The University of Sheffield

Department of Mechanical Engineering

Development of a Novel Ultrasonic Method for Non-invasive Measurement of Oil Films in Piston Ring Contacts

---

Author:

Emin Yusuf Avan

Supervisor:

Prof. Rob Dwyer-Joyce

This thesis has been presented by the above author in partial fulfilment of the requirements for the degree of

Doctor of Philosophy

April 14, 2013

This PhD Thesis is dedicated to

my beloved parents Saniye and Şuayıp.

Abstract

Piston ring-liner contact in an internal combustion engine highly influences the amount of friction, oil consumption and wear that occurs. Proper lubrication of this contact is, therefore, necessary and is an important research area for the engine manufacturers to improve fuel efficiency and achieve the emission reduction targets proposed by authorities. However, the lubricant film formed in piston ring-liner contact is very thin and its measurement is challenging. Although the computer simulations, a low cost tool, are widely used to estimate the piston ring-liner interactions, they require a robust data for the validation of the mathematical models.

In the past several techniques based on optical or electrical characteristics of the lubricant have been developed and applied to measure lubricant film thickness in piston rings, such as capacitance, resistance, eddy current and laser induced fluorescence methods. The main characteristic of these techniques is that they are invasive and require access to the piston ring-liner contact, and so penetrate the cylinder liner. Hence these measurement methods disturb the nature of the contact and influence ring lubrication. This thesis demonstrates the development of a novel ultrasonic method for non-invasive measurement of oil films within the piston ring contacts and the feasibility of the technique on a reciprocating test rig and a fired engine.

After successful implementations of ultrasonic technique, the investigation results showed that the ultrasound technique can be used for the piston ring film thickness measurement. The ultrasonically measured film thickness values were consistent with those of other published data in the literature. The effects of load, speed and viscosity on the lubricant film formation were shown in the reciprocator tests. The investigation of the single cylinder engine test showed that the bespoke ultrasonic sensors could survive at high temperature that liner exterior surface experienced. The minimum lubricant films between the compression ring and liner were measured during the engine's power stroke and were typically less than 1 μm at TDC and $\sim$4 μm at mid stroke.

It has been shown that the ultrasonic technique demonstrates significant promise as a non-invasive and effective tool to assess the lubricant condition within the ring-liner contact. As being insensitive to test environment and more compact technique compared to the current measurement technologies, the ultrasonic method has a potential to be employed in a test vehicle.

Thesis Supervisor — *Author*

Prof. Rob Dwyer-Joyce — **Emin Yusuf AVAN**

Contents

List of Figures

List of Tables

Acknowledgements

I am heartily thankful to my supervisor, *Prof. Rob S. Dwyer-Joyce*, whose encouragement, supervision and support from the preliminary to the concluding level enabled me to develop an understanding of the subject. I appreciate all his contributions of time and ideas to make my PhD experience productive and stimulating.

I would like to acknowledge the financial support of *Turkish Government - Ministry of Education* during my PhD. I am very grateful to *Prof. Metin U. Salamci* for his encouragement, guidance and motivational support.

I would like to thank research technician *Dave Butcher* and all the researchers in the Leonardo Tribology Centre for providing enjoyable research atmosphere. A special thanks to *Robin Mills* who gave great support especially during the fired engine tests. I would like to thank *Andrew Spencer* for the sharing of his numerical data in Chapter-6.

I also would like to thank my friends in Türkiye, particularly *H. Anıl Salman*, *Eralp Ekiz* and *Murat Seyhan* who have given a grateful friendship to the author. I wish to thank *Ahu* and *Murat Coşkun*, *Öykü* and *Melih Bozkurt*, *Edita* and *Özden Işbilir* who gave me the moral support and fantastic social life in Sheffield. I am extremely grateful for the good advice, support and friendship of *Serdar G. Tombul* which have been invaluable on both an academic and a personal level.

I reserve a special thank you to my fiancee, *Esengül Ayaz* for her understanding, kindness support and above all her love and devotion through all my ups and down. Finally, I greatly appreciate the endless support and patience of my beloved parents *Şuayıp* and *Saniye* and my sister *Yeliz*. Without their support this study would never have been possible.

Emin Yusuf AVAN

The University of Sheffield

April 14, 2013

Nomenclature

A ..... area of fluid layer

A_i ..... incident wave amplitude

A_l ..... wave amplitude

A_o ..... initial wave amplitude

A_p ..... area of conductive plates

A_r ..... reflected wave amplitude

B ..... bulk modulus of lubricant

c ..... speed of sound in medium

C ..... capacitance

d ..... distance between the conductive plates

E ..... young's modulus

f ..... frequency of ultrasound

f_m ..... resonant frequency

h ..... thickness of layer

h_{min} ..... minimum thickness of lubricant layer

K ..... interface stiffness

l ..... thickness of material

L ..... reference length

m ..... mode number of resonant frequency

p ..... applied normal pressure

R ..... reflection coefficient

S ..... non-dimensional group

t ..... time

u ..... approach of surfaces

U ..... sliding velocity

V ..... volume of layer

z ..... acoustic impedance of medium

α ..... attenuation coefficient

λ ..... wavelength

λ^* ..... dimensionless film parameter

μ ..... dynamic viscosity of the lubricant

ρ ..... density

σ^* ..... combined roughness

σ_L ..... roughness of the liner

σ_R ..... roughness of the ring

ε ..... permittivity of dielectric material

ω ..... angular frequency of pulse

Abbreviations

BDC ..... bottom dead centre

DPT ..... digital piezoelectric translator

FFT ..... fast Fourier transform

HA ..... honing angle

IC ..... internal combustion

LIF ..... laser induced fluorescence

MOFT ..... minimum oil film thickness

OFT ..... oil film thickness

PZT ..... lead zirconate titanete

TDC ..... top dead centre

ToF ..... time-of-flight

UPR ..... ultrasonic pulser receiver

UV ..... ultraviolet

1

Introduction

1.1 Overview of Piston Rings

In an internal combustion (IC) engine, piston rings play a major role while the piston is converting the high combustion pressure into a reciprocating mechanical movement. The piston rings operate in extremely harsh conditions; their temperature reaches about 250°C or more [1], and the piston speed varies from zero to its maximum speed, generally in the range of 5 to15 m/s, depends on engine type [2]. At these conditions they should provide a gas seal between the piston and cylinder liner, control the amount of oil being passed up the cylinder bore, provide heat-conducting paths from the piston to the water-cooled cylinder liner for the effective cooling of the piston, resist corrosion and keep their shape and tension.

The location of the piston rings in an IC engine is illustrated in Figure 1.1a. The piston rings could be broadly categorized as compression rings and oil control rings. These rings are placed into ring grooves with a specific arrangement. Although the number of piston rings installed on each piston and their line up arrangement are different from engine to engine, the most commonly used one is 'three ring-pack' . In the typical three ring-pack arrangement shown in Figure 1.2, there are three piston rings: generally the

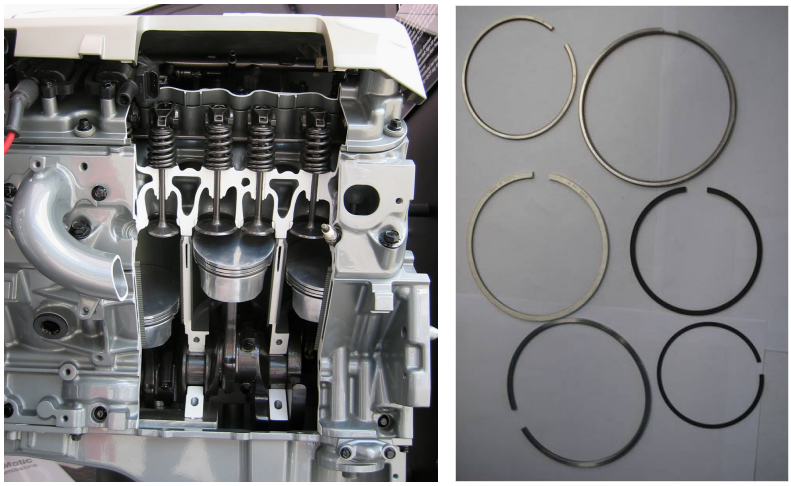

(a) (b)

Figure 1.1: (a) Cutaway of an internal combustion engine showing the piston assembly [3] (b) Several piston rings.

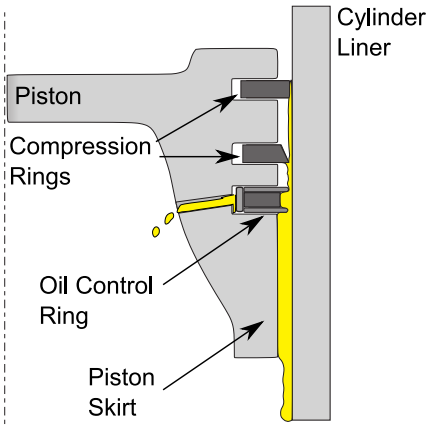

Figure 1.2: Typical configuration of piston ring pack.

top two are compression rings and the last one is oil control ring (terminology is given in Appendix A). As illustrated in Figure 1.1b, the piston rings have incomplete circular shape providing end gap. Although this gap is very small in the installed condition, it allows combustion gas to leak to the crankcase as the engine in operation. The ring gaps are therefore circumferentially staggered when they are installed to piston grooves.

1.1.1 Compression Rings

Compression rings are located in the top grooves of the piston. Each piston groove is produced slightly greater than the piston rings dimensions for both axial and radial directions (roughly 75-125 μm). This allows combustion gas to flow into the groove. The high pressure gas acts on the back of the piston ring and push the piston ring towards the bore. Thus this force enables the ring to seal the combustion chamber and limit oil consumption. Ring radial pressure distribution depends on the ring profile.

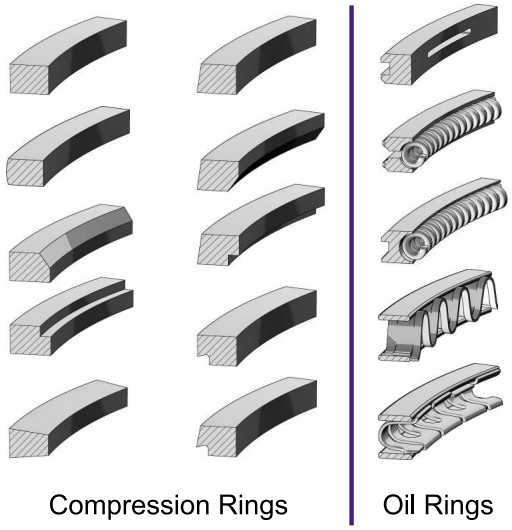

Figure 1.3: Schematic views of typical piston rings used in engines as compression rings (left) and oil control rings (right) [4].

Piston rings can be made of grey cast iron, alloyed cast iron, nodular cast iron or steel depending upon engine conditions and cost effectiveness. However, grey cast iron, which is cheap and readily available material, is generally used as the main material for piston ring production [5, 6]. Its good running properties, good friction and wear resistance are unique and make it an optimal material for piston rings.

A change in ring profile can change the oil control or frictional characteristics of the ring. Many different ring designs have appeared over the years, some of them are illustrated in Figure 1.3. Today barrel-shaped profile rings are widely used in the top groove in

diesel and petrol engines since they give quick bed-in, long life and good scuff resistance [6]. Generally, the peak of the barrel is at the centre but this could be changed relative to the centre line according to the engine designer and application. The ring face may also be coated with chrome, molybdenum to improve wear and seizure resistance.

In typical three-ring pack, a second compression ring has a dual function. It should seal the combustion gas seeping past the first ring and more importantly sweep away any oil layer left over by the oil control ring. Virtually most secondary rings have been formed by considering their oil scraping function. Having a tapered face, which contacts to the cylinder bore with its bottom outer edge, is the main characteristics of such piston rings. This provides rapid running-in and improves oil scraping at the downstroke. The gas pressure force acts on the tapered running face and this gives some sort of pressure relief at the ring cylinder bore contact. This ring is commonly positioned into second groove due to its oil scraping ability but in some petrol engines, they are also installed into the top groove [4].

1.1.2 Oil Control Rings

There have been different designs of oil control ring in today's engines which consist of one, two or three pieces. Their main task in the ring-pack is to control the lubricant oil on the cylinder bore surface and convey the excessive oil to the engine crank case via its perforated structure. One-piece oil control ring could have drainage holes (*i.e.* circular or slotted) in the peripheral direction in order to transfer the oil accumulation between the outer lands as the ring travels from top to bottom inside the cylinder bore. Tangential force is applied to the bore by only the ring's inherent tension because there is no gas pressure behind the slotted oil ring. Two-piece oil control rings consists of a coil spring which provides extra tension and better conformability by increasing contact pressure. An ordinary there-piece oil rings consist of two thin steel rails and a corrugated expander ring which is placed between the rails and holds them in axial position. The rails do not have inherent tension and the expander ring force the rails to both piston

groove side faces and cylinder bore. Such rings perform better adaptation to cylinder deformations and piston tilt. Due to cost reasons, they are preferred in modern gasoline engines whereas two-piece oil control rings are commonly used in diesel engines [5].

1.1.3 Piston Ring Lubrication Regimes

The piston rings operate in various tribological conditions from boundary to hydrodynamic lubrication regime. Generally, the Stribeck curve, which relates the friction coefficient to a velocity, load and viscosity parameter, is used to demonstrate these lubrication regimes. The relative sliding velocity between the ring and liner which entrains lubricant into the contact is substantial at mid-stoke and zero at the dead centres (*i.e.* top and bottom of the stroke). Hence a most satisfactory lubricant film formation between the ring and liner may exist at mid-stroke with hydrodynamic lubrication conditions. However, at top dead centre, especially the top ring is exposed to highest pressure and temperature comparing with the other rings in the ring pack. Therefore, mostly boundary lubrication or partially mixed lubrication regime could occur and the friction is mostly dominated by asperity interactions between the surfaces.

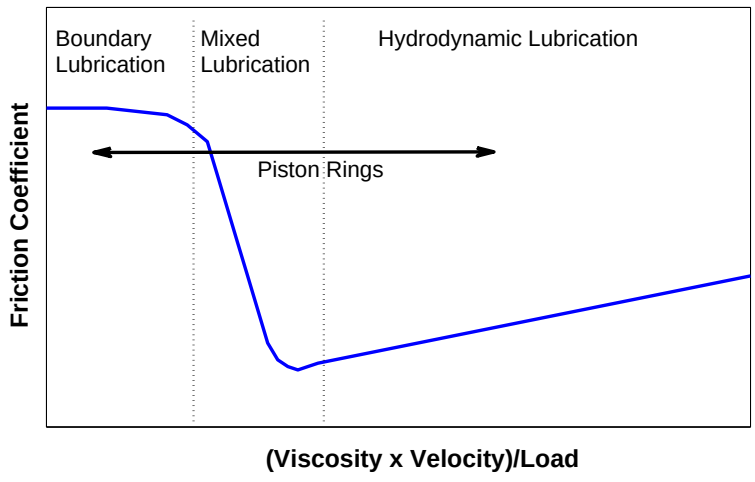

Figure 1.4: Stribeck diagram showing different lubrication regimes.

1.2 The Importance of Piston Ring-Liner Contact

The internal combustion (IC) engine is one of the major sources of anthropogenic carbon emission. According to the recent regulation published in the official journal of EU [7], only road transport is the second largest greenhouse emitting sector in the European Union. The automotive industry is under pressure to improve engine's fuel efficiency in order to meet more stringent emissions standards set by authorities. Since the piston ring-liner conjunction significantly influences engine power loss, lubricant oil and fuel consumption, it has received more attention from engine designers and lubricant suppliers.

Typical distribution of fuel energy is illustrated in Figure 1.5. Broadly, the energy dissipated uselessly in the form of heat during the cooling process of the engine or through the exhaust pipe is around 60 %. A further 15 % of total losses are dissipated as mechanical losses and amongst them the friction between piston assembly and cylinder liner is the single largest contributor with 45 %. Of course these numbers might show some differences depending on the type of engine, loading and driving conditions [8]. During an urban cycle, Andersson [9] showed the distribution of fuel energy usage for a medium sized passenger car and similarly reported that piston assembly is a major source of mechanical losses and responsible for about 40-60 % of the total mechanical losses. The work by Spearot [10] showed only piston ring contribution to the entire

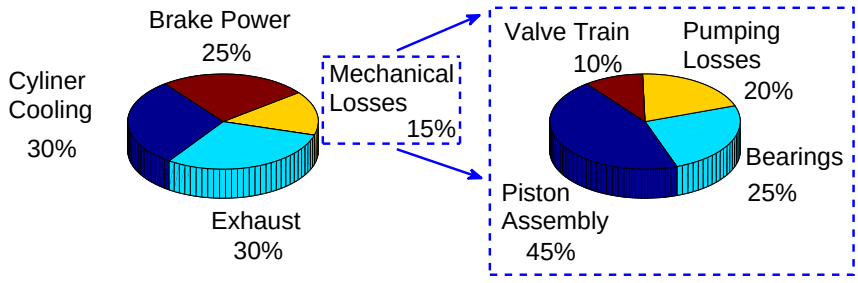

Figure 1.5: Pie charts showing typical dissipation of the fuel energy and typical distribution of mechanical losses in an IC engine [8].

friction loss is 19 % in a light duty vehicle. The tribological performance of the piston rings becomes therefore supreme importance in terms of engine reliability and efficiency [11]. If the amount of reciprocating IC engines in service today has been considered, even the smallest improvements in engine efficiency, emission levels and durability can have a significant effect on the world fuel economy and the environment in a long-term [12].

As mentioned, the major function of piston ring is to provide a mechanical seal between the combustion chamber and engine crankcase as the piston reciprocates. If the sealing action is poor, the combustion pressure in the chamber drops and this results in a reduction in power output of the engine. Exhaust gas leakage also leads to rapid oil deterioration in the engine crankcase. Besides their sealing function, they distribute lubricant oil along the cylinder liner. If the film is too thin then surface contact can occur, leading to high friction and wear. However, if there is excessive oil present in the contact, it will be burnt away and this boosts the exhaust emission. This oil control function has a direct influence on oil consumption in engine, the reliability and life of the rings [11]. Optimum lubrication of the piston rings is therefore necessary.

To achieve a better insight into all of these phenomena, monitoring of the oil film in the ring-liner contact and thickness measurement become very important. The measured film thickness would aid understanding the lubrication process in the contact and validating numerical simulations as well. Most recent techniques utilizing the electrical or optical properties of lubricant to determine the film thickness have been successfully applied to the engine and achieved to measure the lubricant film thickness in piston rings. However the penetration of the cylinder wall is required for these methods and inevitably this disturbs the nature of the contact and hence the lubricant formation in the contact.

In this thesis, a non-invasive ultrasound approach is developed to measure the lubricant film thickness formed between piston ring and cylinder liner. Firstly, the technique

and measurement system are proved on a trial motored engine and then it is applied to reciprocating bench tests. The effects of parameters (*i.e.* load, speed, viscosity and different liner surfaces) on the lubricant film thickness are investigated. In final stage, the technique is employed on a single cylinder engine. The lubricant film thickness measurements between the ring and liner are conducted in fired engine conditions.

1.3 Project Objetives

The aim of this project has been to develop the ultrasonic technique of film measurement for piston ring-liner contact by increasing the understanding of the theory behind it, comparing it against numerical predictions, and extending its use from bench test rig to fired engine test rig. The objectives of this work have been to:

- Devise an ultrasonic method which allows the thickness of oil film formed between the piston ring and liner to be measured non-invasively. All previous measuring methods require the need to penetrate the cylinder liner in order to access the ring-liner conjunction.

- Develop a reciprocating bench test to improve the technique practically. Intensive modification and instrumentation are required for the engine tests and this inevitably increases the time and cost of the tests. Since the most of the operating parameters, such as speed, load, lubricant rate, are controllable in the bench test, this useful low cost tool, provide detailed information about how the different parameters influence the piston ring lubrication.

- Apply the technique to the fired engine and monitor the lubricant films formed in the ring-liner contact. Demonstrate applicability and robustness of the ultrasonic sensors at the elevated temperatures experienced on the engine cylinder wall.

1.4 Thesis Layout

This thesis is divided between the following chapter headings: Piston Ring Film Thickness Measurement-Literature Review, Ultrasonic Background, Generic Method, Ultrasonic Imaging of the Piston Ring Liner Contact, Piston Ring Oil Film Measurement in a Reciprocating Bench Test, Parametric Study of Oil Film Thickness and Friction, Ultrasonic Film Thickness Measurement in a Fired Engine and finally Conclusions and Recommendations. A brief summary of each chapter is given as follows;

- Ch2. Piston Ring Film Thickness Measurement: Literature Review. This chapter reviews the developments in piston ring-liner lubricant film thickness measurement. The aims of this chapter are to appreciating existing measurement methods and understand the gaps in the current state of affairs.
- Ch3. Ultrasonic Background. This chapter reviews the principles of ultrasound and the equations that govern ultrasonic reflection from the interface. These equations are extended to measure thin liquid layers and the spring model widely used in this thesis is outlined. The generation of ultrasound and typical ultrasonic sensors are presented.
- Ch4. Generic Method. This chapter reviews the individual generic parts of an ultrasonic apparatus and generic measurement methodology and signal processing.
- Ch5. Ultrasonic Imaging of the Piston Ring-Liner Contact. This chapter introduces the initial attempt to apply the ultrasonic measurement technique on a motored engine. Reflections from the ring-cylinder wall are identified and captured by developed high speed pulsing and triggering system. Imaging of ring-liner contact is performed and reflection coefficient measurements are made at near TDC, BDC and mid stroke.
- Ch6. Piston Ring Oil Film Measurement in a Reciprocating Bench Test. In this chapter, a reciprocating tribometer modified for the piston ring-liner contact is

introduced. Bespoke small piezoelectric sensors and their application to the test rig are presented. The initial lubricant film thickness results are discussed and compared with a computational model.

- Ch7. Parametric Study of Oil Film Thickness and Friction. Several experiments are performed to investigate the effect of normal load, reciprocating speed, different liner surfaces and viscosity on the measured lubricant film thickness between the ring and liner. The experimental results and the correlation between measured friction and film thickness are presented in this chapter.

- Ch8. Ultrasonic Film Thickness Measurement in a Fired Engine. The ultrasonic method is applied to a four-stroke single cylinder gasoline engine based at Loughborough University. In firing condition, ultrasonic piston ring film thickness measurements at several fixed sensor positions over the liner are conducted.

- Ch9. Conclusions and Recommendations. The main conclusions drawn in the thesis are surveyed and the potential future works and further development of the technique are discussed in the last chapter.

2

Piston Ring Film Thickness Measurement: Literature Review

The availability of lubricant film in a piston ring is important for IC engines and it is intimately responsible for friction loss, oil consumption and wear. The piston ring lubricant film is very thin and the measurement of this essential variable is difficult. In the literature, there have been several methods developed and used in order to visualize or measure the lubricant film thickness formed between piston ring and liner. Test works have been carried out using piston ring-liner simulators or real engines operating in motored or fired conditions. This chapter gives a brief overview of these measurement techniques and their applications to the piston ring-liner case.

2.1 Optical Methods

2.1.1 Laser Induced Fluorescence

2.1.1.1 Transparent Windows

Early optical studies were based on visualization of the piston lubrication mechanism. The conventional cylinder was replaced to transparent cylinder made from perspex or

glass, allowing the light to pass through the cylinder and illuminate the piston ring contact area [13, 14, 15]. Although these early studies did not provide quantitative results, they have been very helpful for guiding to further works.

In one of the earliest studies, carried out by Greene [15], two complementary photographic methods were developed and applied to a motored test ring. Traditional photography techniques could not be employed due to the extreme thinness of oil film. The new techniques were the ultraviolet (UV) light method and the scattered light method. In the scattered light method, the light introduced into the perspex material was reflected by the cylinder walls and the photographs were taken from the front. Some light refracted through the surface and was scattered wherever oil adhered to the cylinder wall. The idea of the ultraviolet light method, also called a fluorescence method, was to use mineral oil's inherent fluorescent property. This property was also enhanced by addition of highly fluorescing compound in the oil. In this technique light source and camera were both located at the same side of the glass cylinder. As the ultraviolet light was projected to the transparent cylinder wall, an UV light illuminated the cylinder and oil doped with fluorescent dye. UV light was absorbed by dye and the dye re-emitted light of a longer wavelength. Hence, the intensity of the reflected light depended on the thickness of the oil film. At that stage, these techniques did not present quantitative results but they provided valuable visual indication of the mechanism of piston and

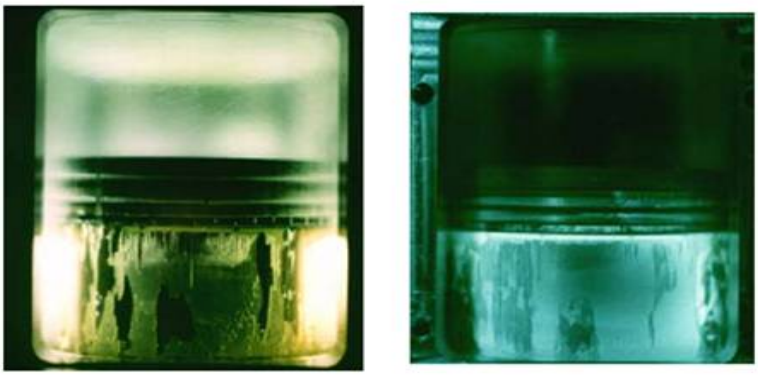

Figure 2.1: Scattered light method (left)- fluorescence method (right) [16].

ring lubrication. A process called fluorescence assay, was later developed and able to measure the film thickness directly by comparing intensity of fluorescent emissions from oil films in the transparent cylinder with emission from films of known thickness. This also allowed identification of cavitation effects [17].

Smart and Ford [18] applied fluorescence assay to open surfaces using a 100 W mercury lamp as a source of ultraviolet illumination. The measurable range of thickness depended on the optical absorption characteristics and degree of fluorescence of the film. For a light lubricating oil, films down to 0.1 μm local thickness were been able to measured successfully. This system was modified by replacing the mercury lamp with a laser light source to excite fluorescence [19]. This offered many advantages, such as reducing the oil deterioration problem, the capability of measure a wider range of film thickness, better stability in fluorescence activity and simplified optical construction. Ting [20] first utilized laser induced fluorescence (LIF) technique for the examination of oil film thicknesses between piston rings and piston skirts on a transparent cylinder engine. It was reported that the calibration of the fluorescence signals was complicated due to the nonlinear response of the dye, therefore uncalibrated assessments of film thickness along the cylinder for a range of speeds were obtained. However, this pioneering work clearly established the feasibility of LIF method to measure the piston ring film thickness.

Alternative to the transparent cylinder, the optical access to piston rings was achieved by inserting a small transparent window into cylinder wall. Researchers successfully measured oil fluorescence in an operating engine through a liner-mounted window [21, 22, 23] and suggested several calibration procedures which related the measured fluorescence intensity to a known oil film thickness. Hoult and co-workers [21] employed the LIF method using a quartz window. To calibrate the output signal, they used a bench top calibration cell where oil was sandwiched between a polished metallic plate and microscope slide separated by a spacer of known thickness. They also suggested one of the first in-situ calibrations of the LIF technique by comparison of a known piston ring profile.

Brown et al. [23] used a single-cylinder research diesel engine for the fluorescence measurements of the oil film thickness between the liner and piston. A fused silica window was positioned flush with the inside of the liner. A laser was fired from Argon-ion laser and steered through the liner-mounted window using a conventional and a dichroic mirrors as detailed in Figure 2.2. The ring-pack oil film thickness was measured for two fully formulated lubricants as a function of engine speed and torque. The minimum film thicknesses under the rings were ranging from ~ 0.5 to 16 μm. The lower viscosity lubricant gave thinner films in the ring pack region. The compression rings were lubricated by a thicker film during the down strokes than the up-strokes with an only exception occured for the top ring films during the expansion stroke.

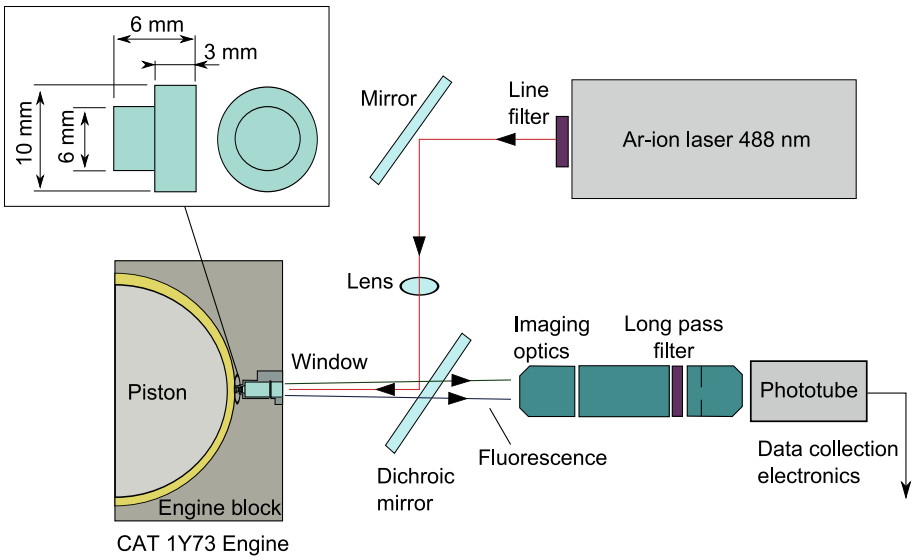

Figure 2.2: Experimental configuration and detail of fused silica window (top-left) reproduced from [23].

Transparent cylinder or liner-mounted window tests have provided useful information about piston lubrication and oil film behaviour around piston ring but they are limited in many ways. Although glass cylinders known as 'optical engines' have successfully run under fired conditions, the materials cannot satisfactorily resist the long term firing engine conditions compared to the conventional cast iron cylinders. The wear on the transparent surface could disturb the illuminating light and alter the results of the study.

Also quartz particles due to the wear of the window would affect the tribology of the engine. The surface of the transparent cylinder must have high quality finish but this finish is not comparable to the honed finished on real cylinders or liners.

2.1.1.2 Fibre Optic Setups

A less intrusive system that combined laser induced fluorescence method (LIF) and fibre optics technology was developed to measure oil film thickness under fired conditions [24]. In this system, the light from laser source was conveyed by the fibre onto the piston or piston rings, then the fluorescence reradiated from the oil film was returned through the same fibre to a detector (*i.e.* photomultiplier (PMT)), measuring fluorescence intensities or levels of light. When compared to previous designs using conventional optics, this combined system improved the ease of installation, portability, durability and signal-to-noise ratio [25].

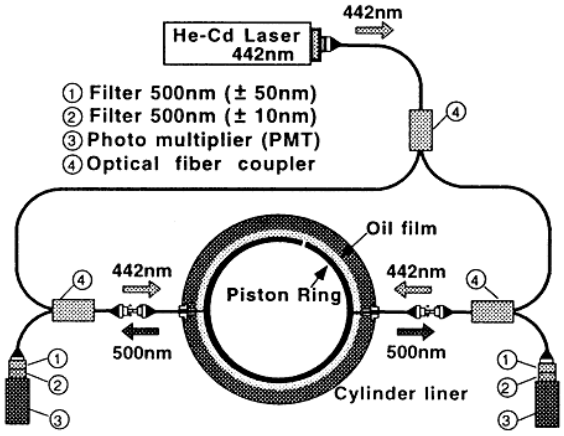

Figure 2.3: Schematic reproduced from [26] showing arrangement of optical system.

In early studies [24, 25, 27, 28] the optical access was still achieved by transparent windows. The optical fibre was coupled a focusing probe mounted in the engine. Hence, the focussed laser beam was passed through the window and traversed the oil film at the window location. This method was also applied to a reciprocating test rig [29]. A reciprocating fixture was connected to a ring guide and a ring holder which were used

together to hold a piston ring segment against a liner segment supported by a floating holder mounted on a pair of linear bearings. Friction force measurement was sensed by a load cell connected to the floating liner holder as schematically illustrated in Figure 2.4. Normal force exerted on the ring segment was adjusted by a pneumatically driven air cylinder and this force was sensed by a sub-miniature load cell mounted at the interface between the ring holder and the ring guide. Two LIF probes were placed into a side plate and light was focused through quartz windows on the liner. This made the measurement of the film thickness under the ring at mid-stroke possible. The tests were carried out at different speeds and loads. The piston ring oil film thickness at mid-stroke varied between approximately 0.5 and 4 μm. However the order of 40% uncertainty of the LIF film measurement was estimated.

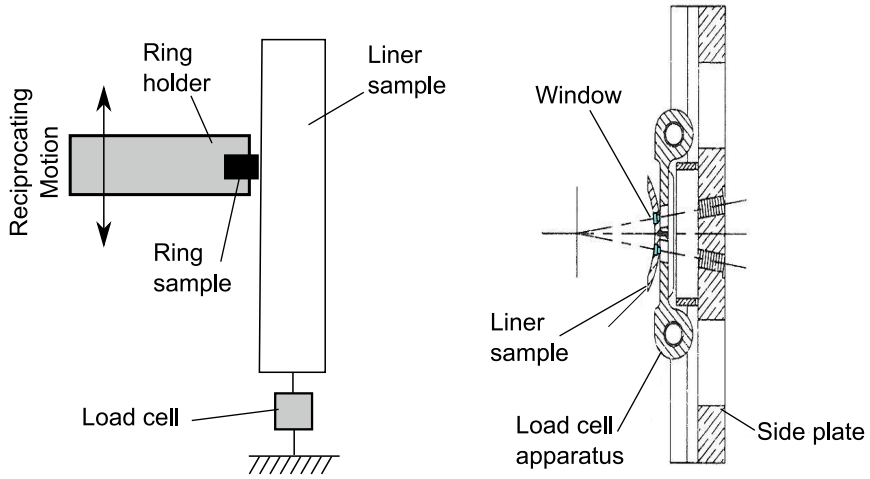

Figure 2.4: Concept of the ring friction measurement (right) and LIF measurement set-up (left) adapted from [29].

With development of fibre optic technology, the laser beam was directly transferred onto the oil film through the optical fibre [26, 30, 31, 32]. The measurement diameter was significantly reduced from ~3 mm to 50 μm and this increased the spatial resolution. Takiguchi et al. [26] employed the method on a pre-combustion type mono cylinder diesel engine. Since the surface of fibre optic became the measuring and sliding surface, it was mounted flush with inner surface of the cylinder wall by means of an adapter

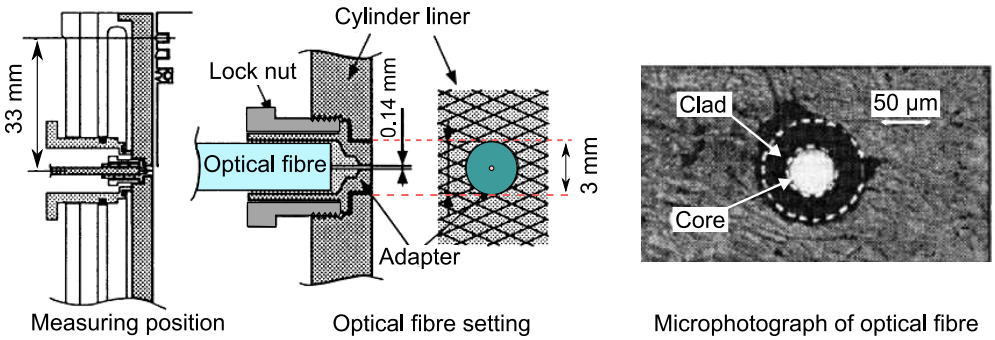

Figure 2.5: Schematic optical fibre setting from [26], microphoto (right) showing an optical fibre mounted in the cylinder liner.

housing the fibre (see Figure 2.5). Two fibre optic probes were placed at the thrust and anti-thrust sides of the cylinder. The stroke to stroke variation of the film thickness of each ring on both sides varied noticeably and the thinnest oil film thickness was recorded for the top ring, ranging from 0.6 to 0.9 μm. The amount of oil supplied changed with the piston slap motion and this motion had more effect on the piston ring film thickness than the engine speed or load. The same engine and system were also used by Seki et al. [31] to study oil film thickness variation in different ring sets. Lubricant film thicknesses were simultaneously measured at four points on the thrust side of the engine. The results showed the measured film thickness values of oil control rings were much thicker than the theoretical values. Oil control ring film thickness increased where the ring tangential tension was reduced while it decreased with reducing the ring width. These effects were observed mainly around TDC. However, the use of tension reduced oil control rings increases the oil consumption under high speed engine operations [32].

LIF method has brought substantial benefits to the piston ring film thickness measurement but it has some drawbacks. This method reduces the required size of entry into the cylinder due to small diameter of the fibre core (about 50 μm). This enables laser light to capture at multiple locations on cylinder liner, as well as increases the measurement accuracy of the ring film thickness. On the other hand, the installation of the fibre optic probes to the cylinder is invasive and requires tedious works (*i.e.* post grinding and honing). There are also many factors that affect LIF beam intensity such as the

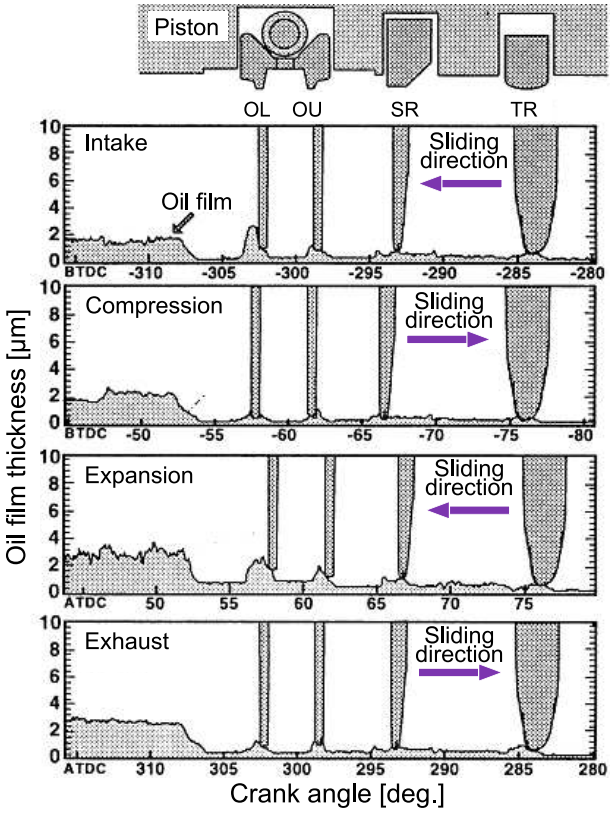

Figure 2.6: Example plot showing variation of oil film thickness in each stroke. Oil film was measured by LIF method as the engine speed of 2000 rpm with a full load [26].

concentration of fluorescent dye, optical filters, the alignment of the laser beam into the fibre, PMT voltage and photo bleaching. Combustion illumination, temperature and soot accumulation can also disrupt the assessment of light intensity for the fired engine tests. Further, an appropriate verification method is required to convert the PMT output to film thickness. In the literature, a pair of glasses with a wedge space between them [33] or an optical fibre mounted flush with the anvil of the micrometer [30] have been used as a static verification and a piston ring with a known step on the sliding face has been used in a test engine as a dynamic verification [26, 31].

2.1.2 Optical Interferometry

The other method used for film thickness measurement has been optical interferometry [34, 35], which is based on the coloured interference pattern produced by the reflected

light from the lubricated contact. Typically a contact is formed between a reflective steel ball and glass disk. The glass surface can be coated with a very thin, semi reflective layer of chromium or titania. The light shines onto the lubricated contact using optical arrangements and then splits into two beams with almost equal intensities. One is reflected back from the semi-reflective coated glass surface and the second travels through any oil film and is reflected back from the steel ball surface. These two beams then interfere and the extent of interference corresponds to the additional distance travelled by the second beam passing through the oil film[36]. This can be then used to determine film thickness. The useful range depends on the source of light, if monochromatic light is used, the useful range is from about 0.1 μm to several micrometres. This becomes more limited for the white light, 0.1-1 μm, due to interference of the different wave lengths of the reflected light [37].

This technique was applied on a reciprocating test rig to measure the film thickness between a piston ring specimen and a plane glass plate[38]. The cyclic change of film thickness during the reciprocating motion was obtained relatively close to theoretical value. However, the coherence of the illuminating light was reduced by increasing the separating gap. This proportionally reduced interference image quality and ultimately film thickness measurements were no longer available. The other limiting factor to optical interferometry is the requirement of reflective coatings which are expensive and are prone to wear [39].

2.2 Electrical Methods

Attempts to examine oil film thickness using electrical principals can be divided into three main groups: resistance method, inductance method and capacitance method. Brief descriptions of these methods will be presented in the following subsections.

2.2.1 Resistance Method

Researchers studied the oil film condition in piston ring using electrical resistance method where the oil film was used like a resistor [40, 41, 42]. To do this, the piston ring must be electrically insulated from the rest of the piston assembly. When a current passed from this ring to the cylinder liner, the potential would drop across the oil film. This could be calibrated in terms of resistance and therefore correlate to the separating oil film.

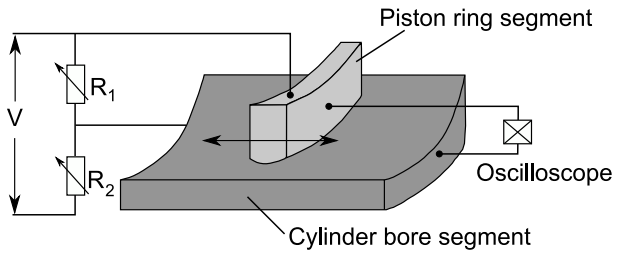

Figure 2.7: Schematic of electrical contact resistance measurement between piston ring segment and cylinder segment (Reproduced from [42]).

In an early study carried out by Courtney-Pratt and Tudor [40], a second compression ring of a single-cylinder water-cooled engine was insulated by thin mica sheets. The experiments were carried out with a series of commercial mineral oils. Although the quantitative results were not presented due to the lack of regular and clean changes in resistance, the conditions of lubricant were interpreted over the length of the piston stroke. It was reported that the ring and liner were never separated by a continuous oil film throughout the entire cycle; a varying degree of intermittent breakdown of the oil film was observed even with higher viscosity oil in use.

Furuhama and Sumi [41] introduced a test apparatus which had a stationary piston ring and reciprocating cylinder liner. The ring load could be varied by means of a rubber tire acting on the back of the piston ring as the compression fluid was pumped into it. A different type of ring instrumentation containing three local electrodes placed into the ring was tested, along with using the whole piston ring as an electrode. The results

showed no difference between these two types of electrodes. As another technique, an anode was placed in the ring end and the film thickness formed between the ring and liner was obtained by means of measuring the circumferential displacement of ring gap. The results obtained from these different instrumentations showed thin oil film thickness mainly near the top and bottom dead centres while thick film near the midpoint of stroke.

In recent study [43], electrodes were embedded into the electrically non-conductive coated rods. The rods were then placed into the inner liner surface of the single cylinder AVL engine as illustrated in Figure 2.8. The differential voltage drop between the piston ring and cylinder liner contact surfaces was measured and converted to the film thickness using an oil film thickness calibration (e.g. each 140 mV equivalent one micron of oil film thickness). It was highlighted that this calibration would vary with different lubricant package. The measurements were taken at five locations and the top compression ring had minimum film along the piston stroke when compared to the other rings. The top ring film thickness varied from 10 μm near mid-stroke to 0.5 μm at TDC.

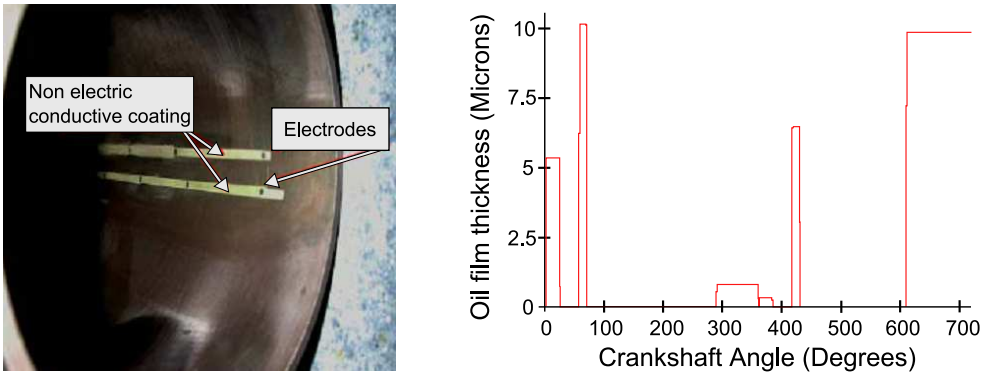

Figure 2.8: Reproduced figures from [43]: AVL liner instrumented with two rods housing electrodes (left), variation of oil film thickness between top piston ring-liner at 2200 rpm engine speed and engine torque of 92 lb-ft (right).

The main drawback of electrical resistance method is to maintain the electrical insulation for the piston ring, especially for the fired engine tests. This prevents resistance measurements from being popular for the assessment of piston ring film thickness; how-

ever, this method is sensitive to the degree of contact between the ring and liner. As a result, this method became more practical for the information about oil film development or the asperity contact than oil film thickness measurement.

2.2.2 Inductance Method

As a current flows through a wire, it generates a magnetic field around it. Likewise, a change in magnetic field produces a different current and a voltage is induced proportionally to the rate of change in current in the wire. This working principle becomes the base of an inductive transducer schematically shown in Figure 2.9. Here any change in the distance between moveable armature and core is responded by change of induced voltage.

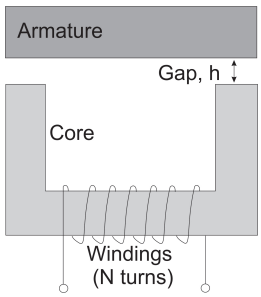

Figure 2.9: Inductive transducer [44].

In an early application, the method was applied to a diesel engine where inductive type proximity transducers were placed into the top piston ring groove and second piston land [45]. The piston ring was used as an armature for the transducer since the coils were too large to be mounted in the ring itself. After appropriate processing of the inductance change in the coils, the clearances from piston to ring and from piston to liner were monitored and the oil film thickness was deduced. The inductive transducers designed to have a high sensitivity in the region of a few micrometers had poor temperature stability and suffered from errors due to changes in resistance of the windings with temperature. To overcome this, Lewis [44] designed a miniature mutual inductive proximity transducer that was calibrated against a jig with a micrometer head. It was shown that this limitation might be amended by measuring the mutual inductance between two

separate windings on the transducers. This type of transducer could increase sensitivity and improve temperature stability. It was suggested that the transducer might particularly be useful for the measurement of oil films between piston rings and cylinder liners.

The indirect measurements of the film thickness using inductive method continued in later years. Ring end gap measurements, similar to that developed by Furuhama [41], were employed on a motored test rig by Dow et al. [46]. The variation in gap size of the ring was measured by a proximity probe embedded in the ring end and the average film thickness around the ring was estimated by using geometric principles. Film thickness measurements were made for a range of operating speeds, oil viscosities and temperatures. Typical film thickness measurements for the flooded and starved conditions are given in Figure 2.10. The maximum film thickness, which occurred at the maximum piston speed, was about 50 percent greater for the flooded as compared to the starved lubrication condition. Recently the eight sensors were mounted on the ring (see Figure 2.11) in order to measure the distance between the liner and ring and estimate film thickness [47]. A rather large ring-liner distance, in a range between 12 and 16 μm, was measured under motored and fired operation. The measured distance variation over

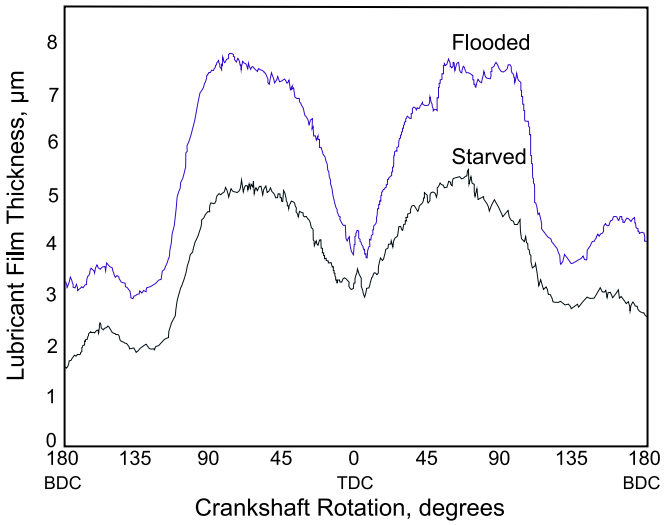

Figure 2.10: Film thickness measurements for two lubricant supply conditions (Reproduced from [46]).

the piston stroke was found less than 2 μm. This method could provide continuous film thickness for a whole stroke. However, the inductive transducer has poor temperature stability and the deduction of film thickness depends on bore circularity such that inaccurate measurement or bore distortion could cause major errors in the measurement.

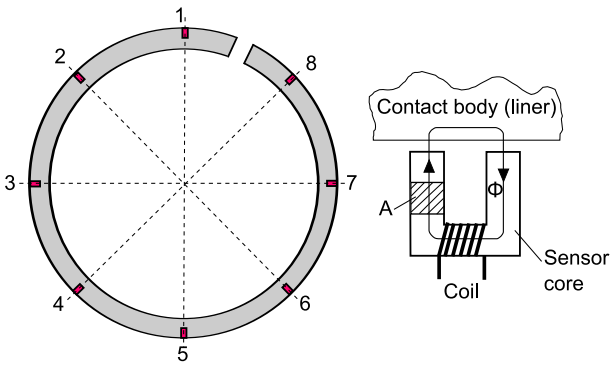

Figure 2.11: Inductive sensor positions within the top piston ring (left) and details of sensor (right) [47].

The minimum lubricant film thickness of piston rings has been measured under motored [48] and fired engine conditions [49] using eddy current sensors. Similar to inductance sensors, the operating principle of the eddy current sensor is also based on electromagnetism. The essential difference between the two methods is that the inductance sensors use the induced voltage whereas the eddy current types use the current induced due to alternating magnetic field [50]. When a high frequency alternating current is passed through a coil embedded into a sensor housing, the electromagnetic field of the coil induces eddy currents in a conductive target material. If the target is close to the sensor core, the induced current reduced the flux and produces low input impedance. As the target moves away, the coupling decreases which increases the input impedance [51]. This change of impedance produces an electrical signal which is proportional to the distance of the target material and the coil in the sensor.

By means of eddy current sensors, Tamminen et al. [49] carried out an experimental research to determine oil film thickness between the cylinder liner and piston ring.

Four eddy current sensors were located in the cylinder liner close to TDC, BDC and at mid-stroke, hence the target material was the piston ring. The sensors were capable of surviving in harsh engine condition but the absolute values of the measured film thicknesses were impossible in this study. This was partly because of the offset installation requirements for the sensors; their inner ended at least 50 μm below the inner surface of the liner. This disturbed the oil film and made the determination of the zero point complicated. Additionally, the eddy current sensor was extremely sensitive to the material of the target. Individual calibration was performed for each piston ring and the measured oil film thicknesses were arranged as sensor-ring pairs. The minimum oil film thickness value of each sensor-ring pair was set to 1 μm. The other measured oil film thickness of each individual sensor-ring pair were expressed as increase in micrometer readings above the minimum value of 1 μm. Therefore, relative oil film thickness values were presented.

2.2.3 Capacitance Method

If voltage is applied on two conductive metal plates (electrodes) separated by a dielectric material, charge will be stored on the surfaces of the plates. Capacitance of these parallel plates, defined by the amount of the charge divided by the voltage applied, varies in inverse proportion to their separation. This is shown in parallel plate formula,

$$C = \frac{\varepsilon A_p}{d} \tag{2.1}$$

where, C is capacitance, d is distance between the plates, ε and A_p are the permittivity of dielectric material and area of conductive plates respectively. This constitutes the basis of industrial proximity transducers. The size required for the piston ring film thickness measurement is too small and researchers tend to design their own capacitance transducers rather than using large commercial proximity transducers [17].

Capacitance method has been widely used to measure the film thickness formed between the piston ring and cylinder wall [52, 53, 54, 55, 56, 57, 58, 59]. An electrode is mounted

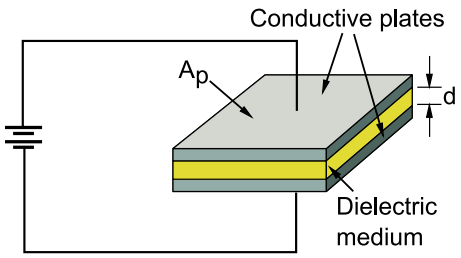

Figure 2.12: Parallel plate capacitor.

either in a liner or in a piston ring and the parallel plate capacitor is formed between the electrode and a matching surface which acts as the other plate of the capacitor. Oil film can be thought as a dielectric material and its thickness change leads to change in capacitance formed between the plates. The oil film thickness is therefore deduced from measured capacitance by assuming the ring-liner contact is fully flooded.

Hamilton and Moore [52, 53] placed three capacitance gauges into the thrust face of a liner to measure piston ring oil film thickness in small diesel engine (see Figure 2.13). In the design of the capacitance probe, a small wire was used as a central electrode and surrounded with a metal screen to eliminate stray capacitance effect. Both electrode and screen were electrically insulated from each other and the rest of the engine. The capacitance gauges were calibrated by a combination of slip blocks and surface pro-

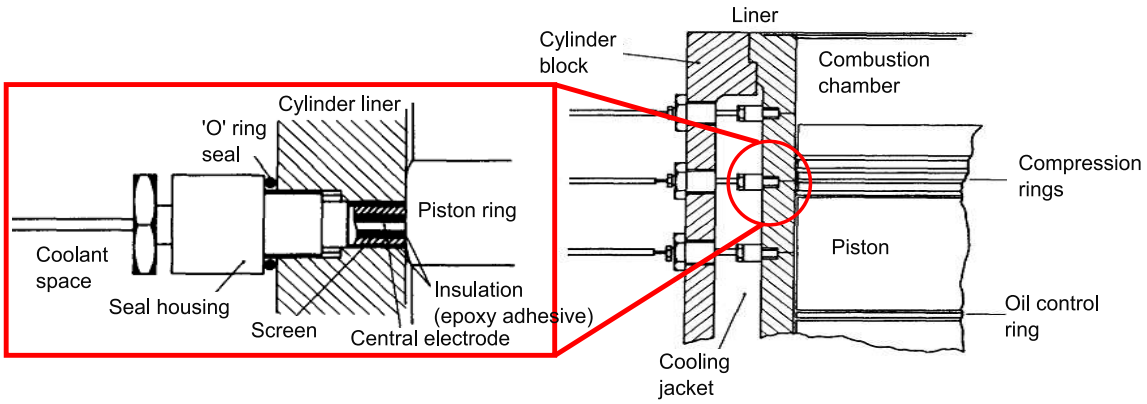

Figure 2.13: A schematic view of the cross-section of the cylinder block and the position of capacitance gauges (Adapted from [52]).

filometer. The calibration showed that the gauges became insensitive beyond 10 μm. The study showed that small capacity gauges were quite successfully operated in the difficult engine conditions. The film thickness between piston ring and cylinder liner was found to be in the range 0.4 to 2.5 μm. Electrical breakdowns attributed to metal to metal contact occurred sporadically all over the cylinder wall. These appeared very often when the film thickness was less than 0.5 μm.

Custom made capacitance probes were small enough to be installed in a piston ring [54, 55, 60]. This made continuous measurement possible over the whole stroke, but some serious modification of the test rig (*i.e.* mechanical linkage illustrated in Figure 2.14) was necessary to maintain electrical contact with the probe comparing with a single point measurement on the water-cooled liner. The electric capacitance type electrodes were embedded into a groove located on sliding surface of the top piston ring using a resin withstanding high temperatures (see Figure 2.15). A thin aluminium oxide layer formed on the face of the electrodes by an electrochemical method was used to complete their insulation. This layer reduced the electrical short circuits caused by metal to metal contact and provided more stable measurements.

Figure 2.14: An example of telemetry linkage from [61]

This type of sensor was used in Furuhama's work [54] and three sensors were located at circumferential direction of the top ring. Then circumferential movement of the ring was restricted using a ring stopper to protect the wiring against shearing off. A calibration curve was drawn by using shallow grooves of 2 and 6.5 μm in depth on the cylinder wall. Oil film thickness was found to be much thinner than theoretical

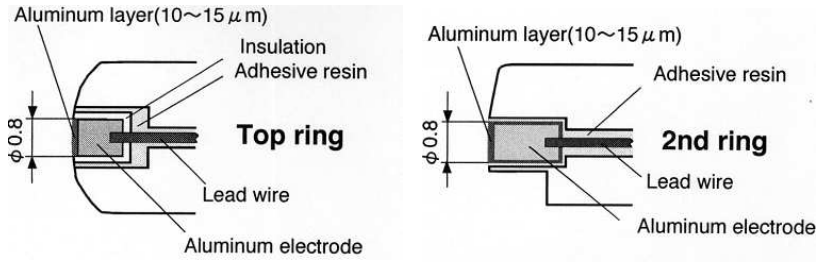

Figure 2.15: Sectional view of the typical ring electrodes from [60]

value when a normal ring arrangement was applied. This was attributed to the lack of lubricating oil supply. A piston without oil control ring was also tested to ensure an adequate supply of lubricating oil. The results showed thicker oil film for the top ring compared to the normal ring arrangement (see Figure 2.16) and the film thickness values were approximate to theoretical values. The inclination of the ring sliding surface against cylinder liner was measured using a twin electrode method, where there were two electrodes in the top ring in use. The effect of the inclination was negligible for thin oil film thickness but it was significant when the film thickness was thicker.

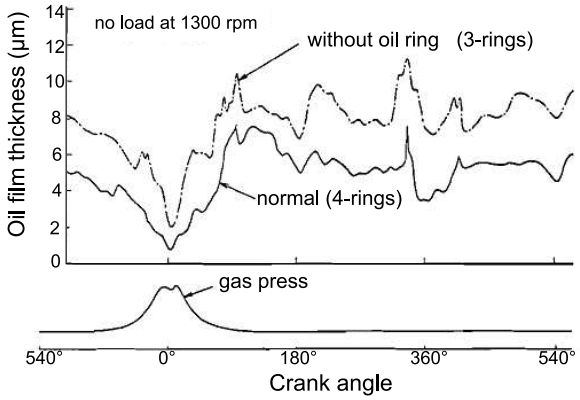

Figure 2.16: The effect of oil ring on the top ring oil film formation from [54]

Ducu et al. [58] carried out a detailed study that analyzed potential error and noise sources in the measurement, such as the fringing of the electric field, curvature of the ring face profile, roughness of the ring profile and the tilt angle of the ring face. They found that the fringing effect, which is the curvature of the constant potential lines near

the edge of the electrode plate, could effectively be eliminated by surrounding the capacitance probe with a metal shield (*i.e.* driven at the same potential that the electrode has). The capacitance probe should be designed as small as possible to increase the spatial resolution. However, the strength of the capacitance signal depends on the electrode area: a large area increases the capacitance input. Therefore, a rectangular probe with a high aspect ratio was suggested as an optimum [58]. The small length in axial direction of piston movement could provide high spatial resolution and additionally, sufficient signal strength could be obtained by having a longer width in circumferential direction. Recently, a rectangular capacitance probe, as shown in Figure 2.17, was utilized to measure lubricant film thickness between piston ring and liner in a motored engine [63, 62]. The lubricant film was measured in a range of 0.2 and 8 μm. Another experimental study has been carried out by adopting the use of capacitance based sen-

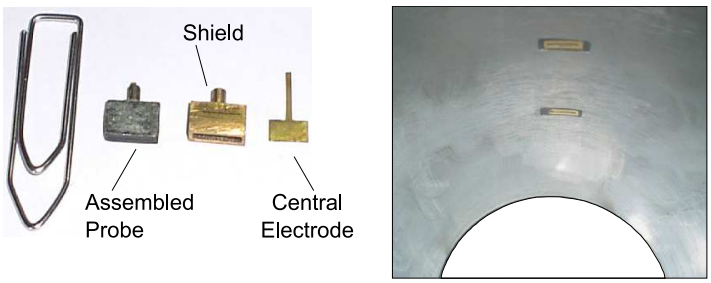

Figure 2.17: A rectangular capacitance probe and a liner installed with the probes [62].

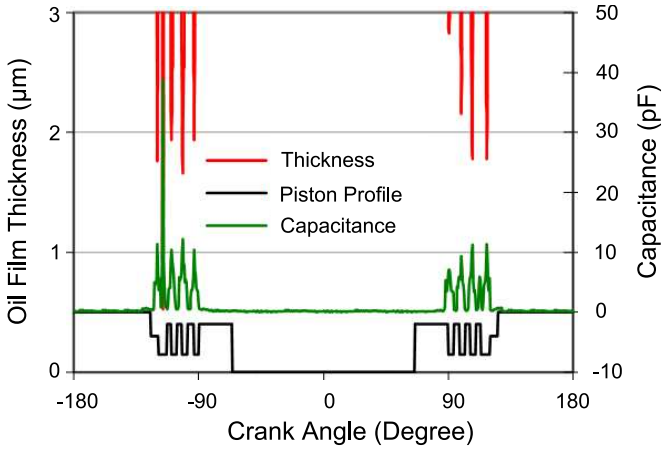

Figure 2.18: Capacitance and oil film thickness at mid-stroke when the motored engine run at 1395 rpm [63].

sor in a Perkins diesel engine [59]. Several oils with different viscosity grades have been tested under a range of engine loads at a constant speed of 2000 rpm. As a general trend, smaller minimum thickness was seen for lower viscosity lubricant and there was no significant effect of load on oil film thickness.

Capacitance method was applied to a purpose-built test rig constructed to allow investigation of boundary conditions for modelling piston-ring lubricant film properties [64]. The capacitance transducer was mounted on the stationary ring specimen thus the full cycle film thickness measurements under the ring were successfully obtained. The predictive performance of various boundary conditions was examined and a delayed cavitation was identified immediately after the dead centres.

Although the capacitance method offers a relatively straightforward way of measuring oil film thickness, it has some limitations. Insulation and shielding are necessary since insufficient shielding of the electrode leads to a nonlinear relationship between film thickness and the capacitance output. The dielectric medium between the electrodes is assumed to be clean and fully flooded. In fired engine, piston rings operate under different lubrication regimes and the cavitation could arise under the piston ring. Thus the medium is filled with air, oil or mixture of them and this leads to a change in the output of the capacitance sensor [65]. Furthermore, oil could contain metal debris or other contaminants which affect the permittivity value of the oil. Erroneous results could be obtained as a group of dissimilar materials are formed for the capacitor due to different thermal expansions and wear rates. The calibration is again required.

2.3 Conclusion

Lubricant film between the piston ring and liner is a vital parameter for engine operation. Its measurement helps the design and optimization of the ring liner conjunction. Several methods, broadly split into optical and electrical methods, have been applied to enable ring-liner film thickness measurements. Early optical methods have been used

to the visualization of the piston lubrication mechanism. With the development of fibre-optic technology, the optical method has been enhanced and LIF method has been successfully applied on a production engine. Many factors have an effect on the assessment of light intensity such as photo bleaching, combustion illumination, limiting its use.

Electrical resistance, capacitance and inductive methods have also been used to measure piston ring-liner film thickness. Resistance method requires electrical insulation for the piston ring to avoid electrical breakdowns in the measurement signal. The inductive method suffers from the probe's poor temperature stability. They are extremely sensitive to the material of the target and individual calibration of the sensors are required. Both methods may not give absolute film thickness but they could provide the extent of the separation between ring and liner. Capacitance method is more popular among them; however insulation and shielding of the electrode are necessary and the dielectric properties of the gap depend on the oil condition in the contact.

A wide range of experimental works has been carried out in the literature. Table 2.1 summarizes measured OFT range and operating conditions for selected references. All of these methods have some degree of success; however, they require the need to penetrate the cylinder wall or liner in order to access the ring-wall contact area. The ultrasound technique is based on sensing the reflections from the ring-wall contact. Therefore the ultrasonic sensors do not have to be mounted in contact with the oil film. Post grinding of the cylinder bore could be enough to place the sensor on the liner. This provides localised non-invasive measurements. The ultrasonic measurement of piston ring film thickness measurement would aid to monitor lubricant condition and make significant contributions to the literature.

Table 2.1: Measured ring film thicknesses in literature. * Approximate range deduced from the graphs. (LIF: Laser induced fluorescence, Res.: Resistance, Ind.: Inductance, Cap.: Capacitance, F: Fired, M: Motored, RT: Reciprocating test rig)

References	Method	Engine	OFT (μm)	Engine Speed (rpm)
Baba et al. [33]	LIF	M	5.0* - 18	300 - 1200
Brown et al. [23]	LIF	F	0.5* - 16	500 - 1800
Dearlove & Cheng [29]	LIF	RT	0.5 - 4.0	200 - 600
Frølund et al. [27]	LIF	F	3.5 - 7.0	3200
Seki et al. [31]	LIF	F	0.4 - 4.0	1500 - 2000
Takiguchi et al. [26]	LIF	F	0.6 - 3.5	2000
Taylor and Evans [28]	LIF	F	1.0 - 4.5	1000
Saad et al. [43]	Res.	F	0.5 - 15	1400 - 2200
Dow et al. [46]	Ind.	M	0* - 7.8	200 - 800
Tamminen et al. [49]	Ind.	F	1.0 - 19	900
Wing and Saunders [45]	Ind.	F	5 - 12.7	950 - 1330
Arcoumanis et al. [64]	Cap.	RT	0.25* - 11	300 - 500
Dhar et al. [62]	Cap.	M	0.2 - 8.0	1300 - 1400
Furuhama et al. [54]	Cap.	F	1.0 - 10	1000 - 1900
Hamilton & Moore [52]	Cap.	F	0.4 - 2.5	950 - 1500
Hamilton & Moore [53]	Cap.	M	1.45 - 4.0	200 - 400
Söchting & Sherrington [59]	Cap.	F	4.0 - 23	2000

3

Ultrasonic Background

This chapter presents ultrasound and the physical principles behind it. At the beginning, types of ultrasonic waves are defined and material properties and their effect on ultrasound are explained. Following this, the generation of ultrasound and type of ultrasonic transducer used for film thickness measurement are given. In the final section, the ultrasonic reflection from the interfaces is detailed and the spring model for thin layered system is introduced.

3.1 Basic Ultrasonic Principles

Ultrasound is acoustic energy in the form of mechanical waves having a frequency higher than the upper limit of human hearing range, *i.e.* greater than 20 kHz (see Figure 3.1). Today, ultrasound is used in many fields, from a basic car parking sensor to an advanced medical sonography to visualize internal organs and fetuses in the human womb. It is also widely used in manufacturing industry as a non-destructive tool for the inspection of imperfections in a solid body.

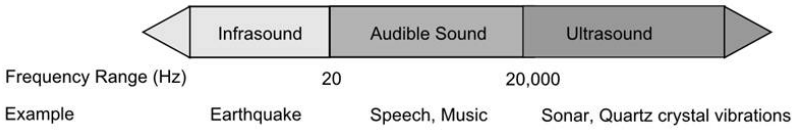

Figure 3.1: Sonic spectrum with some examples.

3.1.1 Ultrasonic Wave Propagation

The physics behind the ultrasound is exactly the same as that of sound. Ultrasound waves are mechanical waves in which oscillation of pressure propagates through a host medium. The host medium can be thought of as a group of particles which are in balance by elastic forces [66]. These elastic forces and the particles can be represented by springs and individual masses respectively. This model can be visualised as shown in Figure 3.2. Assuming such medium is not stressed by compression or tension beyond its elastic limit, the particles can perform elastic oscillations. If the leftmost plane of particles is excited collectively in step with the sinusoidal oscillations, this motion will be transmitted to the neighbouring plane by the elastic forces with the same amplitude and frequency. This process will repeat itself for following planes of particles in the medium and therefore the vibratory movement of the particles will propagate through the medium. If all points are connected rigidly, this displacement will be simultaneously and remain constantly in the same state of motion, *i.e.* in the same phase. However, this is not the case for elastic materials; the displacement requires a certain time to transmit the motion from one plane to the next. This results in phase lag between the subsequent

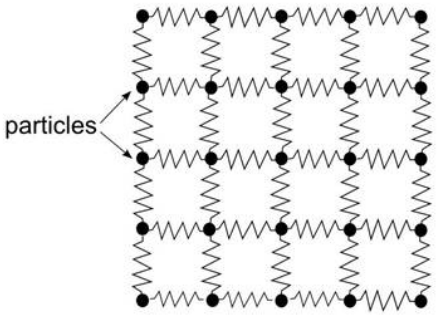

Figure 3.2: Model of an elastic body or medium.

planes and creates compression zones which the particles approach each other closely. This is shown in Figure 3.3 where, λ, is the wavelength which is the distance between two planes.

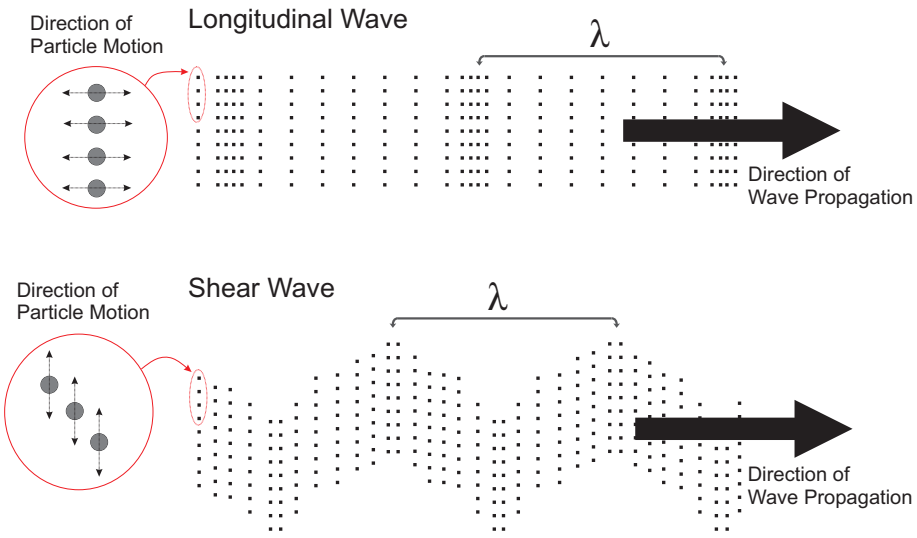

Figure 3.3: A longitudinal wave with particle motions along the direction of propagation and a shear wave with particle motions perpendicular to the direction of propagation.

In the longitudinal wave, the particle motion and the wave propagation are in the same direction. This sort of longitudinal wave is also called a compression wave. The other form of propagation is that of transverse waves depicted in the bottom of Figure 3.3. In this type of propagation, the motion of particles is perpendicular to the motion of wave. This wave is also known as a shear wave. The wavelength of shear wave is indicated between two planes in which particles are in a similar state and instantaneously pass through their position of rest in a direction from top to bottom. It is important to note that, in general, shear waves can be practical only for the testing solid bodies with an appreciable penetration distance since liquids and gases are incapable of transmitting shear [67].

If elastic waves are constrained by a boundary, guided waves occur. This boundary is required for their existence and most common guided waves are Lamb and Rayleigh (Sur-

face) waves [68]. They are combinations of longitudinal and shear waves. In Rayleigh waves, the particles follow an elliptical path and the solid material must have sufficient thickness perpendicular to the surface that the wave propagates on. Unlike Rayleigh waves, Lamb or plate waves only occur in thin plates. They are widely used for damage and flaw detection in the object being tested. These waves are beyond the scope of this investigation and more information could be found in references [69, 67]. This study is primarily concerned with longitudinal waves which were sent through the cylinder wall to measure oil film thickness.

3.2 Acoustic Properties of Materials

As mentioned, ultrasound propagates by transmitting vibratory movement of the particles within a medium. Ultrasound wave and its propagation depend on the properties of the transmitting material. In this section, the factors which characterize the ultrasonic waves are described with their relationship to the host material.

3.2.1 Speed of Sound

The speed of sound is the velocity of propagation of an ultrasound wave. Elastic forces between the constituent particles have an essential role on the propagation of the sound wave so different materials transmit the ultrasound wave at different rates. While the wave propagates at 6100 m/s in a steel medium, its speed is reduced to 1500 m/s for a water medium. Equation (3.1) and Equation (3.2) show the relations of speed of sound with materials density and the Young's modulus for a solid and the Bulk modulus for a liquid [70]. Since these are temperature dependent, the speed of sound is also influenced by temperature changes.

$$c_{solid} = \sqrt{\frac{E}{\rho}} \tag{3.1}$$

$$c_{liquid} = \sqrt{\frac{B}{\rho}} \tag{3.2}$$

The speed of sound is generally constant for a given material at any frequency, f, and wavelength, λ. However, if the material has a heterogeneous structure (*i.e.* crystalline materials in which the elastic properties usually differ in different crystal directions) and a small admixture of a foreign substance (*i.e.* gas pores in porcelain), the velocity of sound speed could change [67]. The relation is given below is valid for all wave types.

$$c = f\lambda \tag{3.3}$$

The frequency of the ultrasound wave is unaffected by the host medium, while the speed of the wave is specific to the material. A source produces ultrasonic waves of a given frequency and they are sent through a sample with a known thickness. The time for the ultrasonic waves to pass through this thickness is measured. This allows the speed of sound to be calculated from a simple time-of-flight equation.

3.2.2 Acoustic Impedance

Acoustic impedance or sound resistance of a medium, z, can be defined as the product of density and velocity of sound.

$$z = \rho c \tag{3.4}$$

The units for acoustic impedance are $kg\ m^{-2}\ s^{-1}\ 10^6$, also known as $MRayls$. Acoustic properties of some materials are given in Table 3.1. Materials with high sound resistance are called sonically hard, on the other hand, materials with low sound resistance called sonically soft. For instance, steel with 47 MRayls, is sonically harder than water with 1.5 MRayls [67].

3.2.3 Attenuation

As the wave passes through a material, the amplitude of a sound wave reduces and the sound weakens. This concept is named as attenuation which could be explained by a combination of true absorption and scattering.

Table 3.1: Acoustic properties of some materials (*at 1 atm and 0°C).

Medium	Density (kg/m^3)	Velocity(m/s)	Impedance ($kg\ m^{-2}\ s^{-1}$)
Air*	1.3	330	0.4 x10^3
Water	1 x10^3	1.5 x10^3	1.5 x10^6
Perspex	1.2 x10^3	2.7 x10^3	3.2 x10^6
PZT (Ceramic)	7.5 x10^3	3.8 x10^3	3 x10^7
Aluminium	2.7 x10^3	6.4 x10^3	1.7 x10^7
Steel (Stainless)	7.8 x10^3	6.1 x10^3	4.6 x10^7

Absorption occurs during the propagation of the ultrasound wave as part of the energy contained in the sound wave is converted to heat. Several processes can be responsible for this [71]. The absorption tends to increase with the frequency of the sound wave. The reason is that the particles within the material oscillate faster at higher frequencies, hence increasing resistive frictional forces and more energy converted into heat [66].

The other source of the attenuation is that ultrasound waves could be scattered as well during its propagation in the medium. Scattering arises due to the nature of materials such that they are not strictly homogenous, for example cast iron or alloyed materials. Additionally, they may have either foreign inclusions, gas pores or voids of which density and speed of sound could be vary. These influence the strength of the pressure wave and results in deflection of waves. The wavelength of the signal is important as the larger size of the void or inclusion relative to the ultrasonic wavelength, the greater the scattering of the sound signal. In the case of grain boundaries, the scattering of the ultrasonic signal is minimal up to a point that the grain size is greater than one hundredth of the ultrasonic wavelength. Of course, the scattering of the signal is total as the ultrasonic wavelength approaches the grain size.

These two losses set practical limitations to the testing of materials in slightly different ways. Absorption weakens the transmitted energy and the amplitudes of ultrasonic echoes. To cancel out this effect, the transmitter voltage and the gain can be amplified

or the lower absorption at lower frequency can be exploited. However, the scattering is not only reduces the amplitudes of the echoes but also produces numerous echoes with different transit times so echo of interest cannot be distinguished from the others [67]. The attenuation law of ultrasound in material is defined by,

$$A_l = A_o e^{-\alpha l} \tag{3.5}$$

where α, is an attenuation coefficient, A_o, is initial amplitude of a wave , A_l is the amplitude of a wave after it has passed through a thickness of material, l. If Equation (3.5) is rearranged and natural logs is taken,

$$\alpha l = ln\frac{A_o}{A_l} \tag{3.6}$$

Attenuation coefficient is expressed in terms of dimensionless number of *nepper*s per unit length, *i.e.* Np/m. However, for the practice in electrical measurement, attenuation is commonly expressed in terms of decibels per meter (dB/m) as defined in Equation (3.7). In this way, the attenuation in bearing steel was measured to be $\alpha = 1.5f^2$ dB/m by Dwyer-Joyce et al. [72].

$$\alpha l = 20lg\frac{A_o}{A_l} dB \tag{3.7}$$

3.3 Generating Ultrasound

Acoustic transducers, which convert one energy form to acoustical energy and vice versa, are utilized to generate and receive the sound waves. There are several types of acoustic transducers that use different techniques such as heat shock by suddenly heating the surface of the body [73, 74], optical methods and laser [75], electromagnetic methods [76, 77]. However, many of these methods produce weaker signals. Ultrasound induced by crystal oscillators, which are based on the piezoelectric effect, is therefore the most popular one [67]. Since ultrasonic transducers which utilize the piezoelectric effect will be used in this study, the other generating method will not be detailed here but the

more information regarding these methods can be found in references [67, 78].
The piezoelectric effect, which was discovered in 1880 by the Curie brothers, occurs in crystals having one or more polar axes or the absence of a centre of symmetry. If a plate is cut from such crystals, electrical charges are generated on its surface as the plate is deformed by external mechanical pressure. The reverse effect, in which the material deforms by being placed in an electrical field, was predicted by Lippmann in 1881. Thus, piezoelectric materials are used in many applications as the first piezoelectric effect provides the basis for measuring and the reverse effect for producing mechanical pressures and oscillations. These effects constitute the base of ultrasound receivers and transmitters for the non-destructive testing, e.g. ultrasonic transducers [79].

Various piezo materials are used for generating and receiving ultrasound. Today, piezoelectric ceramics such as lead zirconate titanete (PZT), lead titanete, lead metaniobate and barium sodium niobate are mostly in use for material testing. Piezoelectric monocrystals which are quartz (*i.e.* the oldest known piezo material), lithium sulphate, lithium niobate, lithium tantalite, zinc oxide and ionic acid are rarely used.

3.3.1 Ultrasonic Transducers for OFT

Several types of ultrasonic transducers are available and designed for specific areas, such as medical imaging and NDT. In this section the ultrasonic transducers used for OFT measurement are going to be classified. The other types ultrasonic transducers are such as angle probes to produce surface waves are beyond the scope of this investigation.

The tree diagram in Figure 3.4 shows types of ultrasonic transducers. A bare element comprises of a piezo material and electrodes. As mentioned above, piezo material can be varied; however lead zirconate titanete and lead titanate are used in most ultrasonic transducer due to their relative ease of manufacture [80]. Standard vacuum deposited electrodes are made from chrome/gold, chrome/silver, chrome, copper, aluminium etc. The piezo element can be produced in various types; round (disc), square, rectangular,

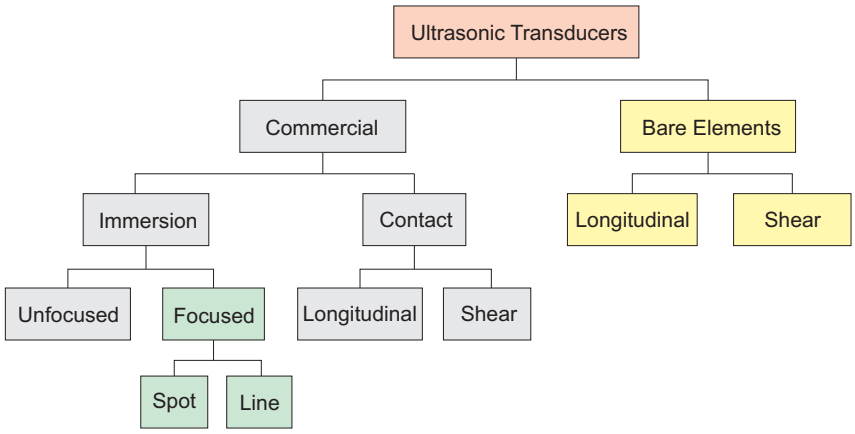

Figure 3.4: The diagram illustrating types of ultrasonic transducers for film measurements.

triangular. This piezoelectric element can also be assembled into a commercial transducer or used directly for emitting and receiving ultrasound waves. If this element is properly bonded to the test piece, it produces shear wave or longitudinal wave depending on its type. Figure 3.5 shows the comparative size of piezo discs which is extensively used in this study and commercial transducers.

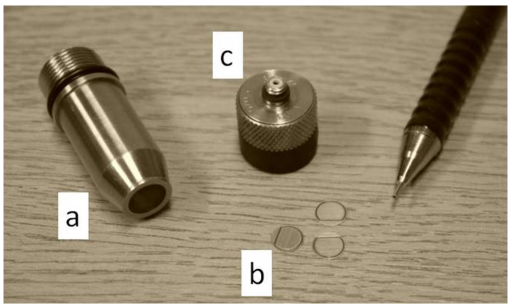

Figure 3.5: Photograph of ultrasonic transducers: a) immersion type transducer b) piezoelectric elements c) contact type transducer.

Commercial transducers consist of a piezo element, a backing material, a wear plate and possibly an electrical matching element. They are built into a rigid housing with an electrical connector. A simple cutaway view of a commercial transducer is shown in Figure 3.6. The piezo element will oscillate when it is exposed to a short duration voltage. Because of a constraint of the element, oscillation will die down rapidly and

so ultrasonic pulse is transmitted into the constraint medium. The piezo element is bonded to a protective wear plate. The main purpose of using this plate is to protect the piezo element against wear and corrosion. The wear plate material must be selected by considering its acoustic impedance which should be between that of the element and that of the material to which the transducer is coupled [81]. The best compromise is reached if its thickness is a quarter wavelength [82, 83] so for this reason, the wear plate is also known as quarter-wave plate. The back of the piezo element is filled with backing material which is most commonly a high attenuative and very dense material. By absorbing the energy that radiates from the back face of the piezo element, the backing material controls the vibration of the piezo element. Thus a short pulse is generated rather than a continuous wave train.

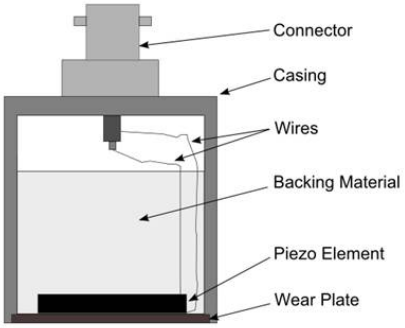

Figure 3.6: Design of typical commercial transducer.

Commercial transducers can be divided into two categories, *i.e.* contact and immersion, according to how they are coupled to the test specimen. Contact transducers are directly coupled onto the specimen surface by a couplant layer. This layer is necessary to avoid air gaps occurring between the transducer and test object because the trapped air disrupts the transmission of the sound pulse. Pastes and some liquids such as oil, glycerine etc. can be used as a couplants. Dry coupling made of soft plastic could also be used in some applications where the liquid couplant is not allowed or unsuitable. The advantage of liquid coupling is that the transducer can be move freely and this brings scanning and focussing features to the transducer.

The other type of commercial transducers is immersion transducers, which means the gap between transducer and the test object is filled with water. Thus its ultrasonic pulses firstly propagate through the water and later reach the test object. This provides uniform coupling and reduces variations in sensitivity. They are built in same way of the contact transducer and available in different configurations in terms of sound beam shape; unfocused or focused transducers (see Figure 3.7). Focusing is achieved by either the addition of a lens or by curving the piezo element itself. Ultrasound can be focused down to a line known as cylindrical focusing, or more commonly a point known as spherical focusing. Since ultrasound waves are concentrating into a very small area, focused transducers provide higher sensitivity and resolution.

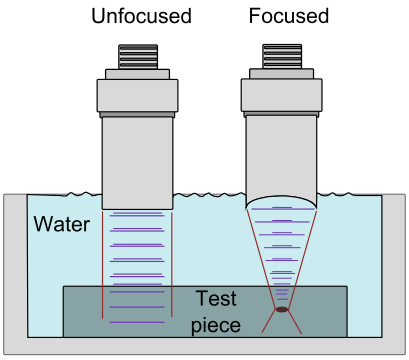

Figure 3.7: Examples of immersion transducers.

Figure 3.8a illustrates a typical waveform from an ultrasonic transducer. A spectrum, shown in Figure 3.8b, is created by performing a Fast Fourier Transform (FFT) on the waveform. The spectrum indicates that the waveform has energy over a range of frequencies. The frequency corresponding to the peak of the amplitude is called the centre frequency. The pulse emitted from the transducer contains intense energy around the centre frequency. In general non-destructive testing, the centre frequencies of transducers vary from 0.5 MHz to 50 MHz depending on the application. However, the information is extracted from the bandwidth region because the outside of this region contains very little energy and so little effect on the analysis. The bandwidth is defined as the useful frequency range over which amplitude of the pulse is greater than

half the maximum amplitude. This corresponds to a 6 dB reduction from the maximum amplitude.

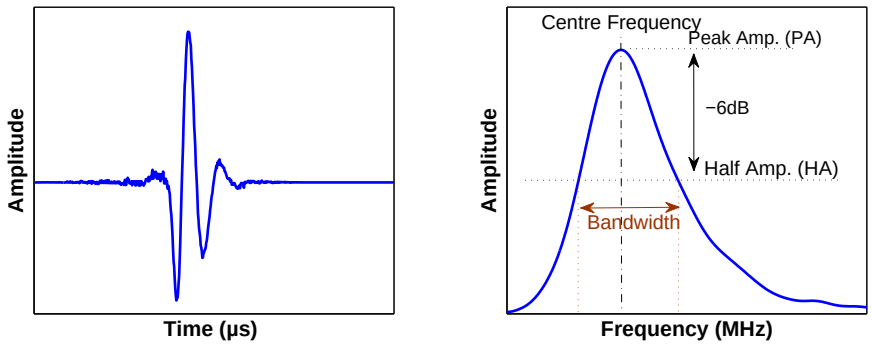

(a) (b)

Figure 3.8: Graphs showing (a) typical pulse in time domain, (b) FFT of the pulse

3.4 Ultrasonic Reflections and Measurement of Layer Thickness

In this section, the behaviour of an ultrasonic wave reflecting from layers will be explained along with a parameter known as reflection coefficient which quantifies the reflections. This section also introduces how the reflection coefficient can be linked to the thickness of the layer.

3.4.1 Reflection from a Perfectly Bonded Interface

When a beam of longitudinal ultrasonic waves strikes a perfectly bonded interface between two materials, some of the wave amplitude is transmitted and the remainder is reflected back. This situation is represented schematically in Figure 3.9. The proportion that is reflected is known as the reflection coefficient, R, is given by;

$$R_{12} = \frac{z_1 - z_2}{z_1 + z_2} \tag{3.8}$$

where, z, is the acoustic impedance and the subscripts denote the materials forming the interface.

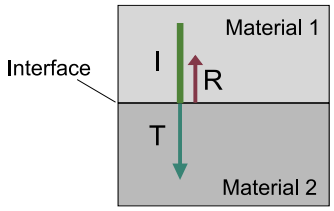

Figure 3.9: Ultrasonic reflection and transmission at a perfectly bonded interface (I: incident wave, T: transmitted wave and R: reflected wave).

If the materials either side of the interface have the same acoustic impedance, the reflection coefficient becomes zero, meaning that a sound wave will be fully transmitted through. If the materials either side of the interface have considerably different magnitudes of acoustic impedances, the reflection coefficient will be close to unity and almost the entire waves are reflected back. The acoustic impedance of air is around an order of magnitude lower than that for most solids. So the most of incident waves are reflected back as it come across with an air interface. This phenomenon constitutes a base for the common flaw detection device such that cracks and flaws including air are discovered using the echoes produced by reflected waves.

It is important to note that the reflection coefficient can be either positive or negative depending on acoustic impedances of the materials. As an example, water/steel interface has a reflection coefficient of -0.94 and steel/aluminium interface has a reflection coefficient of 0.46. A positive reflection coefficient indicates that there is no phase shift between the incident and reflected wave, conversely a negative reflection coefficient means a phase shift occurs between them.

3.4.2 Reflection from an Embedded Layer

For the durability of machine elements, the contact surfaces should be separated enough from each other as they are in operation. This separation is ensured by a liquid oil film

layer. If the film is too thin then surface contact can occur, leading to high friction, wear and seizure. The surfaces of the materials which are in relative motion to one another and oil film constitute a three-layered system, in other words, an embedded layer. This structure can be found in many machine elements such as the ball/oil film/raceway in rolling-element bearing, shaft/oil film/bush in journal bearing, or piston ring/oil film/liner in IC engine.

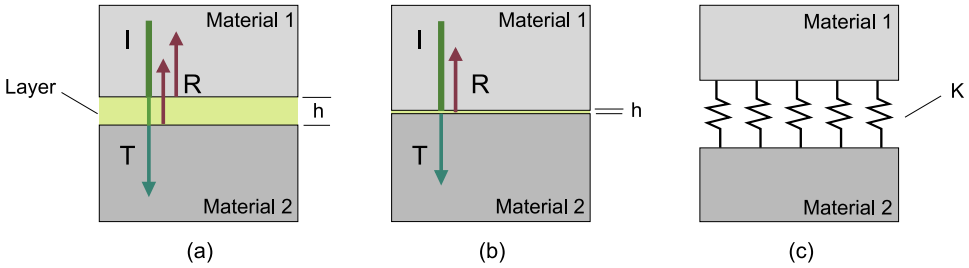

Figure 3.10: Schematic diagrams of a three-layered system: (a) thick film (b) thin film and (c) spring model.

Figure 3.10 shows an ultrasound wave incident on a typical lubricated contact which is a three-layered system. The incident waves are reflected back from the front and back face of the layer. If the layer is sufficiently thick (Figure 3.10a) , these reflections will be discrete in time. This means that if the speed of sound in the lubricant is known, by measuring the time-of-flight (ToF) between these reflections the thickness of the lubricant film can be calculated using Equation (3.9).

$$c = \frac{h}{t} \tag{3.9}$$

where, t, is the time between the reflections, c, is the speed of sound in the layer, and h is the thickness of the layer. Here the motion of the wave is assumed to be uniform and not subjected to any acceleration or deceleration in other words attenuation. This approach is used extensively in thickness gauging of metallic components.

3.4.3 Measurement of Thin Film Thickness

If the layer is very thin (Figure 3.10b) then the two reflections are close together and even overlap. It is noted that h$\rightarrow$ 0 since c $\neq$ 0, then Equation (3.9) becomes inappreciable and difficult to measure the discrete reflections. Typically, when lubricant film is less than 50 μm, the ToF approach becomes less accurate and is rarely applicable [84]. To extract the thickness information from the overlapped reflections in time domain, two alternative approaches which are continuum model and spring model are discussed in detail.

3.4.3.1 Continuum Model

Continuum models have been developed and used by many authors [85, 86, 87] in order to predict the reflection and transmission of ultrasound waves incident on the multi-layered system. The models are based on continuity of stress and strain at each boundary in the multi-layered system.

Pialucha and Cawley [88] used the continuum model approach to show that the resonant frequencies of an embedded layer are related to its thickness, h, and acoustic properties. This relationship is given in Equation (3.10) where, c, is the speed of sound in the lubricant layer, m, is the mode number of the resonant frequency and f_m is the resonant frequency in Hz of the mth mode.

$$h = \frac{cm}{2f_m} \tag{3.10}$$

By considering Equation (3.10), the thinner layer thickness gives the higher resonant frequency. This is also shown in Figure 3.11 illustrating a continuum model prediction of the reflection coefficient spectrum for 0.1, 1.0, 15, and 20 μm thickness mineral oil layers between two steel half-spaces. It can be seen from the figure that the reflection coefficient spectrum contains sharp minima at the resonant frequencies. Therefore the upper operating frequency becomes critical for this approach. As an example, if a lubricant layer in a journal bearing is below 10 μm, the resonant frequency will be above

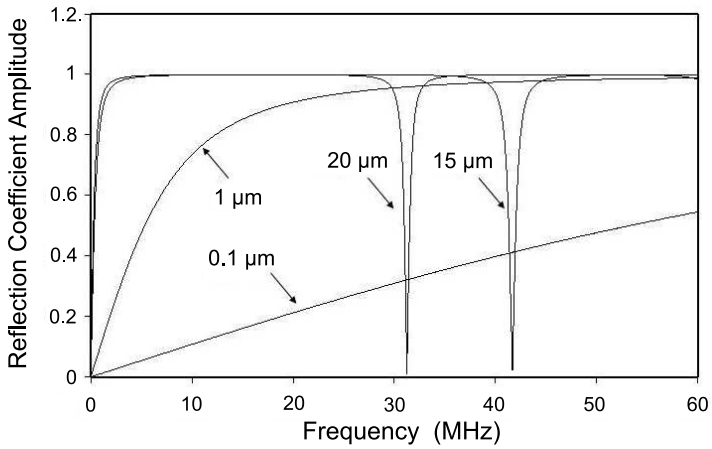

Figure 3.11: Continuum model predictions for the reflection coefficient from a layer of mineral oil, between steel half spaces [80]

the measurable range limitation because in practice, frequency is limited to below 40-60 MHz by the attenuation of the ultrasonic pulse in the bearing materials [84].

3.4.3.2 Spring Model

When the interfaces on either side of the layer are in very close proximity such as if the layer is very thin with respect to the ultrasonic wavelength, the discrete reflections from these interfaces are close together and the layer acts as a single interface. This situation can be modelled by using a quasi-static spring model (see Figure 3.10c). Tattersal [89] demonstrated that the reflection coefficient for a thin layer is defined by,

$$R = \frac{(z_1 - z_2) + i\omega/K(z_1 z_2)}{(z_1 + z_2) + i\omega/K(z_1 z_2)} \tag{3.11}$$

where ω is the angular frequency of the ultrasonic wave ($2\pi f$) and K is the stiffness of the interfacial layer. In the model, the reflection coefficient is highly dependent on the stiffness of the layer and it is assumed that mass and damping have no significant effect on the coefficient of reflection. It could be seen that if the layer is infinitely rigid, $K = \infty$, Equation (3.11) turns into Equation (3.8) which is the general expression of reflection coefficient for perfectly bonded interface. However, if the layer is infinitely slack, $K = 0$, it means that the materials are not connected anymore and the boundary

of the first material becomes a free surface. There is, therefore, no energy transmission through the second material and it means total reflection.

If Equation (3.11) is separated into real and imaginary parts by multiplying the complex conjugate of denominator, then Pythagoras's theorem is applied, after the rearrangement the layer stiffness can be described in terms of reflection coefficient modulus, $|R|$.

$$K = \omega z_1 z_2 \sqrt{\frac{1 - |R|^2}{|R|^2 (z_1 + z_2)^2 - (z_1 - z_2)^2}} \tag{3.12}$$

The relationship above allows layer stiffness to be determined from a reflection coefficient of an ultrasound wave sent through the layer. In the past, this relationship has been used for determining the stiffness of dry contacts [90, 91, 92] or partially lubricated contacts [93]. In both cases, the interface between two rough surfaces, composed of regions of asperity contact and air gaps (*i.e.* dry case) or oil (*i.e.* lubricated case), acts like a layer of reduced stiffness. The stiffness of the interface defined by the pressure required to cause unit approach of surfaces mean lines is given by,

$$K = -\frac{dp}{du} \tag{3.13}$$

where, p, is the applied nominal pressure and , u, is the approach of surfaces. In the same way, this approach can be applied for a liquid layer, *e.g.* oil film, hence the term of the approach of surfaces, u, could turn into an oil film thickness, h. The bulk modulus of a liquid layer, B, is defined by,

$$B = -\frac{dp}{dV/V} \tag{3.14}$$

where, V, is the volume of the layer. If the wavelength of the ultrasound is large compared to the layer thickness, then liquid layer is constrained and deforms only across its thickness [72]. Thus, the rate of volume change equals to the rate of layer thickness change as the fluid area, A, remains constant.

$$B = -\frac{dp}{d(Ah)/Ah} = -h\frac{dp}{dh} \tag{3.15}$$

Combining Equation (3.13) and Equation (3.15) gives,

$$K = \frac{B}{h} \tag{3.16}$$

The speed of sound in homogeneous liquids, already given in Equation (3.2), is independent of frequency. This equation is also called the Laplace equation or the Newton-Laplace equation [94]. The stiffness of a fluid layer, K, (Equation (3.16)), can be rewritten by substituting the Laplace equation.

$$K = \frac{\rho c^2}{h} \tag{3.17}$$

where, h, is the liquid layer thickness, c, is the speed of sound in a liquid layer and ρ is density of liquid. Layer thickness can be obtained by combining Equation (3.12) and Equation (3.17). This gives,

$$h = \frac{\rho c^2}{\omega z_1 z_2}\sqrt{\frac{|R|^2(z_1+z_2)^2-(z_1-z_2)^2}{1-|R|^2}} \tag{3.18}$$

where R is the reflection coefficient. Equation (3.18) gives the layer thickness in terms of reflection coefficient and acoustic properties of the oil and materials either side of the interface. This relationship is valid for the different materials on each side of the layer. From the equation above, Figure 3.12 has been plotted out for an aluminium-oil-steel layer showing reflection coefficient values against frequency. As seen, the range of reflection coefficient amplitude for the layer is limited by a value which is equal to that given by Equation (3.8) for a perfectly bonded interface. This is because the reflection coefficient can never have a value lower than that for the interface with no layer present (*i.e.* aluminium-steel). If the materials are identical where is z_1 equal to z_2, then Equation (3.18) reduces to;

$$h = \frac{2\rho c^2}{\omega z}\sqrt{\frac{|R|^2}{1-|R|^2}} \tag{3.19}$$

Figure 3.13 has been plotted for the case of an oil between steel plates (*i.e.* steel-oil-steel). Here the range of reflection coefficient amplitude is bigger than that of given in Figure 3.12 and there is not a minimum reflection coefficient value due to having

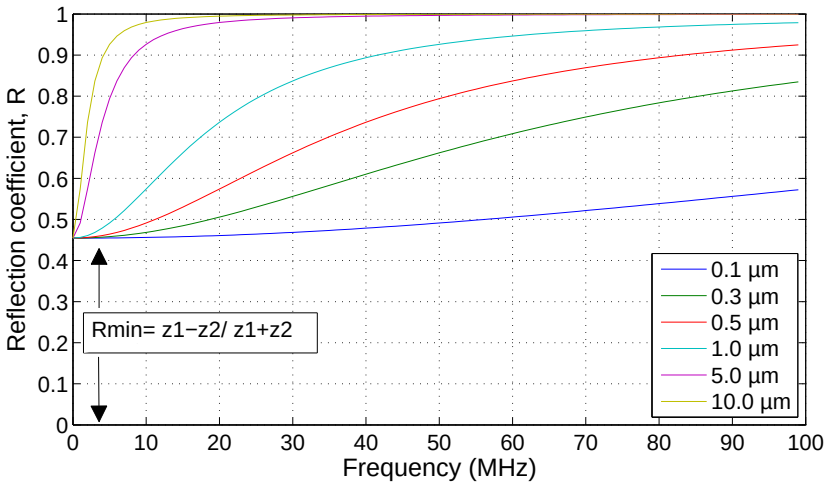

Figure 3.12: Reflection coefficients calculated over a range of frequency and oil film thicknesses (Aluminium-Oil-Steel).

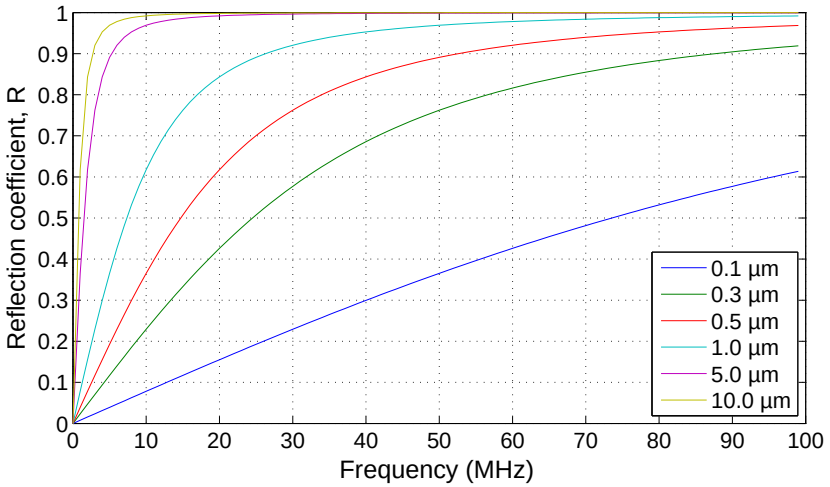

Figure 3.13: Reflection coefficients calculated over a range of frequency and oil film thicknesses (Steel-Oil-Steel).

similar materials. It can be seen that at a constant frequency, the reflection coefficient decreases as the film thickness decreases. This is expected that the layer becomes stiffer and more of the wave is transmitted.

3.4.4 Calibration of Spring Model Approach

The spring model approach has been used previously to quantify lubricant film in machine elements such as thrust pad bearings [95], hydrodynamic journal bearings [96] and a rolling element bearing [72]. The technique is inherently based on physical principles of the system; quantification of thickness is derived by direct physical correlation. The experiments to determine the validity of the ultrasonic film thickness measurement have been carried out in several studies using digital piezoelectric translator (DPT) technique [97], liquid wedge, journal geometry [84, 98] and glass plate test [99]. Overall an excellent agreement was found for the quasi-static spring model technique.

Two sheets of float glass separated by a shim of known thickness at one end were immersed in a water tank as illustrated schematically in Figure 3.14. The focussing type immersion transducer was mounted above the liquid wedge on a computer controlled x-y positioning frame. Film thickness values measured by ultrasonic method were compared with predictions of the thickness determined from the geometry of the liquid wedge. The results are given in Figure 3.15 where the data below 25 μm correspond to measurements performed using the spring model, while the data above 25 μm have been determined from the measurement of film resonances. As seen, there is good agreement for the spring model data.

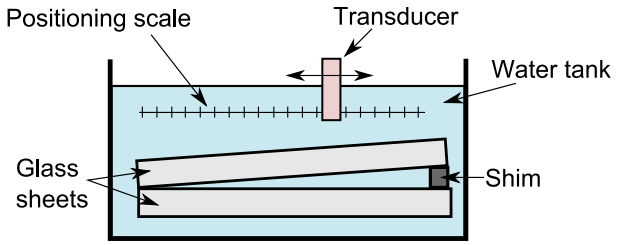

Figure 3.14: Schematic of the liquid wedge test set-up, reproduced from [84]

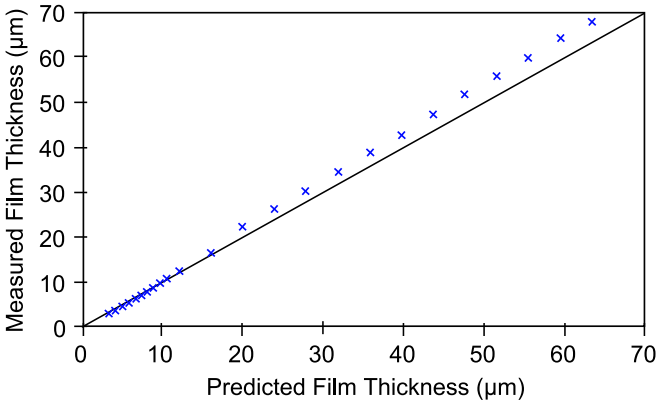

Figure 3.15: The results from the liquid wedge experiment, reproduced from [84]

The DPT test set-up illustrated in Figure 3.16 was used to generate a thin lubricant film between two steel discs. An immersion transducer was fixed onto a 3-axis automated linear scanning system. The DPT fixed to a base plate via rigid clamping system was controllable to 2 nm. Ultrasonic reflections were recorded against DPT displacement and the spring model was used to calculate the thin film thicknesses (0.5 - 1.3 μm). Excellent agreement was obtained and so in this way the spring-layer model was validated.

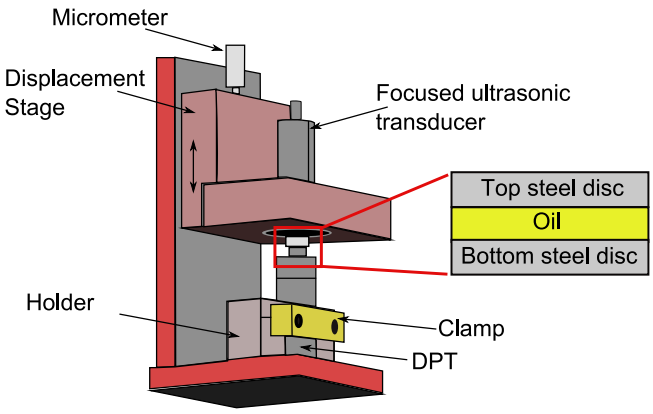

Figure 3.16: Schematic diagram of the DPT test set-up, reproduced from [97]

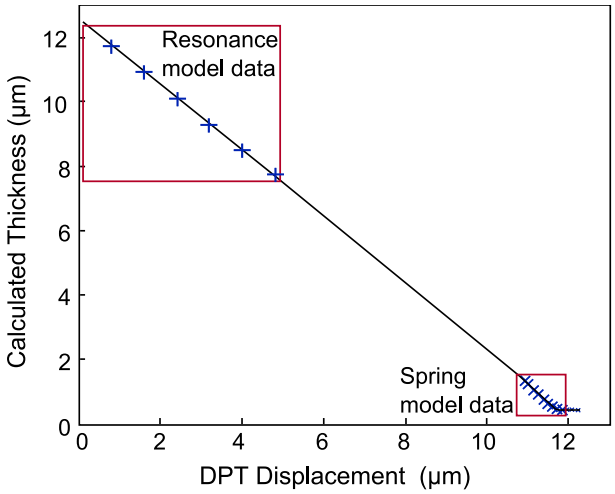

Figure 3.17: Film thickness measured by the spring-layer model and the resonance-layer model compared with the DPT displacement, reproduced from [97]

3.5 Conclusion

Ultrasound is widely used in industry during manufacturing and inspection processes due to its non-invasive, portable characteristic. The principles of ultrasound and acoustic properties of the materials have been defined in this chapter. The generation of the ultrasound and the piezo electric effect have been explained. Bare elements exclusively used in this work and the commercial type transducers, contact and immersion, have been detailed. Typical transducer waveform and its FFT spectrum illustrating bandwidth, centre frequency have been introduced.

The behaviour of the waves at interfaces and layers have been detailed. The thickness measurement of thin layer which is seen in most of the tribological applications has been explained by three ultrasonic approaches: the time of flight, continuum model and the spring interface model. Amongst them, the spring model has been detailed and applied to two different layered systems which are formed between dissimilar and similar materials. In the final section some experimental methods used for the validation of spring model have been presented.

4

Generic Method

This chapter shows how oil film thickness is measured ultrasonically. Ultrasound equipment for the thickness measurement, such as transducer, ultrasonic pulser-receiver, is introduced. The lubricant speed of sound value, which is essential for film thickness measurement, and its relation with temperature are analyzed. Generic reflection coefficient measurement and signal processing are explained in detail with a basic perspex sandwich test (*i.e.* perspex-oil-perspex layer) as an example.

4.1 Ultrasonic Apparatus

The ultrasonic measurement equipment consists of an Ultrasonic Pulser-Receiver (UPR), an ultrasonic transducer, a digitizer and a dedicated computer. The photo and schematic view of the equipment set-up are illustrated in Figure 4.1 and Figure 4.2 respectively.

4.1.1 Transducer

Ultrasonic transducers used for film thickness measurement have been detailed in Chapter 3. Depending on the application, the type of transducer should be selected. If an oil film being measured is in a concentrated contact (e.g. oil film in a ball bearing), a focusing type transducer could be chosen. If there is a space restriction for liquid

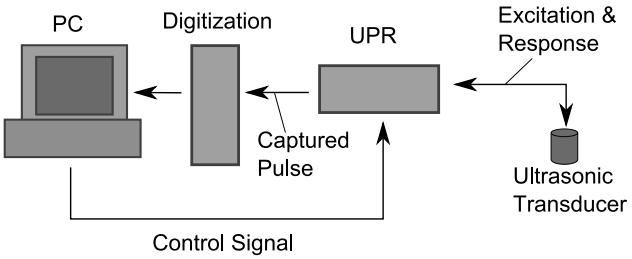

Figure 4.1: Schematic diagram showing a configuration of ultrasonic apparatus.

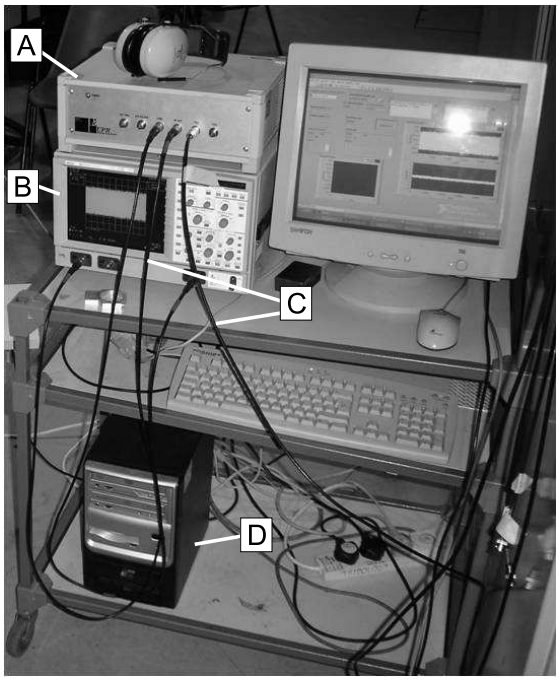

Figure 4.2: Photos showing the ultrasonic measurement kits. (A: ultrasonic pulser receiver, B: oscilloscope (digitizer), C: connections and D: computer.

coupling or enough contact area, bare elements or contact type commercial transducers can be used. The other criterion is the selection of central frequency of the transducer. The optimum choice should be made considering the expected oil thickness (see Equation 3.18 and Figure 3.12) and also the attenuation rate of ultrasound in the specimen especially when the use of high frequency transducer is needed.

The transducer is coupled to the test specimen using liquid coupling layer for commercial type transducers or coupled permanently for bare piezo elements using adhesive. The

coupling surface must be free from pits and irregularities. Adhesive should be chosen by considering the acoustic characteristic of the bonding line that would affect the signal-noise ratio.

4.1.2 Ultrasonic Pulser-Receiver

UPR allows various characteristics of the excitation signal (*i.e.* frequency, voltage, pulsing rate) to be tuned in order to obtain the optimum response of the transducer. Voltage is the amplitude of the excitation signal in volts and a value of the voltage can be adjusted depending on the size of the piezoelectric element and damping level of the probe. Frequency is the reciprocal of the period of the excitation pulse and the excitation frequency is usually set to match the centre frequency of the transducer. Excitation signals are sent to the transducer at a specified rate, called repetition rate, meaning that how many pulses are sent through the medium in a second, for instance 5000 pulses per second. This is an important parameter for high speed applications where the high rate of data capturing is necessary.

The transducer operates in a pulse-echo mode. This means that the reflected pulses from the inspection area are also received by the transducer. As well as providing voltage signals for transducer, the other function of UPR is to amplify the voltage of reflected pulses.

UPR used in this system was NDT Solutions UPR which had a complex circuitry in order to provide an appropriate rapid switching between the high voltage pulsing circuit and low voltage receiving circuit. The UPR was controlled by computer software called 'WinUPR' which allowed to the excitation signal to be tuned before digitization.

4.1.3 Digitizer

The digitizer unit used was a LeCroy LT342 oscilloscope which allowed signal voltages to be viewed additionally to be digitized before downloading the data into the PC for

signal processing. The sampling rate of the scope was up to 500 Msamples/second. It had 250 kB internal memory capacity. The oscilloscope was able to perform mathematical averaging on the captured signal up to 1000 averages. This sort of oscilloscope had a capability to capture small portion of incoming wave form repeatedly. This was known as 'segmenting' which provided extremely quick measurement. Thus the variation of the signal could be stored, digitized and then sent to the computer. The rate for downloading the data to the PC was up to 200k measurements/second.

4.1.4 Computer

Two experimental setups were used in the experiments. In one of them, as shown in Figure 4.2, the digitizer and UPR were involved in the measurement system as individual units. Hence, a personal computer was used to control the ultrasonic settings on the UPR, to acquire the data from the oscilloscopes and to process the data. In the other experimental setup, these units were PCI cards and they were embedded into an industrial computer (*i.e.* detailed in Chapter 6). Reducing incompatibility between the units and increasing mobility of the measurement system were the main advantages of this setup.

4.1.4.1 Software

In both computers, the commercial software package LabVIEW® (by National Instruments Inc.) was used for all data acquisition and signal processing routines. LabVIEW® is a graphical programming environment and the LabVIEW® program is called 'VI' which stands for Virtual Instrument. LabVIEW® is very handy program that allows the user to build customised routines and they can be easily recalled as a sub Vi into the other Vis. Additionally, the program already contains built-in-signal processing routines such as FFT, cross correlation etc. A screen print of a typical LabVIEW® program written for ultrasonic measurement of oil film thickness is shown in Figure 4.3. This program enables to control the settings of the ultrasonic signals, manipulate reflection data from the inspection area and instantly display the film thickness results.

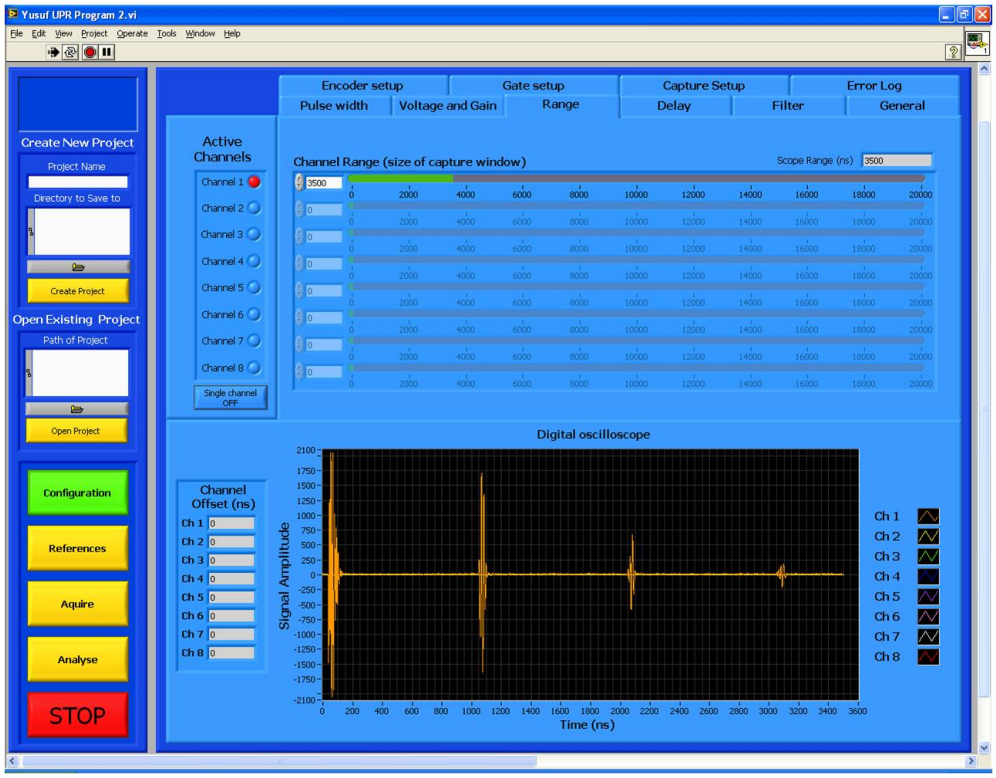

Figure 4.3: A screen print of a typical LabVIEW® program for ultrasonic measurement of film thickness.

4.2 Speed of Sound of Lubricants

According to Equation 3.18, it is necessary to know the speed of sound in the lubricant in order to determine the oil film thickness formed between the materials. In general the speed of sound values for lubricant oils are in the range 1250-1500 m/s. A relatively simple test was carried out to measure the speed of sound in the lubricant oil. As schematically illustrated in Figure 4.4, a chamber of known dimension was used and a piezo element was glued on the outside chamber wall. The chamber was filled with testing oil. When the piezoelectric element was activated, the ultrasonic waves were generated. Therefore, ultrasonic reflections from the inside walls of the chamber, which were opposed to each other, were recorded. The time for passing through the oil depth,

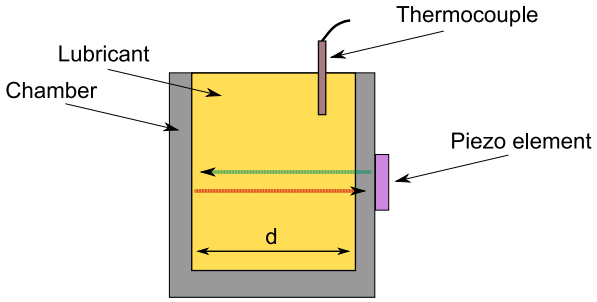

Figure 4.4: Schematic view of measurement device used for speed of sound measurement.

d, was measured by using these reflections. Once the time obtained, the speed of sound calculated from simple time-of-flight calculation.

It should be noted that acoustic properties of the oil vary with temperature due to changing its elastic forces. Thus, the measurement of the speed of sound over a range of temperatures is essential to have an accurate evaluation of film thickness. For this reason, the measurement device was placed into the temperature controlled oven and the speed of sound measurements were performed in a temperature range from 25°C to 120°C. The reflections were recorded for each 5°C increment in oil temperature. A thermocouple was placed into the chamber so the exact temperature of oil was used

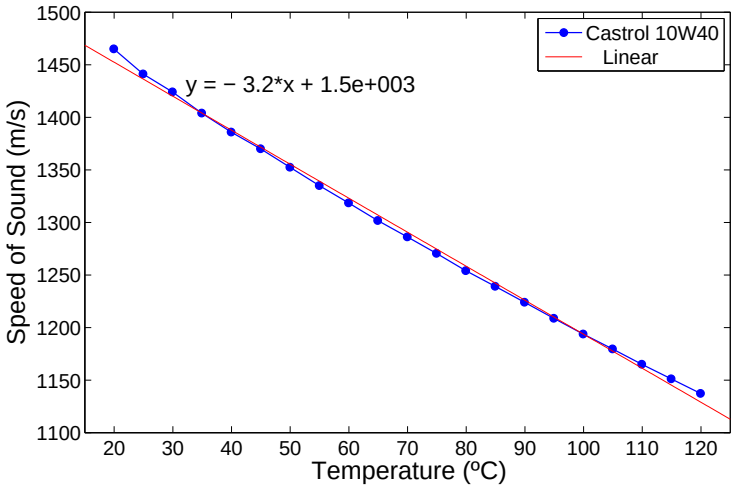

Figure 4.5: Variation of lubricant speed of sound values with temperature

for recording. Figure 4.5 shows the measurement results for the lubricant sample of 10W40 from Castrol. It can be seen that there is a linear inverse relationship between the lubricant's speed of sound and temperature.

4.3 Implementing Ultrasonic Measurement

In this section the generic measurement method will be explained with an example application to a three layered system. The layer was formed using a perspex cylinder, oil and a perspex plate (see Figure 4.6). The perspex cylinder was mounted on the sensor using a screw adapter. Oil was dropped between the perspex plate and the cylinder.

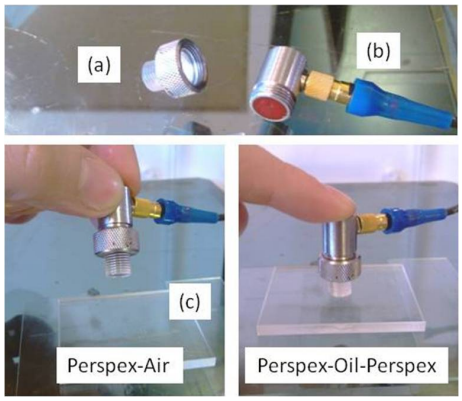

Figure 4.6: Perspex layered test materials: (a) perspex cylinder (b) ultrasonic sensor (c) pespex plate

4.3.1 Selection of Pulse of Interest

When the ultrasonic transducer was excited, it generated the ultrasonic wave through the perspex layered system. The acoustic response from the perspex system is given in Figure 4.7a. The pulses marked with 'A' and 'B' were the first reflections from the multiple interfaces. The pulse 'A' was reflected from the perspex cylinder-oil-perspex plate and the reflection pulse 'B' was from the bottom surface of the perspex plate. These are shown schematically in Figure 4.7b. The rest were the echoes of these pulses occurred inside the layered system. For instance, the pulse 'C' was the second reflection

of the pulse 'B' from the bottom surface while the pulses marked with 'D' and 'E' were the second echoes of 'A' and 'B' respectively occurred inside the perspex cylinder. Thus, in order to measure the oil film thickness between the perspex mediums, the first reflection, pulse 'A' was isolated and used. In this study, this pulse was also called 'pulse of interest'.

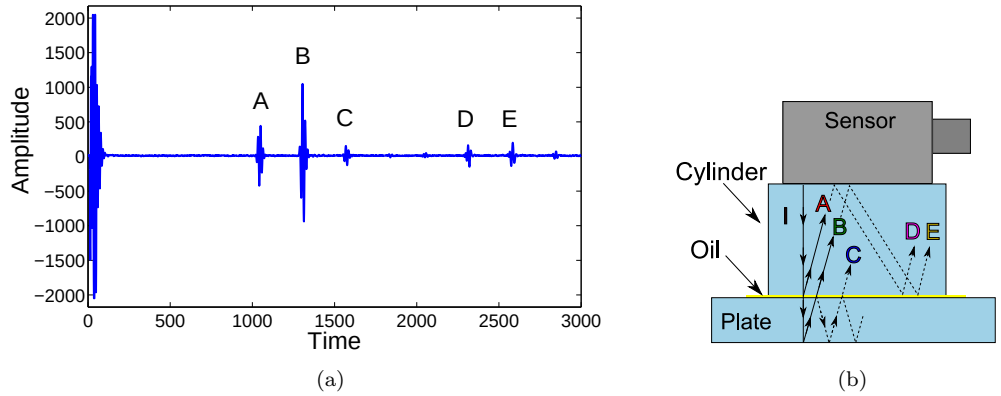

(a) (b)

Figure 4.7: Reflections from the perspex-oil-perspex assembly; (a) in time domain (b) in schematic view.

4.3.2 Reference Signal

As described in previous chapter, the reflection coefficient is necessary in order to calculate film thickness. The proportion of the incident wave amplitude that is reflected is expressed by the reflection coefficient using,

$$R = \frac{A_r}{A_i} \tag{4.1}$$

where A_i is the incident wave amplitude and A_r is the reflected wave amplitude. However it is difficult to measure the incident pulse. Hence in practice it is convenient to record a reflection from an interface formed by materials with a large impedance mismatch.

Air has very low acoustic impedance compared to Perspex and the common engineering materials such as steel, aluminium, brass etc. So if the matching material is air, most of the incident wave is reflected back due to a high acoustic mismatch between the materials (see Equation 3.8). In other words, this means that the pulse reflected from the perspex-air interface almost equals to the incident pulse. Then Figure 4.8, illustrating the reflections from the perspex-air and the perspex-oil-perspex layer, could be thought of as a comparison between incident and reflected pulses. It can be seen from the figure that there is a reduction in amplitude. This is purely because of the partially transmission of the ultrasound wave through the oil layer. Thus, the pulse reflected from the material-air interface is called as a 'reference signal' during this study.

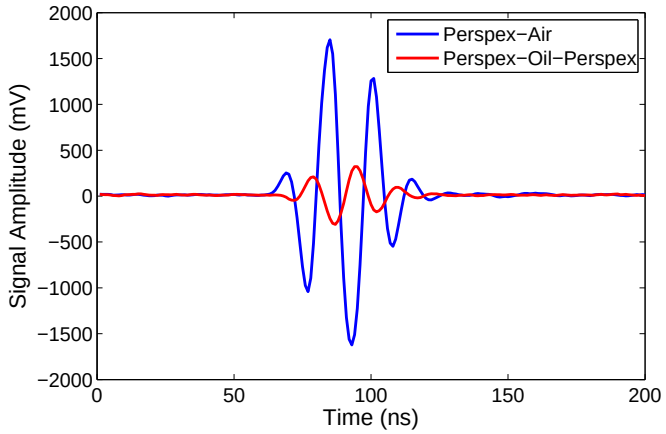

Figure 4.8: Comparisons from perspex-air and perspex-oil-perspex

4.3.3 Generic Signal Processing

Signal processing software programs were written in LabVIEW®. Two slightly different data processing routines, on-line and post processing, were followed according to the experimental setup. However, the main data processing routines for calculating a film thickness remained the same. Once the reference and measurement signal were captured and digitized, several steps depicted schematically in Figure 4.9 needed to be taken.

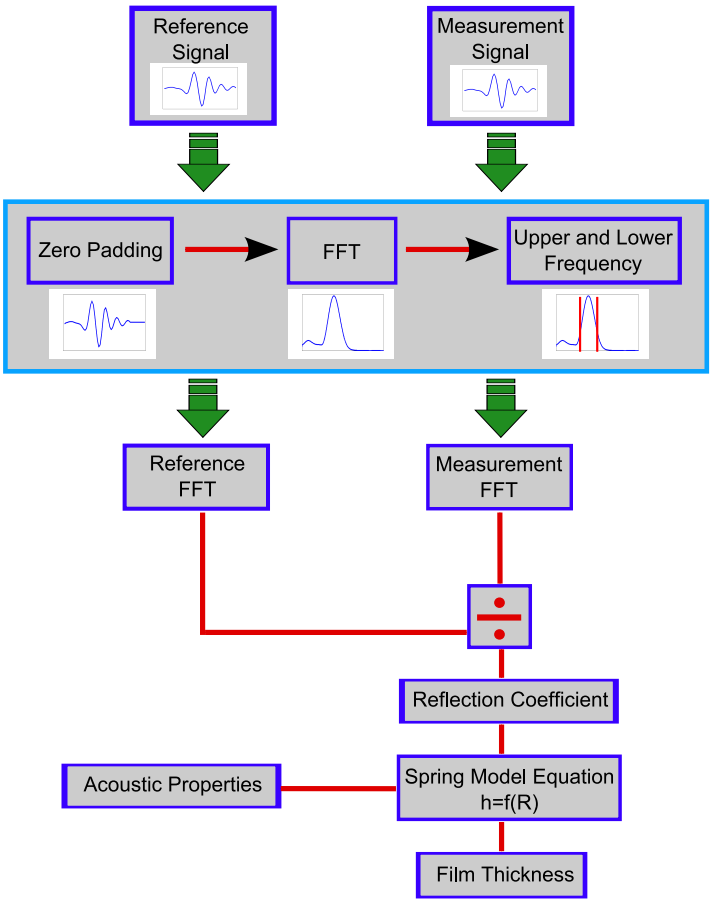

Figure 4.9: Schematic diagram of generic data processing

Since every frequency of the reflected signals was important, firstly a fast Fourier transform (FFT) was performed on both reference and measurement signal. The FFT provided signal amplitude variation in the frequency domain. Before taking FFT, zero padding was also applied on both signals by adding a string of zeros to the end of the input signal. This modification gave sufficient resolution in the resulting spectra produced by a Fourier transform [80]. The reflection coefficient, which was the proportion of the incident wave amplitude that was reflected, was obtained by dividing the FFT of measurement signal by the FFT of reference signal. Once the reflection coefficient was produced and acoustic properties of materials were known, film thickness value was able to be calculated using the spring model Equation 3.18.

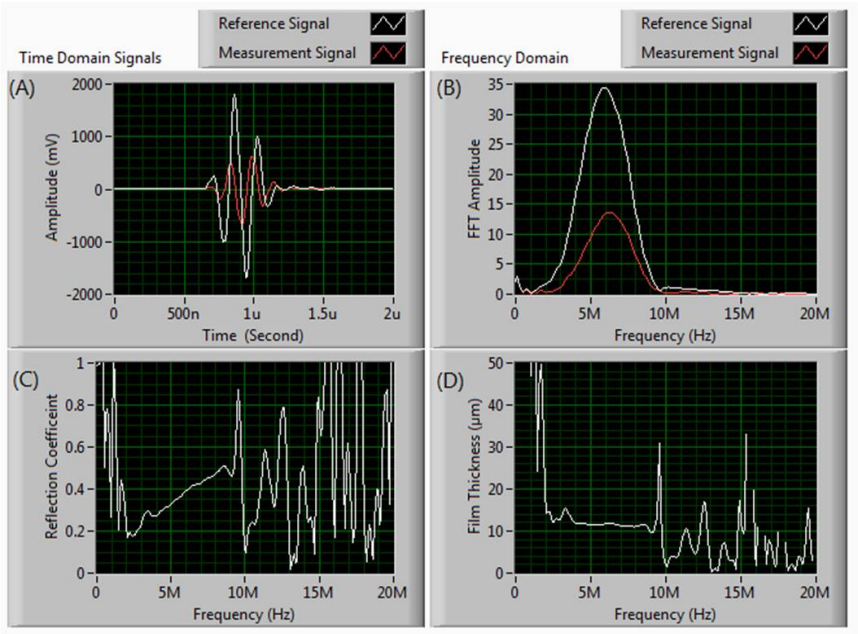

Figure 4.10: Graphical outputs obtained from the Labview sotfware during the signal processing.

Figure 4.10 shows the graphical outputs obtained from the Labview sotfware during the signal processing of ultrasonic pulses given in Figure 4.8. The top left figure shows the reference and measurement signal in time domain. After FFT, the reflection coefficient is obtained from the frequency domain signals (*i.e.* given at the top right) dividing the measurement signal by the reference signal. Calculated film thicknesses are given in the film thickness-frequency graph at the bottom left. As seen, oil film thickness is a flat line in the bandwidth region and it is the independent of frequency. The regions of spectrum outside the bandwidth contain very little energy and the measurement results in these regions effectively depend only on the noise in the signal. In the experiments, to avoid from incorrect measurement, film thickness values in the useful region are only used. This can be seen in the FFT block in Figure 4.9 in which the spectrum inside the bandwidth region is selected by choosing upper and lower frequency on the spectrum.

4.4 Conclusion

This chapter introduced ultrasonic apparatus used for film thickness measurement. Generic measurement methodology containing the pulse of interest and reference pulse was described. The generic signal processing routines to obtain the film thickness value from the ultrasonic reflections were illustrated. These routines written in a LabVIEW® software program will be used as a sub-program for the following chapters.

5

Ultrasonic Imaging of the Piston Ring-Liner Contact

This chapter introduces an initial attempt to apply the ultrasonic system on a motored engine. A contact transducer was located in the water jacket so that ultrasonic pulses propagated through the cylinder and reflected from the inside wall. While the piston rings were passing over the sensing area, reflected pulses were captured using a high speed pulsing system developed along with triggering system. These pulses were processed and the reflection coefficients were successfully generated for the ring pack of the piston. Minimum reflection coefficients of the ring pack were recorded for several engine speeds. However, no attempt was made to translate these reflection coefficients into quantitative film thicknesses because the spatial resolution of the sensor was too low.

5.1 Test Apparatus

5.1.1 The Motored Engine

A Perkins Engine 1100 Series with a bore of 105 mm and a stroke of 127 mm was modified to be driven by an external electric motor (see Figure 5.1). The cast iron engine

block had a vertical in-line configuration with 4 cylinders. Total displacement of the engine was 4.4 litres. The engine did not have a separate cylinder liner insert but rather a homogeneous cylinder wall separating the inside of the engine from the water jacket. The nominal piston diameter was 104.2 mm in the region of the piston ring pack. The skirt diameter was 104.8 mm. The nominal piston skirt clearance was approximately 200 μm. The piston had three rings; top compression ring, second compression ring and oil control ring.

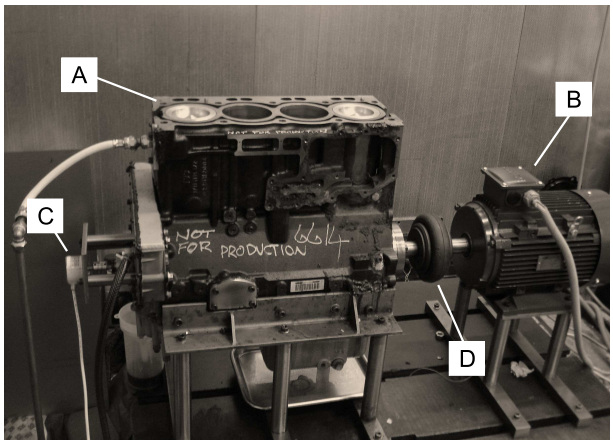

Figure 5.1: A photo of motored engine used in the tests. A: engine, B: electric motor, C: shaft encoder, D: coupling

Table 5.1: Specifications of test engine.

$Number of cylinders$	4 in-line
Bore and *Stroke*	105 mm x 127 mm
Displacement	4.4 litres
Cycle	4 stroke
Rotation	Anti-clockwise

A 7.5 kW three phase motor turning the crankshaft was controlled by an inverter. The inverter provided accurate speed control with its 'soft start and stop' function. A flexible tyre coupling was used to connect the motor shaft and the gear box of the engine for the purpose of transmitting power. The use of this coupling brings some benefits. Firstly,

this sort of coupling permitted some radial, axial and angular misalignment. Secondly, it reduces the heat transfer from the engine and the motor so this would also help to prevent thermal overload of the electrical motor during testing. The engine and motor were mounted on six and four upright posts respectively. These posts were attached to cross-members, which were bolted to a steel test bed.

The engine's head and valve train were removed and the lubricant system was modified to lubricate just the cylinder block. The cylinder wall was splash lubricated. There were a number of access points on the engine to mount the transducer on the outside surface of the cylinder walls. One of them was the rear face of cylinder 4 (the cylinder nearest to shaft encoder). The others were the thrust face and the front face of cylinder 1 (the cylinder nearest to the motor). The surfaces of the cylinder walls at these access points were ground to provide flat surface for the transducer.

5.1.2 Instrumentation of the Engine

A 5 MHz straight beam contact transducer was used together with the ultrasonic equipment which included NDT Solutions UPR, oscilloscope and dedicated PC detailed in Chapter 4. As shown in Figure 5.2, the 5 MHz contact transducer with a 0.25 in of element diameter was coupled to the wet-side of the cylinder wall using a magnetic clamp. Liquid coupling was applied to the interface between the transducer and outside surface of the cylinder wall to prevent air from entering the interface.

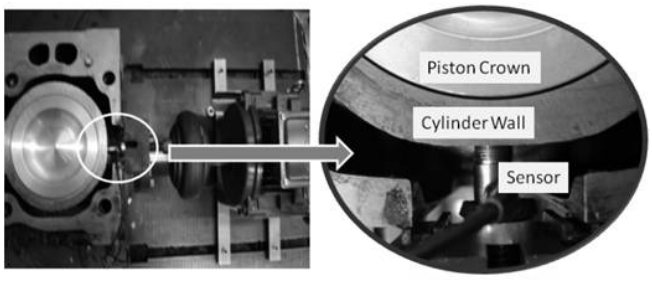

Figure 5.2: A top view of the cylinder showing the transducer coupling on the cylinder wall.

An incremental shaft encoder made by Hengstler was mounted to the crankshaft. This shaft encoder provided two output channels in order to gain a feedback of the engine speed and position of the piston. The first channel produced 3000 pulses per revolution. The second channel of the encoder provided a voltage spike occurring for every complete rotation of the crankshaft. Hence, the piston position at any specific point upon the cylinder bore (the cylinder number 1, nearest the motor) was able to be obtained by making an angle adjustment on the shaft encoder. This spike was called 'timing pulse' and it was very practical to create a trigger point for data capturing. This timing pulse was sent to a function generator, manufactured by Agilent, to acquire an external trigger source for UPR. Thermocouple, K type, was placed to the wet-side cylinder wall, close to the ultrasonic sensor. Temperature of the cylinder was monitored by a digital thermocouple reader and documented during the test.

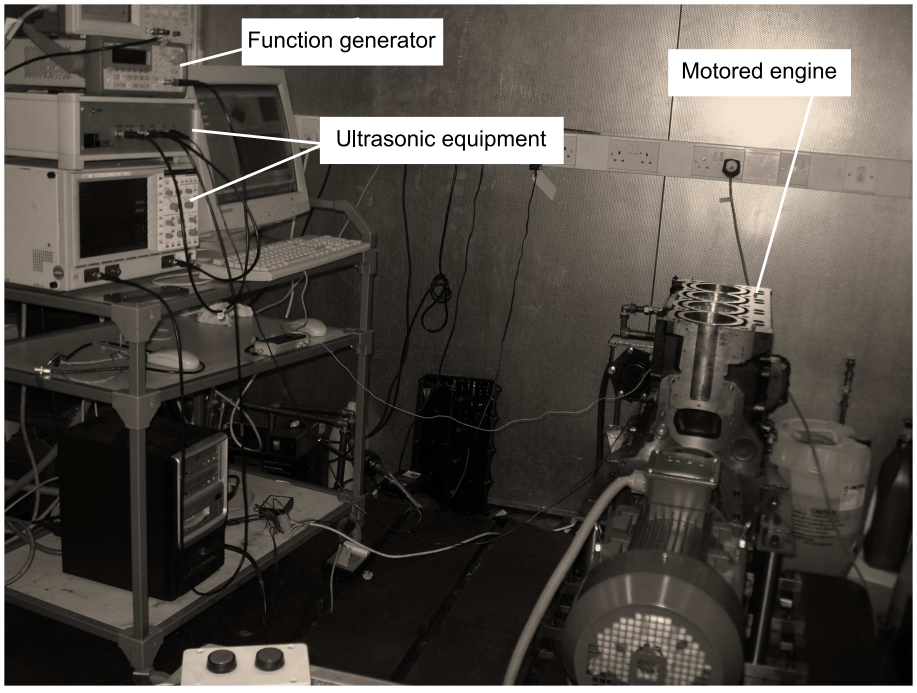

Figure 5.3: A view of the test cell

5.2 Reflections from Cylinder Wall

Figure 5.4 shows a waveform of the reflected signal as the transducer has been coupled to the outer cylinder wall. The first pulse 'a' is a combination of reflection from the outer cylinder wall and sensor initiation, since this pulse does not change with piston movement, it is a stable pulse. Pulse 'b' is reflected from the inner cylinder wall. This pulse changes as the piston rings pass over the sensor location. When no ring is present, the ultrasonic pulse will be completely reflected due to a high acoustic mismatch. Thus the signal reflected from cylinder wall-air interface was used as a reference signal. However when there is a ring present, some of the ultrasound is transmitted through the interface into the ring. The subsequent peaks are the resonances (i.e. second and third reflections) and are of no consequence for these measurements.

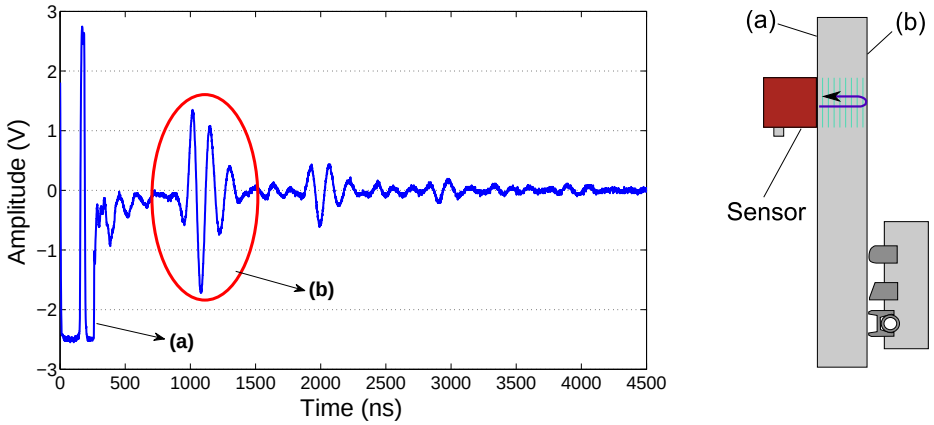

Figure 5.4: Time domain signal showing the reflections from the cylinder wall.

Figure 5.5 shows samples of a reference signal, which was recorded from the reference interface, and a reflected signal, which was captured when an oil film was formed between the piston ring and wall. If the FFT is applied to these samples, the frequency domain pulses, in Figure 5.6, are obtained. It is seen that the amplitude of the pulse is decreasing when oil formed in piston ring. This peak 'b' is isolated from the rest of the signal by oscilloscope and recorded repeatedly during the rings passage. The benefit of this isolation is that data storage requirement of the measurement becomes significantly less.

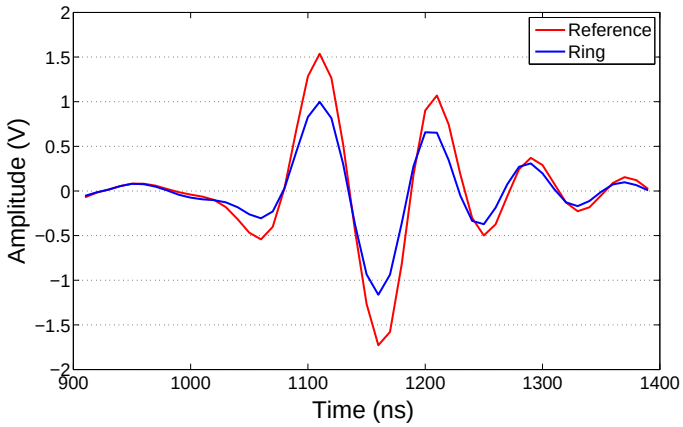

Figure 5.5: Time domain signals showing the variation of peak 'b' as the piston ring is passing over the sensing area

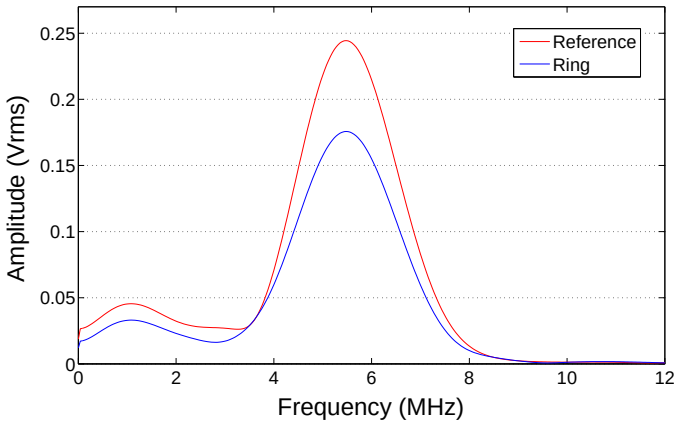

Figure 5.6: Frequency domain signals showing the variation of peak 'b' as oil film is formed between piston ring and cylinder wall

5.3 Test Procedure

The ultrasonic reflection measurements start with a timing pulse from the shaft encoder (see Figure 5.7). The timing of this pulse can be adjusted according to the desired piston position inside the cylinder (*e.g.* TDC), which is called the triggering point. When the piston is on the triggering point, the shaft encoder sends the timing pulse to the function generator, which generates a defined number of square waves (*e.g.* 370 square waves). These square waves are used as an external triggering source for the

UPR, which produces and sends an equivalent number of short duration high voltage signals to the transducer coupled to the wet-side of the cylinder wall. A piezo element inside the transducer is excited by these voltage signals and generates ultrasound waves which propagate through the cylinder wall. The transducer operates in a pulse-echo mode, therefore, it captures the reflections from the cylinder as the piston rings pass over the transducer area. These reflected signals are amplified and sent through the oscilloscope for digitization. Then a digitized pulse sequence constructed by successive pulses is downloaded to the dedicated computer for on-line signal processing. This cycle is repeated for the next timing pulse generated by the shaft encoder.

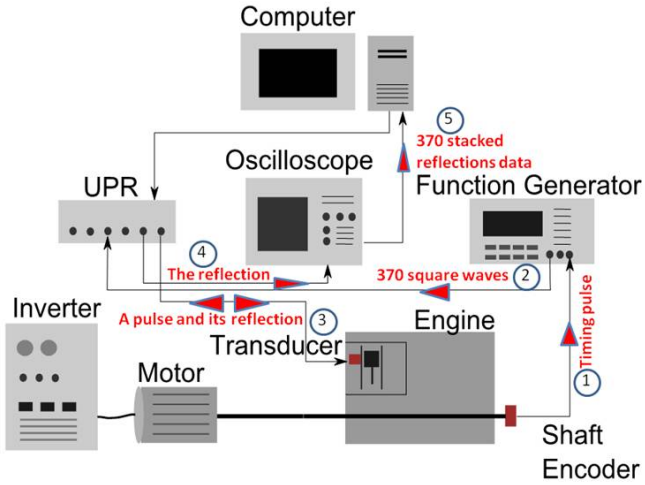

Figure 5.7: Schematic diagram of the test equipments and their connections

5.4 Signal Processing

In this work, online signal processing has been performed using the commercial software package LabVIEW® (by National Instruments). As mentioned in the previous section 5.3 , the high speed pulsing and triggering system allows continually passing pulses of ultrasound through the cylinder wall. The transducer captures the reflections as the rings travel across the sensing area. The pulse of interest ('b' in Figure 5.4) is isolated from the rest of the signal and selected by the oscilloscope for each of the reflected

signals. These selected segments (*i.e.* pulses of interest) constitute a pulse sequence and they are stored in the oscilloscope memory until the last reflection segment is added to a pulse sequence.

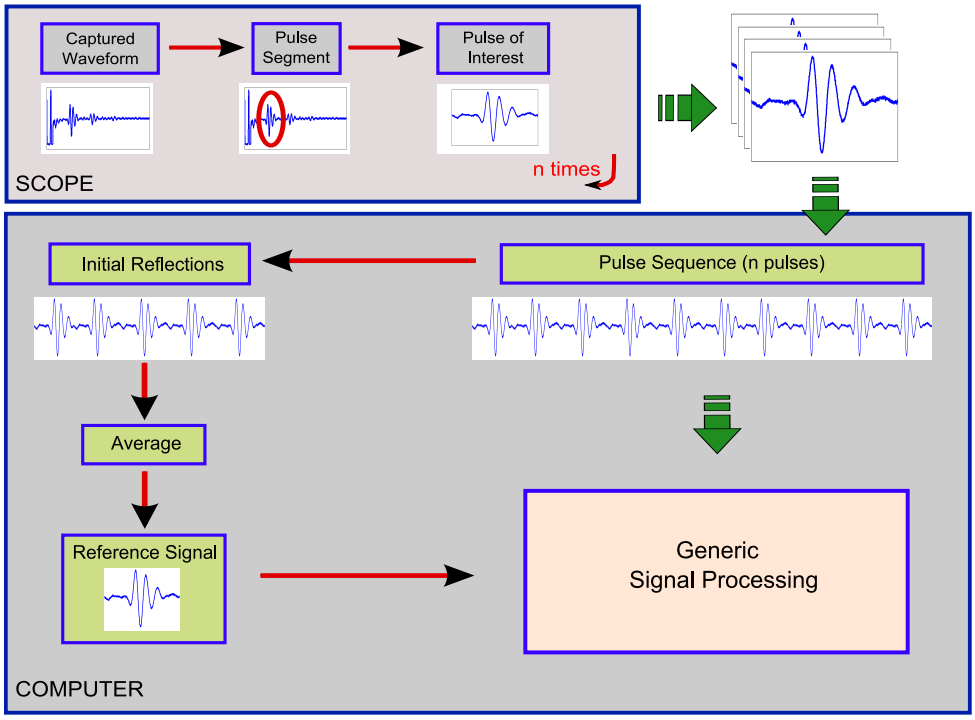

Figure 5.8: Schematic diagram of signal processing stages

The triggering system allows a reflected signal to be recorded at a time before the rings reach the transducer location. Hence, initial reflections in the pulse sequence are from the reference interface and the remainder from the layer (ring-oil-wall). The reference signal is therefore created by selecting the initial reflections in the pulse sequence and averaging them, as depicted schematically in Figure 5.8. Once the reflection coefficient is produced, the main signal processing routine described in Chapter 4 was carried out for each pulse in the pulse sequence.

5.5 Measurements of Reflection Coefficient

During the experiments, a square wave with 370 cycles was produced by the function generator for each shaft encoder timing pulse, hence the contact transducer was excited 370 times by UPR. The average of the first five FFT amplitudes when the piston ring was away from the sensor was used for the reference signal. The number of cycles was determined by the storage limitation of the oscilloscope. Each pulse was sampled at 500 MS/s and this gave 500 data points per pulse. The frequency of the square waves was selected according to the piston speed to ensure that the entire ring pack was captured. For data analysis, the upper and lower frequencies have been set up to 6 and 4 MHz respectively.

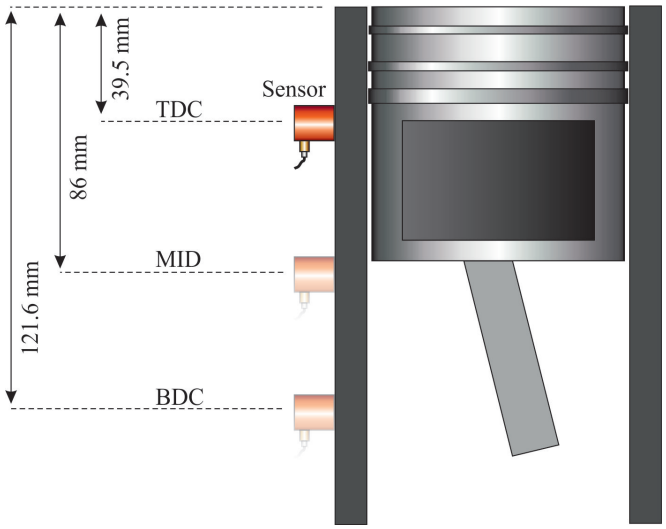

Figure 5.9: Ultrasonic measurement locations

The ultrasonic reflection measurements were taken from three locations which were close to TDC, BDC and middle stroke of the motored engine (MID). Figure 5.9 shows the measurement locations on the cylinder wall. These locations have been chosen to catch all ultrasonic reflections coming from three rings.

As a recap, the reflection coefficient is obtained as the FFT amplitude of the reflected signal divided by the FFT amplitude of the reference signal (*i.e.* the average of the

first five FFT amplitudes). Figure 5.10 shows the reflection coefficient as the sensor positioned at 39.5 mm from the the top of the cylinder. The data was captured when the piston was travelling from TDC to BDC at an engine speed of 840 rpm. The three troughs associated with the three rings can be seen clearly in the figure. The first trough corresponds to the passage of oil ring and the second and the third troughs represent the passage of second ring and the top ring respectively. When the piston ring is far from the transducer's inspection area, the reflection coefficient approaches unity because all the ultrasonic waves are reflected back from the interface. As the piston rings pass through the area, the reflection coefficient becomes less than unity. However, in the figure, there are small spikes and noise which could either be electrical interference or the thin layer of oil on the inside cylinder wall which is inhomogeneous and causes some reduction in reflection.

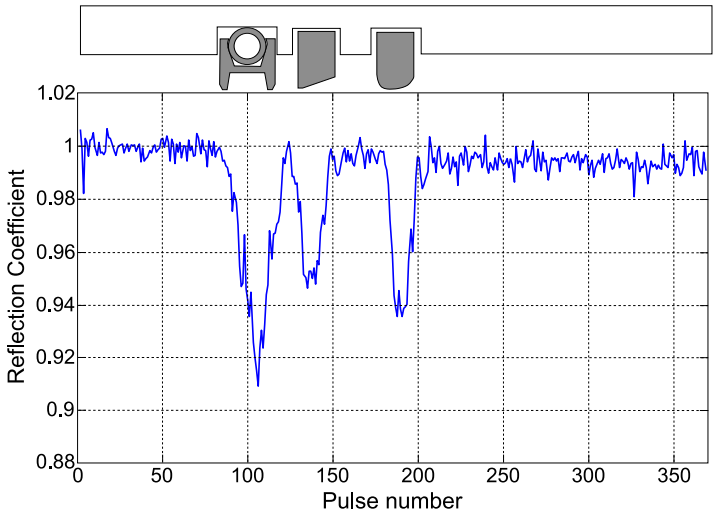

Figure 5.10: Plot of reflection coefficient recorded at close to TDC point for an engine speed of 840 rpm.

By increasing the number of the square waves, more ultrasound pulses can be captured from the interface with a low sampling rate. If the pulsing time is long enough, the reflection coefficients can be recorded for a complete cycle of the piston. Figure 5.11 shows superimposed sets of such data where the sensor was positioned between mid-stroke and BDC and two different triggering points were set-up. It is seen that all the

data sets show the same pattern. When BDC is used as a triggering point, firstly three small troughs corresponding to the ring pack and then a large trough corresponding to the piston skirt were seen in the reflection measurement. Of course, the sequence was reversed for the down stroke in this case firstly the skirt reflection was recorded. In the other case, the triggering point was changed to TDC. For the down stroke (the bottom graph), the sensor firstly captures the reflections from the skirt and then captures from the ring pack. It can be seen in both cases that the reflection coefficients of the rings decreases to around 0.9, therefore 9 % of incident wave is able to pass through into the rings. It is interesting to note that the piston ring signals are relatively stable, whilst the skirt signals have varied much more. This variation in skirt is expected because in nominally cold engine condition, the clearance between the skirt and liner is quite large which causes significant secondary motion and piston cant. Therefore this unpredicted the skirt-liner contact may lead to much more fluctuation in the reflection signal and lubricant film formation in the contact.

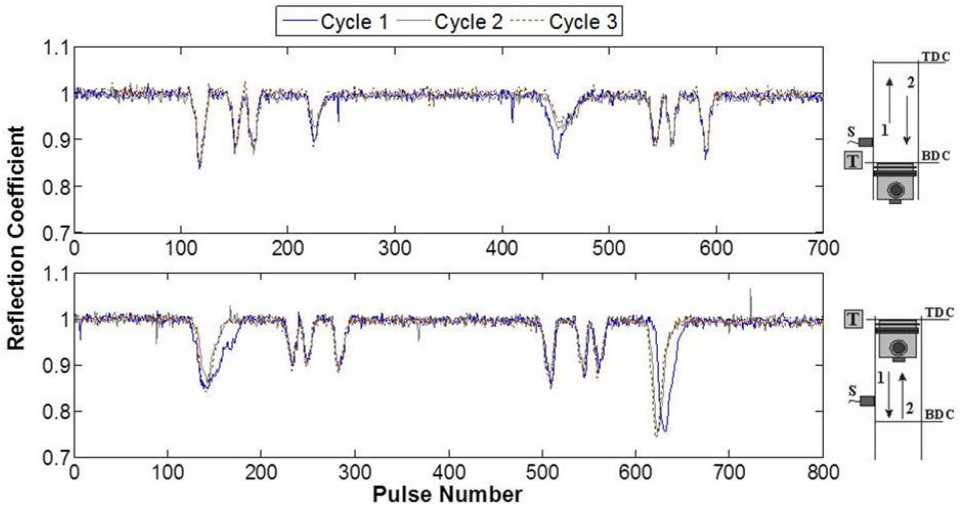

Figure 5.11: Plot of reflection coefficient over the rings and skirt (T: triggering point, S: sensor)

The reflection measurements were recorded from three locations on the thrust side of the engine (*i.e.* close to TDC, BDC and MID). To be able to record the reflections for

the piston down stroke, the system triggering point was separately adjusted for each measurement location. Three engine speeds, 600, 720 and 840 rpm were tested. Unfortunately, further speed increment was not possible because a pump which circulated the cooling water around the engine block was not in an operation due to the sensor coupling.

The minimum reflection coefficients of the piston ring-wall contact are given in Figure 5.12. The reflection coefficients were varying between 0.88 and 0.97. The smallest R values were measured at close to BDC. The reflection values were increased for MID location where the velocity of piston was greatest. The reason could be that the stiffness of the contact decreased due to the thicker film formed in the contact. More ultrasound was, therefore, reflected from the less stiff ring contact. However there is no clear difference between the speed tests. The results indicate that TDC had bigger reflection coefficient than BDC. This could be explain with oil starvation occurred around TDC. Since the lubrication was provided by oil splash, less oil entered into the contact hence the oil-air mixture leaded to increase in reflection. The results also suggested that the

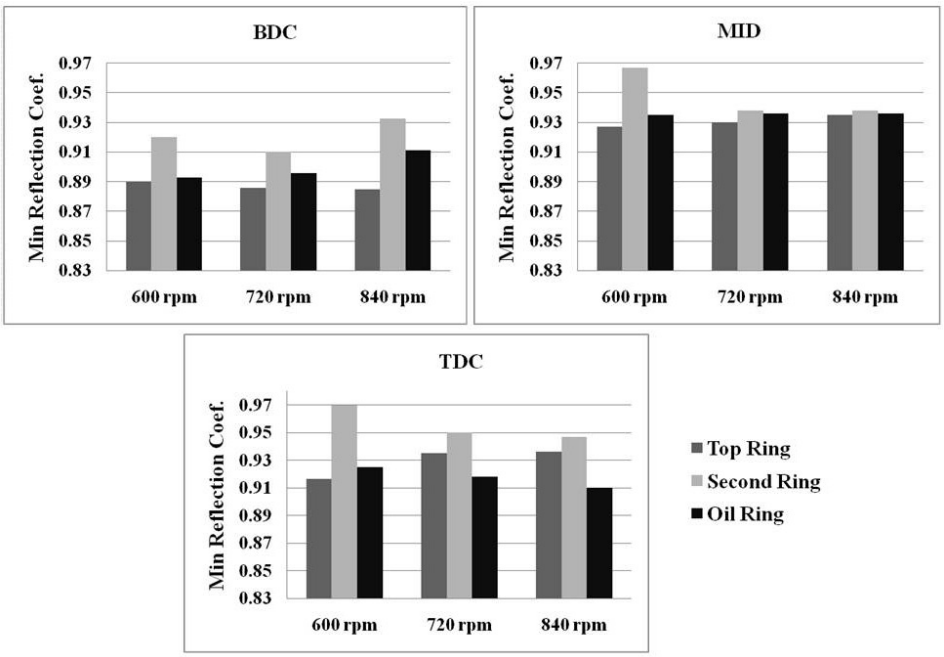

Figure 5.12: Graphs of minimum reflection coefficients for the ring pack.

second ring had consistently larger reflection than the other two rings. The second ring had a tapered face so this might be increased the cavitation region in the measurement area and hence give higher reflection coefficient.

5.6 Discussion

5.6.1 Sampling Rate and Data Capture

Segment numbers have an effect on the accuracy of the measurement because they are successive pulse of interest signals (*i.e* constituting the pulse sequence) in which some of the signals are reflections from the ring. If more segments for the rings are used, more accurate data can be obtained. However, each of the signals in the pulse sequence is digitized at a selected sampling rate and utilizes the internal memory capacity. For example, if a signal with duration of 1μs is digitized at 50 MS/s, it is defined by 50 data points while this signal is presented by 500 data points for 500 MS/s digitizing. The resolution of signal can be enhanced by using more data points.

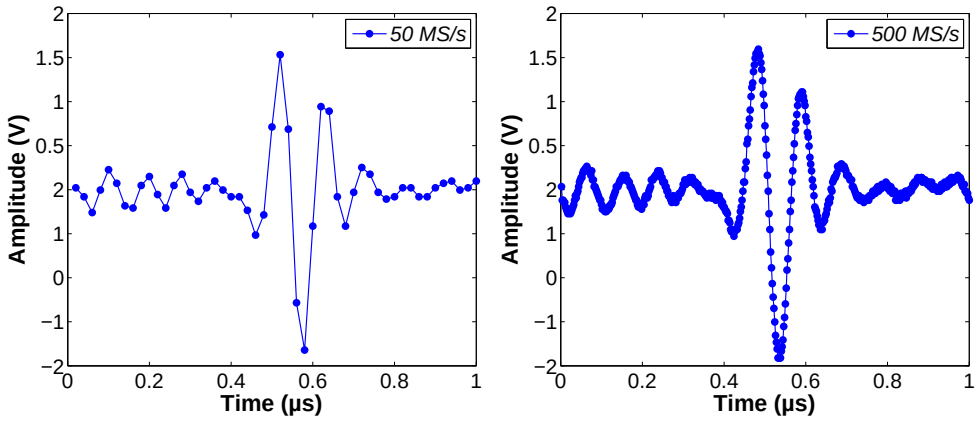

Figure 5.13: Comparison of the signals digitized at 50 MS/s and 500 MS/s.

A number of segments required for covering the entire piston crown by the ultrasonic sensor, depends on triggering frequency and piston speed. Figure 5.14 shows this relationship when a sensor was located 39.5 mm below the TDC point. The system

allows capturing maximum 1000 segments at 50 MS/s, this segment number, however, is limited for a particular sampling rate due to data acquisition memory capacity of the system. The four horizontal lines in the figure indicate this limited maximum segment numbers digitized at corresponding a particular sampling rate. Segment number at a constant engine speed increases with triggering frequency. It means that more ultrasonic signals from a piston crown can be obtained by using triggering signals with shorter time interval. However, sampling rate has an inverse proportional with this increment and so optimum engine speed and frequency should be chosen. The internal memory capacity of the scope is 250 kB. This capacity is used to store the data in real time before transmitting to the PC. In the experiments, 370 segmented signals were digitized at 500 MS/s. An increase in data storage capacity of the system would allow more data points per signals and more segmented signals to be captured.

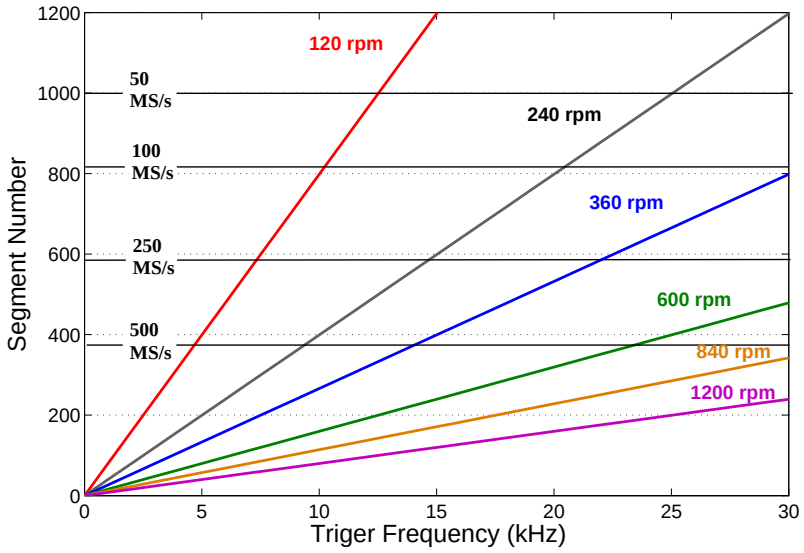

Figure 5.14: System limitations on engine speed and data acquisition when the sensor is located 36mm below from TDC

5.6.2 Spatial Resolution

The transducer used in the tests has successfully detected all the rings but its piezo element diameter is bigger than the ring width and Figure 5.15 schematically shows the effect of this. The ultrasound pulse is emitted over a larger area than the piston ring contact. This means that some of the pulse is reflected from the oil film and some from the wall-air boundary (albeit with a thin oil layer present on the surface). For the top compression ring and second ring, the reflection ratio was 50 % whereas this was roughly 40 % for the oil control ring. Therefore the reflection coefficient is a combination of Equation 3.8 and Equation 3.11. This leads to higher reflection coefficients in the measurements.

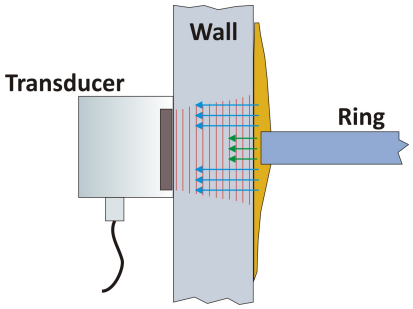

Figure 5.15: Reflections from both ring and wall-air boundary captured by the piezo element

If the incident ultrasound can be confined to fall entirely on the ring surface then only Equation 3.11, which relates the stiffness of the interfacial layer to the reflection coefficient, can be applied. For this reason, no attempt was made to translate these reflection coefficients into quantitative film thicknesses.

5.6.3 Engine Limitations

Although this is an initial attempt to test the ultrasonic technology, there are some restrictions in the operating conditions. This motored test rig does not provide any combustion pressure since as mentioned before the engine head and valve train have

been removed. Therefore the oil film pressure supports only the pressure produced by the inherent radial force. The effect of load variation on film thickness could not been explored. Only limited speed tests have been carried out due to the lack of cooling (no water circulation around the cylinder bore).

5.7 Conclusion

In this chapter, an ultrasonic method for the imaging of the piston ring-cylinder contact has been developed. A transducer was located in the water jacket of the motored engine so that ultrasonic waves were propagated through the cylinder wall and the reflections were recorded as the piston passed over the sensing area. A high speed pulsing and triggering system was built. The reflection coefficients for a complete cycle of the piston were generated. Skirt-cylinder wall and ring-cylinder wall conjunctions were successfully detected. The measurement system was triggered by a timing pulse produced by crankshaft encoder. By adjusting timing pulse, several measurements were taken from near TDC, BDC and mid stroke of the motored engine at different operating speeds. Minimum reflection coefficients were presented for all the rings. It should be noted that these values cannot be used to effectively determine oil film thickness due to the spatial resolution problem. These data can be used in spring model to calculate film thickness only if the incident ultrasound can be confined to fall entirely on the ring surface. This initial non-invasive attempt to monitor the piston ring-cylinder contact showed that the ultrasonic approach would be feasible if the internal memory capacity of the system and the spatial resolution of the sensor are both improved.

6

Piston Ring Oil Film Measurement in a Reciprocating Bench Test

This chapter presents a reciprocating test rig combined with the ultrasonic film thickness measurement system. Special piston ring and liner holders were manufactured to replicate the piston ring-liner contact and smaller piezoelectric sensors were developed. A liner section was instrumented with five ultrasonic sensors and the reflections from the ring-liner contact were successively recorded as the ring reciprocates over the liner. The results of oil film thickness measurement were presented in detail and compared with numerical simulations.

6.1 Introduction

Engine manufacturers and scientists are seeking to improve the tribology of the ring-liner conjunction by formulating new lubricants or designing different materials and surfaces. Laboratory tests carried out in either test engine or bench test have shed light on these developments. Altough the engine tests more realistically recreate the piston ring-cylinder liner contact, they require intensive modifications and instrumentation as briefly mentioned in the literature chapter. These inevitably increase the time and the

cost of laboratory tests. Tribological conditions in the engine tests, particularly in a fired engine, are very sophisticated and there are many factors affecting the lubrication of the piston assembly such as blow-by, dynamics of the piston and ring and thermal deformations.

As an alternative method, simplified test rigs have been developed to investigate the piston ring lubrication mechanism and the related friction phenomena. The designs of these test rigs are wide ranging and depend on the focus of the research. Although whole piston and cylinder liner assemblies have been used in certain designs [100, 101] a typical test rig configuration consists of segments of a piston ring and cylinder liner where one of them reciprocates and the other is kept stationary [64, 102, 103, 104, 105]. These components are tested for different operating parameters, *i.e.* speed, load, viscosity and lubricant rate. However, it should be mentioned that there are several drawbacks of bench tests. The stroke is often an order of magnitude less than that in an engine. Therefore, because of a shorter stroke the maximum speed and acceleration seen by the piston ring is significantly less. In an engine, the loading between the ring and liner is dynamic while it is static in reciprocating bench tests. The test temperature in bench tests is also limited and the thermal expansion of the ring has not been considered. Generally the ring movement is restricted due to the use of ring holder and so dynamics and conformity of the ring is essentially different from the engine.

Since most of the parameters are controllable, the bench test rig can provide a suitable platform for developing the ultrasonic method and detailed information about how the different parameters influence the piston ring lubrication. Additionally, in most of the bench test studies, generally, film thickness data is obtained from the numerical solution of Reynolds Equation. There are very few bench test studies [29, 64] that have been carried out to provide simultaneous and comparative measurement of friction and lubricant film thickness. One successful approach by Dearlove et. al [29] modified a reciprocating test rig with the addition of a laser induced fluorescence (LIF) oil film thickness measurement system. However, a force spike in friction trace was observed

at mid stroke due to the protruding edge of the quartz window on the liner. In this chapter, a reciprocating test bench was instrumented with non-invasive ultrasonic film thickness measurement system, hence simultaneous friction and oil film thickness data were achieved.

6.2 Test Apparatus

6.2.1 Reciprocating Test Rig

A Plint TE-77 high frequency reciprocating tribometer, shown in Figure 6.1, was used in this study. As a well-established research and development tool, the TE-77 was also used in several other piston ring-liner studies [106, 107] to assess the dynamic wear and friction performance of lubricants, materials and surface coatings. The machine configuration involved a special adapter oscillated mechanically over a fixed liner section. The adapter retaining a section of piston ring was loaded against the liner section by a spring balance through a lever and stirrup mechanism. The normal force was transmitted directly onto the moving specimen by means of a needle roller cam follower on the adapter and the running plate on the loading stirrup.

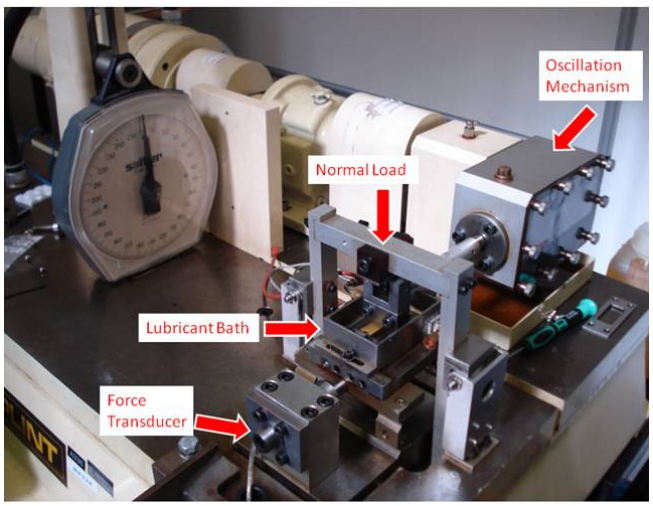

Figure 6.1: TE-77 Plint machine

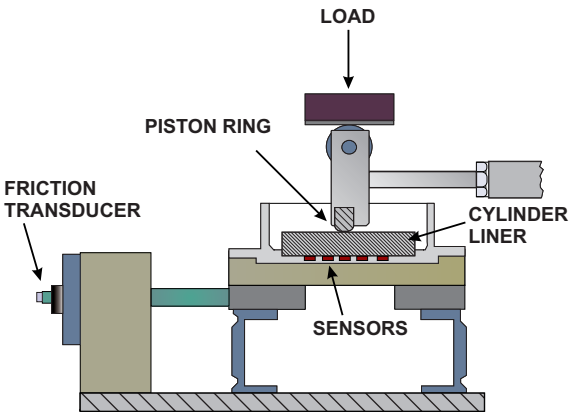

Figure 6.2: Schematic diagram of the modified Plint TE-77.

The oscillations were produced by a variable speed motor with an eccentric cam, scotch yoke and guide block arrangement. A stable oscillating frequency was maintained by a tacho generator feedback system. The whole assembly was mounted on flexible supports, which allowed free movement in the horizontal reciprocating axis. A stiff piezo-electric force transducer connected to the assembly measured the friction force in the reciprocating direction. The possible testing configurations of the Plint are as follows:

- Shape of contact - nominally point, line, area, piston ring / cylinder liner
- Normal load - 5 to 250 N
- Temperature - Room to 250 °C;
- Sliding frequency - 0.1 to 50 Hz;
- Amplitude - 1 to 15 mm in 8 steps or 0.5 to 5 mm in 8 steps.
- Lubrication Conditions - Lubricated/Dry
- Method of Lubrication - Immersed, thin layer, drip fed

Due to the liners horizontal position, it is useful to identify the dead centres where the oscillating ring stops. The dead centre closest to the force transducer is named top dead centre (TDC) and the one closest to the adapter mounting hole is named bottom dead centre (BDC) in this work.

6.2.2 Piston Ring and Liner Specimens

A pair of cast-iron liner and ring segments from the same heavy duty diesel engine were used to create the contact. The liner specimen, 50 mm in length and 20 mm in width, was cut from the cylinder liner with a bore diameter of 130 mm (see Figure 6.3). The acoustic impedance of cast iron piston ring and liner is 34.9 MRayls. The surface parameters of the specimens were measured using a stylus surface profilometer. The cylinder liner had a mean roughness value R_a of 0.32 μm. The liner had a cross-hatched

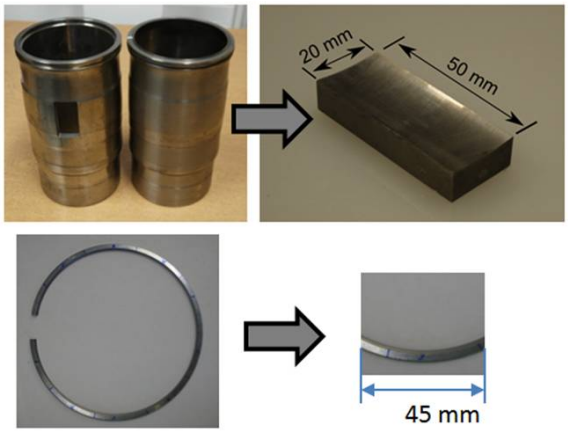

Figure 6.3: Photos illustrating the dimensions of ring and liner sections machined out from the original heavy duty engine components.

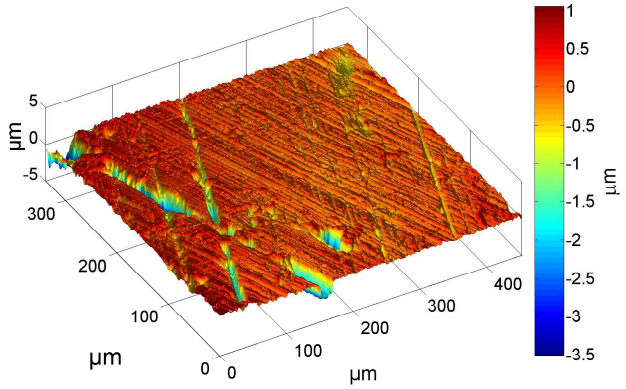

Figure 6.4: 3D image of cylinder liner surface used in the tests, measured with a confocal microscope.

surface finish typical of a plateau honing process as illustrated in Figure 6.4. Although honing angle (HA) of 30° was suggested as an optimum by [108], the liner used in the tests was a standard production liner with 55° HA. The depth of honing grooves and their variation can be observed from a cross-section of liner surface profile given in Figure 6.5.

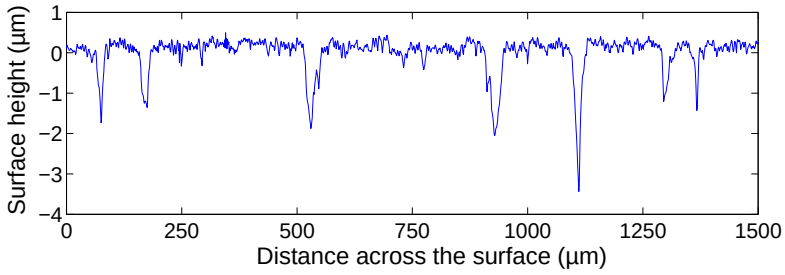

Figure 6.5: Cross-section of the surface profile of the liner specimen.

The used top compression ring from the same engine was sectioned into a length of 45 mm. The width of the piston ring was 3 mm. The piston ring had an asymmetric barrel shaped profile as illustrated in Figure 6.6. The running face of the ring was coated with a chrome ceramic coating (CKS®) developed by Federal-Mogul. In this patented coating system, chromium coating with aluminium oxide particles is deployed on the ring running surface using electrochemical deposition process. This coating provides

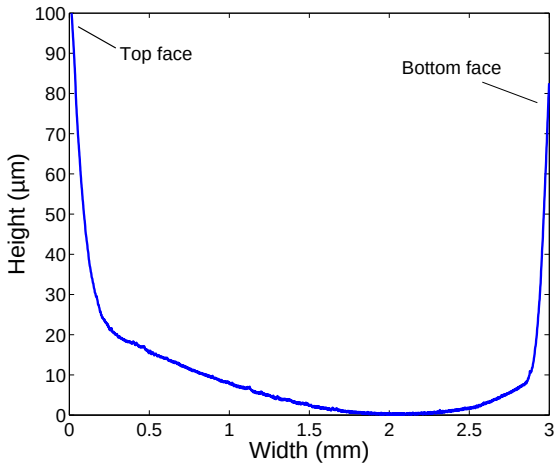

Figure 6.6: Piston ring profile measured by a profilometer.

significantly lower wear rate and scuff resistance compared to hard chromium. Using original piston ring and liner components, the geometry and the metallurgy of the contact were preserved. This allowed representative surface finishes, oils and engine materials to be tested and evaluated.

6.2.2.1 Ensuring Conformability of the Ring-Liner Contact

Consistent conformability between the piston ring and cylinder liner is necessary from test to test. In the engine, the ring is able to conform due to its inherent tension and freedom to move. However, in simulated test rigs, the uncompressed piston ring (the diameter of the ring is bigger than the diameter of the liner) would mean that in its free state the piston ring would only make contact at the edge of the liner. To prevent this, a special ring holder manufactured from an original production piston was designed and attached to the adapter (see Figure 6.7). The conformability of the ring-liner contact was adjusted by two slotted plates located at either side of the ring holder and a grub screw in the centre which pushed the ring from behind. The liner specimen was held in the lubricant bath and secured by six grub screws allowing for axial and lateral alignment of the liner.

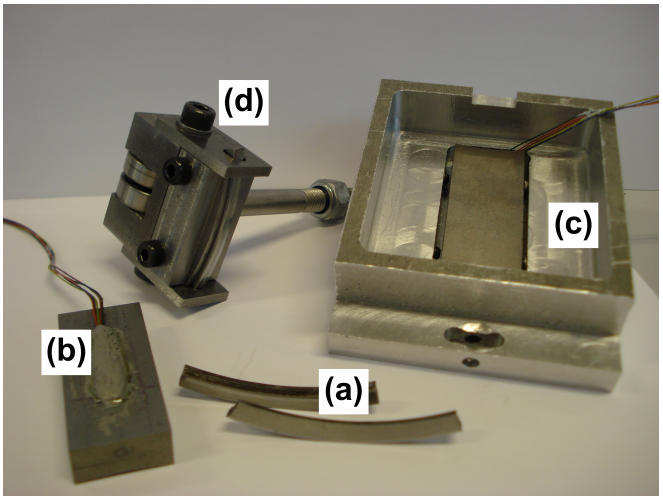

Figure 6.7: A photograph showing the components manufactured for this ultrasonic application: (a) piston ring sections, (b) cylinder liner section with ultrasonic transducers attached to the back side, (c) oil bath and cylinder liner holder, (d) ring adapter.

In the piston ring tribotest literature there is very little information about how the ring-liner conformability was checked or even obtained. In one paper [29], a light bulb was placed behind the ring and the non-conformity was observed. In this work, Fujifilm® Prescale pressure measuring film was used to check the conformability of the contact. The Fujifilm® paper indicating the stages of the ring-liner contact from the initial to final set-up are shown in Figure 6.8. As seen, the progress of obtaining conformability is clear. The ring-liner contact was initially unconformal such that a more dense pink colour appeared at the right hand-side of the liner, indicating a higher contact pressure. After a few adjustments, a more conformal contact where the colour is evenly distributed over the liner surface has been obtained.

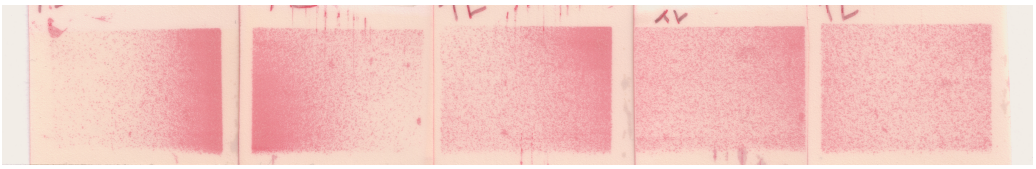

Figure 6.8: Fujifilm® Prescale pressure measuring film used during the conformability adjustment, from the initial attempt (left) through to the conformal contact (right).

6.2.3 Lubricant

The lubricant used in this study was Castrol base oil meaning that there was not any additive package in the lubricant. The lubricant speed of sound was measured using a time of flight measurement from the chamber containing the oil sample as detailed in Chapter 4. The speed of sound in and density of this oil were 1440 m/s and 843 kg/m^3 respectively. The liner specimen was fully immersed in the oil. This does not represent the real lubricant condition in the engine, which would normally be significantly less. However, it ensures that the inlet is fully flooded allowing for good, accurate comparisons with the numerical model which will be given in the following section. It also assists in maintaining a stable temperature of the liner surface during the short tests.

6.3 Sensor Development

The resolution problem has been mentioned in Chapter 5. This problem occurs when the ultrasound pulse is emitted over a larger area than the piston ring contact (see Figure 5.15). It means that some of the pulse is reflected from the oil film and some from the liner-air boundary. Therefore, to increase the spatial resolution, 10 MHz piezoelectric crystals (8 mm diameter) were cut into shape of 2.5 mm in length, 1.3 mm in width and a thickness of 0.2 mm as illustrated in Figure 6.9. By following an installation procedure, these bespoke piezo strips were installed on the liner specimen.

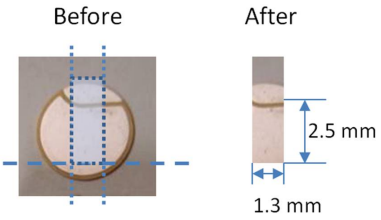

Figure 6.9: Dimensions of piezo electric sensors.

The back of the liner sample was ground to provide a flat mounting surface for the piezo-crystal sensors and was cleaned with acetone using an ultrasonic bath. A guidance template with five rectangulars indicating where the sensors were positioned over the back side of the liner was stacked to a glass surface, hence only sensor positions were free (see Figure 6.10). The positioned array of sensors was removed by means of a heat resistance tape. Then Vishay M-Bond 610 high performance epoxy resin formulated specifically for bonding strain gauges was applied and the array was glued on to the back side of the liner. Later the liner sample was clamped to provide a required pressure during the curing cycle and was placed in an oven for curing process which took minimum 4 hours at 100 °C. By soldering, the electrodes of the sensor were connectted to a small coaxial cable, with a diameter of 0.4 mm, and covered by a protective layer of silicone.

These five ultrasonic sensors placed at the back of the liner were almost equally distributed. The schematic diagram illustrating the ultrasonic sensor array configuration is given in Figure 6.11. The central sensor was positioned at the middle of the stroke

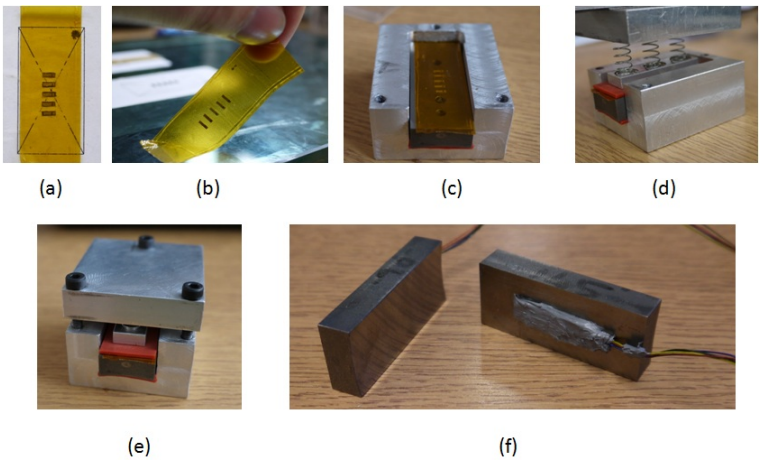

Figure 6.10: Photos showing the installation procedures of the piezo strips on the liner specimen: (a) guidance template, (b) positioned piezo strips on the heat proof tape, (c) the glued strips on the liner specimen, (d, e) clamped and ready to place into an oven (f) final instrumented liners.

by adjusting the liner holder's grub screws located in the axial direction. Thus, the ultrasonic sensors were kept in the stroke area swept by the piston ring and they were able to record the oil film data at five locations between the dead centres.

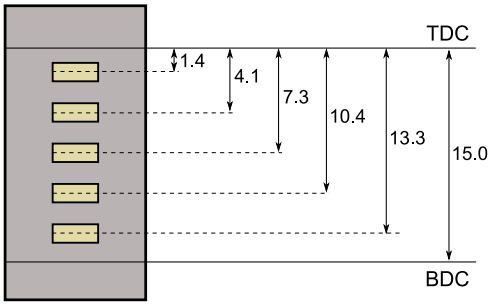

Figure 6.11: Sensor array configuration over the stroke (all dimensions in mm).

6.4 Instrumentation

An ultrasonic pulsing unit and digitizer embedded into a dedicated computer, (FMS-100 ultrasonic pulsing unit from Tribosonics® Ltd.) was used in this study. This unit, illustrated in Figure 6.12, consisted of an ultrasonic pulsing and receiving card (UPR)

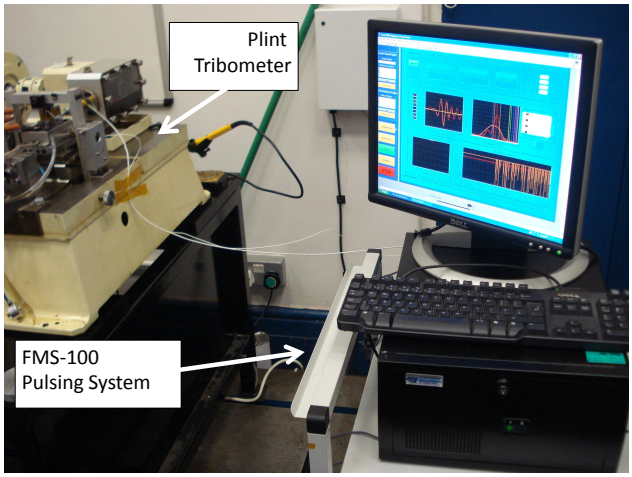

Figure 6.12: A photo showing a FMS-100 pulsing system.

which was equipped with 8 channels and a maximum achievable pulse rate of 80 kHz on a solitary channel. Receiver gain range was between -40 db and +110 db and the receiver bandwidth was from 0.1 to 25 MHz. The UPR card controlling software was written in-house using Labview®.(National Instruments). Each of the ultrasonic sensors was individually connected to the pulsing unit, totalling 5 channels with a pulse repetition rate of 15 kHz for each. The system operated in a pulse-echo mode, meaning that the reflected pulses from the ring-liner conjunction were also received by the sensors. Ultrasonic reflection signals were digitised at 100 MHz with a 12 bit resolution.

The piezo-electric force transducer (Kistler type 9203) with a range of 500 N and normal sensitivity of 50 pC/N was used to measure the friction force. The charge amplifier (Kistler type 5007) converts the charge produced by the transducer into proportional electrical signals with a resolution of 0.001 N. A fixture which applied a calibrating load in line with the normal point of contact between the ring and liner was used for the force transducer calibration. The transducer was calibrated before the experimental stage and the calibration graph is given in Figure 6.13 showing the voltage output versus calibrating load. Uni-directional friction data output was logged to the computer hosting the ultrasonic pulsing unit.

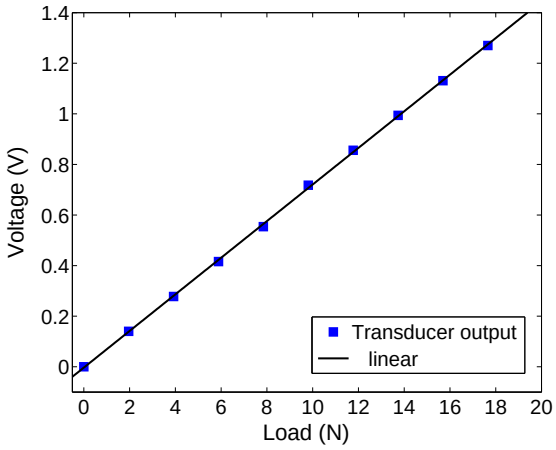

Figure 6.13: Force transducer calibration chart.

6.5 Data Acquisition and Processing

Before starting the test, the inner liner surface was cleaned by acetone. So when the ring was not in a contact with liner, the reference pulse from the liner-air interface, which would fully reflect all incident waves, was recorded for each ultrasonic sensor (see Figure 6.14). Since the system had enough memory (so there was not triggering system), ultrasonic reflections captured by the sensors were continuously recorded as the test progressed. The measurements and pre-stored references were recorded to hard

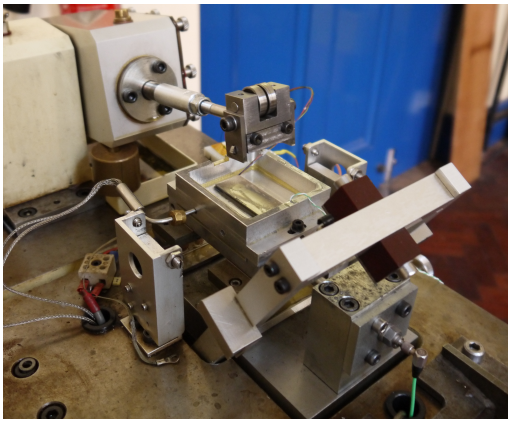

Figure 6.14: A photo showing the position of reciprocating head when the reference signals were recorded for the sensors.

disk in binary file format. Then a post-processing software program, utilizing the same generic signal processing described in Chapter 4, translated the data to oil film thickness.

6.6 Succesive Oil Film Measurements

6.6.1 Reflection and Oil Film Spectra

In this section, FFT analysis of the measurement signals is detailed as the ring passing through the sensing area. The variations of reflection coefficient and film thickness with frequency are given. The acoustic reflections captured by Sensor-3 is illustrated in Figure 6.15. The second pulse 'II' was reflected from the inner side of liner (*i.e.* pulse of interest), as in CH5, this 'II' pulse was therefore isolated by the pulsing system and successively recorded.

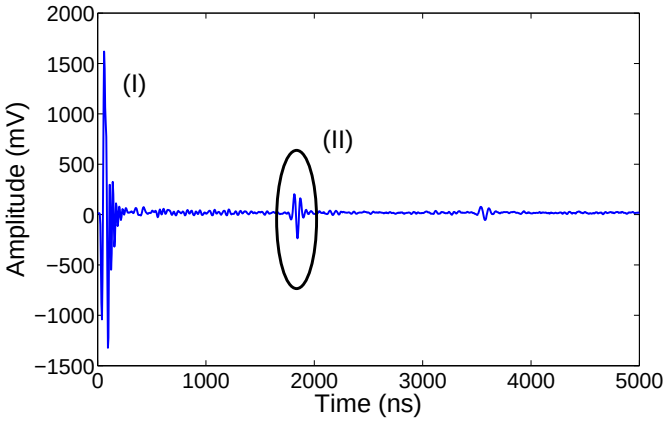

Figure 6.15: A typical waveform measured by Sensor-3 showing the reflections from the liner specimen.

During the piston ring stroke, the ring passed back and forth over the sensor location. Hence, sometimes ultrasonic wave continuously emitted from the sensor (*i.e.* pulse 'II') was reflected from a liner-oil interface and sometimes from the oil film that formed between liner and piston ring (see Figure 6.16).

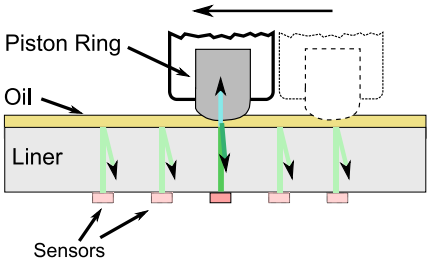

Figure 6.16: Ultrasonic reflections during the piston ring stroke.

As the ring reciprocates over the liner, typical successive reflections recorded by the sensor are illustrated in Figure 6.17a. In the figure, each trough, where the pulses were reflected from the piston ring, corresponded to one of the ring traversals over the sensor area. Figure 6.17b illustrates a close view of the reflections as the ring passage occurred. The initial pulses in the graph were reflected from a liner-oil interface and the amplitudes of subsequent pulses were reduced as the ring passed over the sensor location.

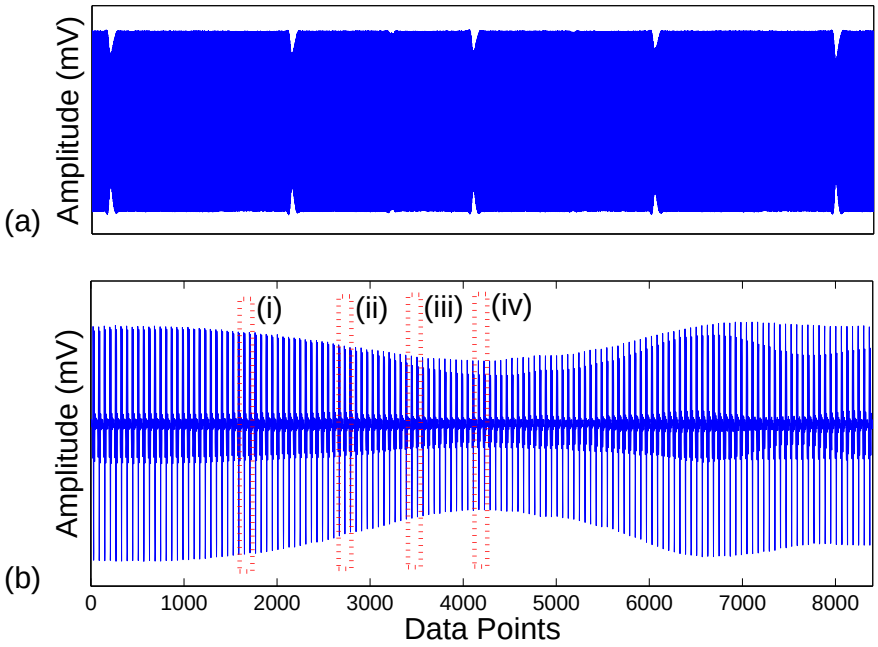

Figure 6.17: (a) Sequence of reflections from the inner side of the liner specimen as the ring reciprocates over the sensor location, (b) Close view of reflections from the inner side of the liner specimen corresponding to the ring passage.

Some pulses were selected from Figure 6.17b for a detailed analysis. Figure 6.18a shows these selected pulses in time domain together with a reference pulse. By applying FFT, amplitude spectra of these pulses are illustrated in Figure 6.18b. As the lubricant film thickness reduces, more of the ultrasound energy passes through the lubricant and is absorbed by the ring. Hence, the amplitude of the reflected pulses decreases. Although the sensors are labelled as 10 MHz, their useful energy distribution is in between 5.5 and 11 MHz with a centre frequency of approximately 9MHz.

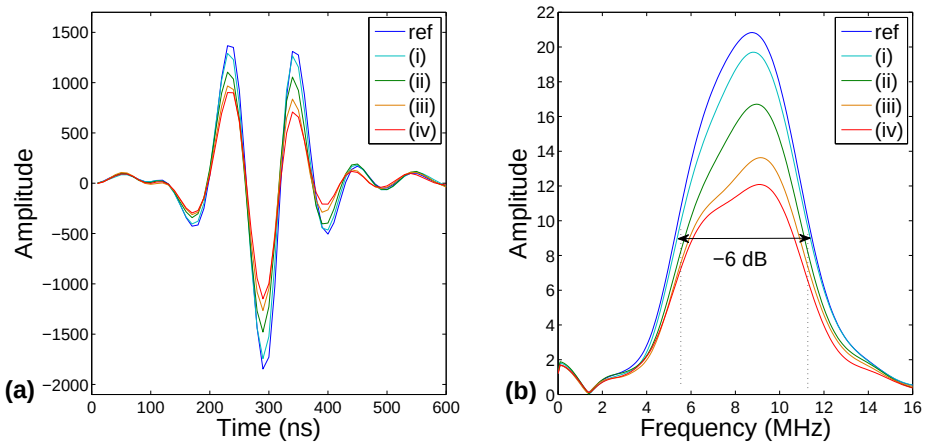

Figure 6.18: (a) A series of time domain pulses. The reference pulse is reflected from liner-air interface and the four other pulses are selected pulses of Figure 6.17b. (b) Fast Fourier Transform of these reflected pulses.

If each selected pulse spectra is divided by the reference spectrum, this gives the reflection coefficient against frequency. This is plotted in Figure 6.19 with the reference spectrum which is scaled to show the bandwidth of the sensor. The lubricant film thickness obtained by substituting each pair of reflection coefficient and frequency data into the spring model equation is plotted in Figure 6.20. In theory, within the -6dB bandwidth of the sensor, the reflection coefficient should be smooth and monotonically increasing with frequency whereas the outside bandwidth, erroneous results have appeared due to low signal-to-noise ratio. Despite the fact that frequency appears in the equation, its effect on h is cancelled by the counter-variation of reflection coefficient with frequency [84, 72, 99]. Clearly, the film thickness should not vary with measurement

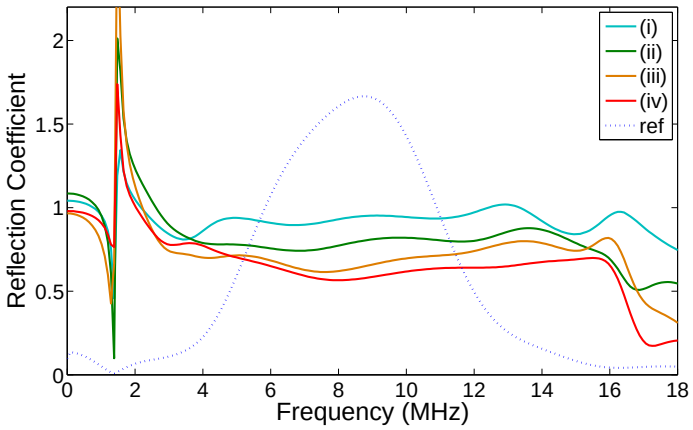

Figure 6.19: Reflection coefficient spectra for the four pulses.

frequency within the bandwidth region. Figure 6.20 shows that this is valid for the ring reflection (iii and iv), a straight line occurs within some part of the bandwidth. But there is some frequency dependence observed for the partial ring reflection (i,ii), so measurement in this region is not strictly valid. Therefore, in this study, a mean value of the reflection coefficient recorded over the reliable part of the bandwidth (from 8.5 to 10.5 MHz), where the film thickness is not frequency dependent, was used to determine the film thickness.

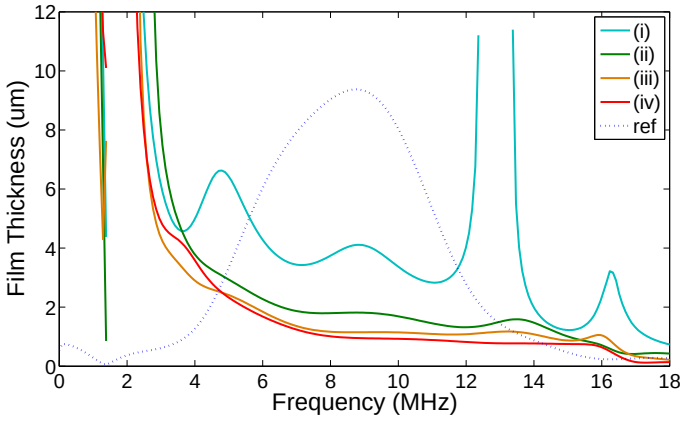

Figure 6.20: Oil film thickness spectra.

6.6.2 Typical Measured Film by a Single Sensor

As mentioned, the ultrasonic data were recorded successively and each pulse was processed and compared to the reference pulse. Figure 6.21a shows reflection coefficients measured by Sensor-1 as the ring reciprocates over the liner. The reflection coefficient should ideally equal to 1 in the non-contact region due to acoustic mismatch. It decreases as the ring in the sensing area; however, in the transition region (ring partially in the sensing area) the reflection coefficient tends to be slightly higher. This is mainly because there is small phase shift in the peak position leading to a minor error in judging the maximum amplitude of the signal [109]. It is seen that the piston ring has passed over the sensing area six times and since Sensor-1 is close to the TDC, there are two repetition intervals between the troughs, short and long. Figure 6.21b shows the oil film thicknesses which were obtained from the data given in Figure 6.21a. One ring passage has been represented by approximately 100 pulses and this number depends on pulsing rate of the ultrasonic system and the ring reciprocating speed.

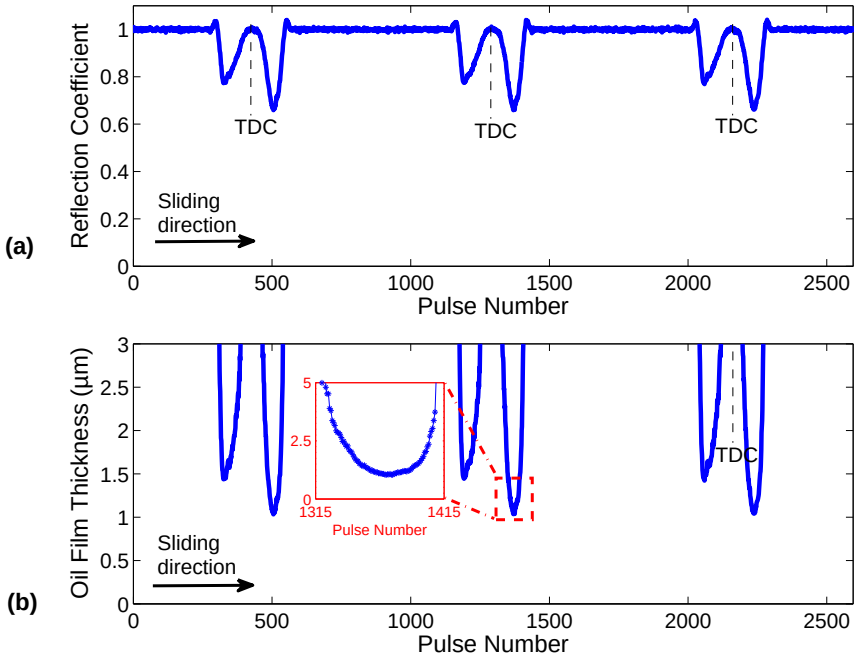

Figure 6.21: (a) Reflection coefficient obtained from the reflections successively recorded by Sensor-1. (b) Oil film thicknesses at the location of Sensor-1 as the ring reciprocates.

6.6.3 Typical Measured Film by Five Sensor Array

Up to now, the film thickness data measured only by Sensor-1 has been presented. In the experimental stage, ultrasonic signals were simultaneously captured by all five sensors. The capturing time and pulse repetition rate for each sensor were the same. Once the signal processing has been performed for each sensor, the film thickness values at the fixed sensor locations could be achieved and superimposed on a single graph. Figure 6.22 shows the measurements of film thickness as the ring reciprocates at 2.5 Hz (0.11 m/s at mid-stroke see Appendix B1) under a normal load of 80 N (*i.e.* 4 N/mm see Appendix B2). It is notable that the film thickness data from cycle to cycle was very repeatable. In the figure, the ring starts its travel from TDC to BDC, thus it is initially captured by Sensor-1 (close to TDC). As the ring moves from one sensing area to the next, the other sensors detect the ring respectively. This roughly provides an overview of lubricant film formation over the stroke.

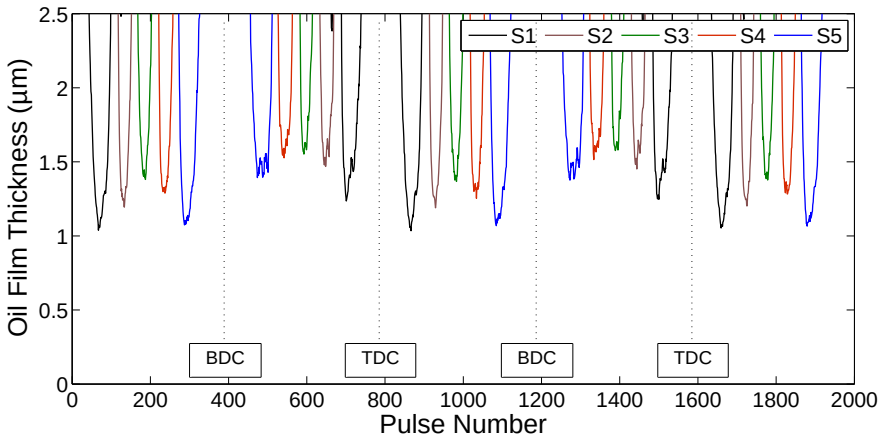

Figure 6.22: Oil film thicknesses measured by the sensors as the piston ring reciprocates over the liner specimen

During testing, there were some fluctuations in the ultrasonically measured ring profiles, especially in the case of the ring travelling from BDC to TDC (see Figure 6.22). This is likely because the interface between the ring and liner is not homogenously filled with lubricant If the oil is partly depleted under the sensing area, this leads to more

ultrasound reflected from the interface due to an air-oil mixture in the contact. This results in bigger reflection coefficients and the impression of greater film thickness measurements being recorded. Two possible factors, cavitation and less oil availability in the ring-liner contact could cause this inhomogeneous region. To show the effect of oil availability, a test was carried out by providing a smaller amount of oil into the contact. The operating conditions of the test were the same that of given in Figure 6.22. The reflection coefficient results of both cases, starved and lubricated contact, are provided in Figure 6.23. It can be seen that the trend of reflection coefficient observed in the lubricated contact (*i.e.* like an arc shape) was changed for the starved condition and more fluctuations have been observed in both reciprocating direction. Clearly, the reflection coefficients are bigger in the starved condition than in the lubricated condition. If there is a plenty of oil in the contact, at least the area covered by the sensor, more smooth shape of the reflection coefficient is observed as shown for the down stroke in Figure 6.23.

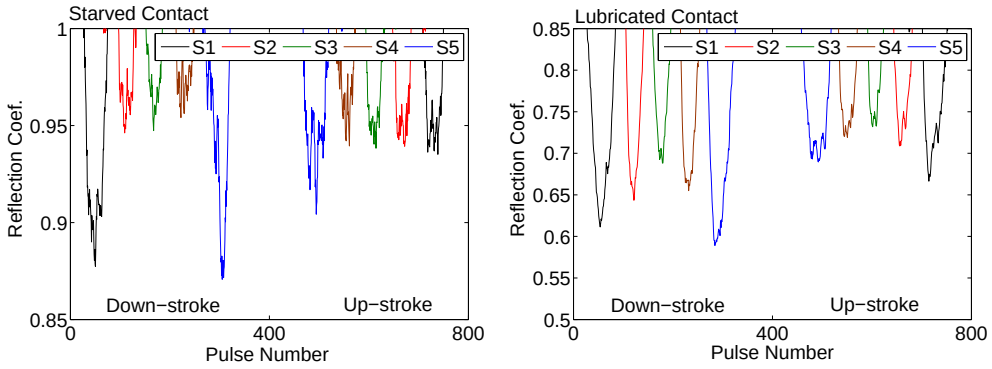

Figure 6.23: Measured reflection coefficients for one complete cycle: starved (left) and flooded (right) contact conditions; higher reflection coefficients values in starved conditions due to the presence of air-oil mixture in the contact.

6.6.4 Effect of Convergence Angle

In the measurements, the ring was installed in the ring holder with the greater converging shape facing towards BDC (see Figure 6.24b). Thus there were not considerable fluctuations in reflection coefficient for the down stroke since enough lubricant could

flow into the contact. However, for the up stroke, the lubricant on the liner was swept away by the rings trailing edge and less oil entered the contact and leading to uneven reflection coefficient. As the ring slides on the liner, possibly cavitation would occur at the diverging part of the piston ring. The non-symmetric barrel shaped piston ring could lead to a different size of the cavitation region according to the direction of the stroke [110]. Because the diverging part of the ring was much smaller in down stroke than in the up stroke, it was expected that the cavitation region on the down stroke was considerably smaller than that on the up stroke. This also could contribute the inhomogeneous layer phenomena for the up stroke.

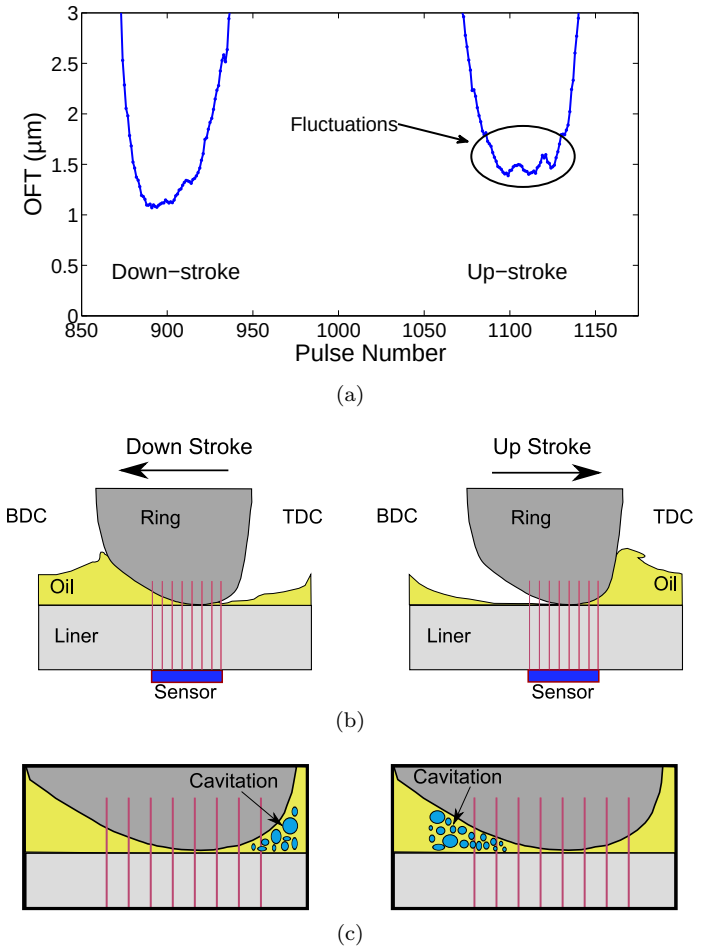

Figure 6.24: Fluctuations in the up stroke: (a) close view of ultrasonically measured ring profiles, (b) lack of oil inside the contact, (c) cavitation occuring in the contact.

Since there is a far larger inhomogeneous region on the up stroke due to lack of oil availability and cavitation in the contact, as is mentioned the ultrasound recorded an anomalously high film thickness in this direction. This is can be seen in Figure 6.22 and Figure 6.24a where oil film thickness is bigger on the up stroke, compared with the down stroke. However, fluctuations on the measurement are clearly discernible. It was concluded that the up stroke data cannot be considered reliable and in this study, the down stroke data exhibiting far less fluctuations has been used to examine the tribological condition in the ring-liner contact.

6.7 Minimum Film Thickness Measurements

Figure 6.25 illustrates an oil film profile for one ring passage over the sensing area. The width of the sensor (1.3 mm) was smaller than the ring width (3 mm). Thus the sensor records an average of the reflection signal over that 1.3 mm 'window' as the ring traverses the region. Hence each film thickness data given in the figure is averaged over the window and the exact ring profile is, therefore, not expected from this kind of profile measurement.

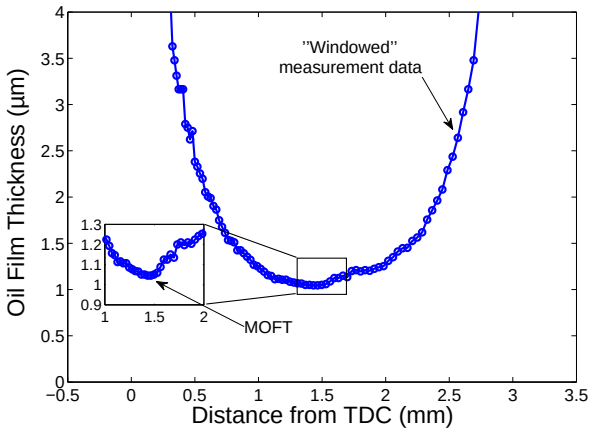

Figure 6.25: Film thickness recorded for one ring passage

Each sensor gives one minimum oil film thickness (MOFT) data for each ring's passage. During the test, therefore, plenty of minimum film thicknesses were recorded. One

sample is illustrated in Figure 6.26 showing the MOFT values measured by Sensor-3 as the test in progress. It is seen that the data is varying between 1.40 and 1.47 μm and the mean of the data is 1.43 μm.

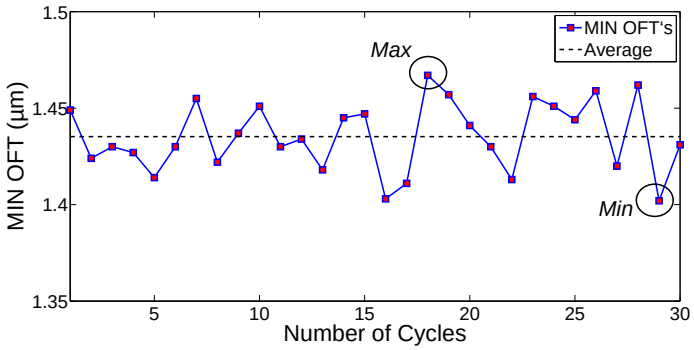

Figure 6.26: Minimum film thicknesses measured by Sensor-3 for a series of cycles (Normal load: 140 N, reciprocating speed: 12.5 Hz).

To see the down stroke MOFT variation along the liner, the mean value of a series of cycles was used for each sensor. Typical MOFT measured by sensors at 12.5 Hz reciprocating speed and under a normal load of 140 N is given in Figure 6.27. The MOFT data in the figure represents the mean value of down strokes and the standard deviation bars gives an indication of cycle to cycle variation. As seen there is more or less similar variation in the data and towards Sensor-3 where lubricant entrainment speed is highest, the MOFT becomes largest due to the hydrodynamic lift of the piston ring.

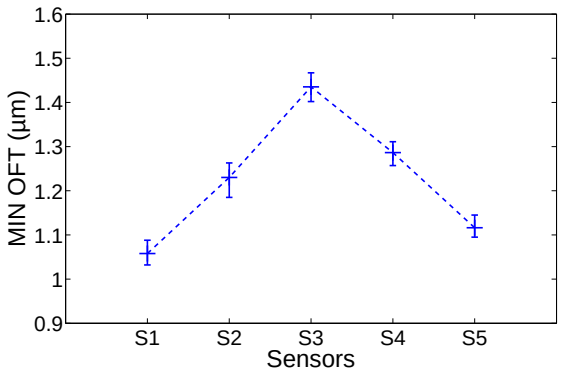

Figure 6.27: Minimum film thickness for down stroke (Normal load: 140 N, reciprocating speed: 12.5 Hz).

6.7.1 Effect of Ring Profile on Measured Minimum Lubricant Film Thickness

In this piston ring-liner application, the matching surfaces are not parallel due to the profile of the ring even though the liner and ring are both concentric. As illustrated in Figure 6.28, if the ultrasound wave is thought of a series of discrete pulses over the sensor area, each local film thickness (h_i, h_{ii}, h_{iii} etc.) would produce its own reflection. Therefore the total reflection captured by the sensor is the cumulative result of these local reflections. This averaging effect leads to the measured minimum film thickness larger than the true minimum value.

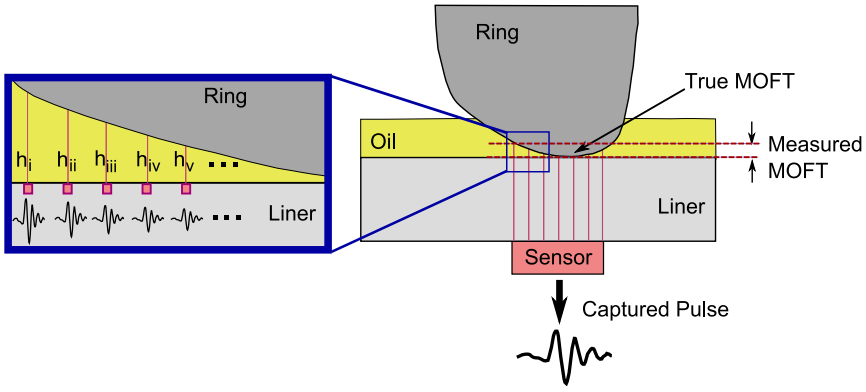

Figure 6.28: Piston ring-liner contact schematic.

A deconvolution algorithm was developed to extract the true minimum film thickness from the measured MOFT data. The algorithm utilized the rearranged form of spring model Equation (3.18) for each discrete local thickness under the sensing area and calculated the equivalent reflection coefficient as the ring rests on the liner.

A computer software program was written in MATLAB® to perform the deconvolution. The routines used in the program were given step by step as follows:

- The ring profile measured by a profilometer was taken and it was discretised together with the sensor window equivalent to the sensor width. The pitch was set

to 1 μm when the profile was recorded so this was used as 'Δx' for the discretization process. At this stage, a filter could also be applied to remove the roughness.

- The minimum point of the ring profile was matched with the zero point supposing that the ring was in contact with an infinitely smooth surface and the separation was completely filled with oil (Figure 6.29a and Figure 6.29b). The average film thickness under the sensor window were calculated across the ring profile (*i.e.* like 'scanning') and so the minimum region in the measured profile was identified.

- Using Equation (6.1) (*i.e.* the rearranged form of Equation (3.18)), the reflection coefficients were calculated for each discrete film thickness value in the region (see Figure 6.29d).

$$R(x_i) = \sqrt{\frac{h_{x_i}^2 \omega^2 z_1^2 z_2^2 + \rho^2 c^4 (z_1 - z_2)^2}{h_{x_i}^2 \omega^2 z_1^2 z_2^2 + \rho^2 c^4 (z_1 + z_2)^2}} \tag{6.1}$$

- Then they were averaged to produce the equivalent reflection coefficient. This could be thought of as the minimum reflection coefficient observed by the sensor when the actual minimum film thickness was zero.

$$R_{equivalent} = \frac{1}{n} \sum_{i=0}^{n} R(x_i) \tag{6.2}$$

- By employing $R_{equivalent}$ into the spring model equation, the film thickness value under the minimum region was achieved. It meant that this film value corresponded to the measured MOFT by the sensor while the true MOFT was actually zero.

- Hence when the separation was increased iteratively by certain amount ($h_{x_i+1} = h_{x_i} + \Delta y$) and the calculations given above were repeated for each case, the true MOFTs against measured MOFTs were achieved.

The results of the iterative calculations for the given ring profile (see Figure 6.6) used in this work were illustrated in Figure 6.30. As seen there was a more or less linear relationship between the measured MOFTs and true MOFTs. However, the non-linearity

of the spring model was observed when the true film less than half a micron, (see box A in Figure 6.30). In this case, 0.71 μm of the measured MOFT corresponding to zero true MOFT, was calculated for the ring profile used in the experiments. The measured MOFT correlated well with the data such that the minimum measured values during the reciprocating testing did not fall below 0.71 μm.

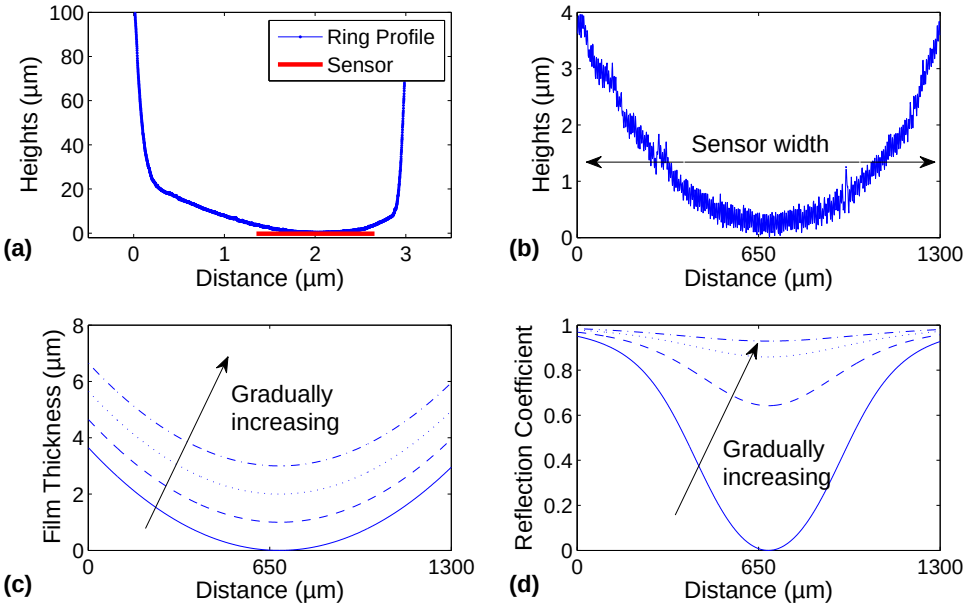

Figure 6.29: Correction steps: (a) ring and sensor, (b) the minimum film thickness region under the sensing area, (c) after filter, the film thickness plot under the region, (d) reflection coefficient corresponding to the film thickness plot in (c).

In these calculations, several assumptions were made. The transmission results from asperity to asperity contact assumed to be very small and negligible. The other assumption is that deformation in the contact was neglected. These are particularly realistic so long as the ring-liner contact operates in hydrodynamic conditions. The contact was assumed to be fully flooded with oil and no cavitation occurring in the contact.

Although the ring shape was measured accurately and the ring adapter was aligned to make sure it sat flat and parallel with the liner sample, it was possible that there was a small misalignment. On the other hand, in engine the piston ring could also be twisted

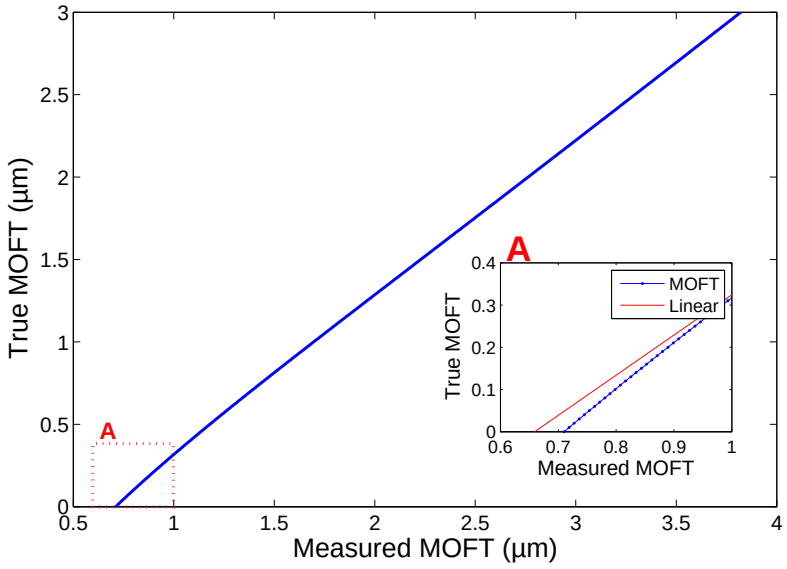

Figure 6.30: Correction of minimum oil film thickness measurement according to the profile of the piston ring.

and this would result in slightly different profile. Such misalignment and twisted ring profile could lead to a slightly different true film thickness. This was not considered in the de-convolution algorithm which assumed perfect alignment and contact geometry. Using this algorithm, the measured minimum film thickness data given in Figure 6.27 was modified and plotted in Figure 6.31 together with the original data.

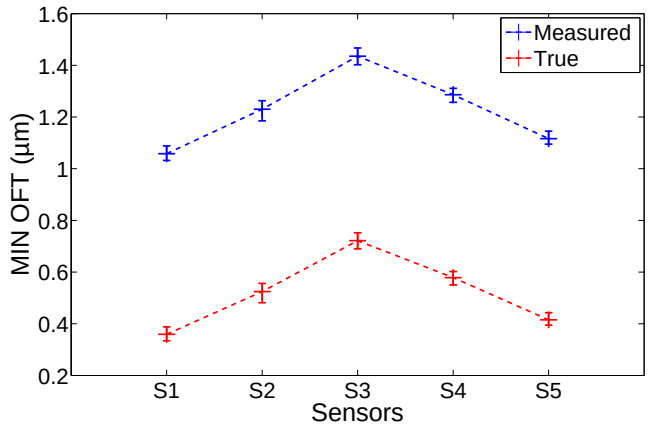

Figure 6.31: Minimum film thickness for down stroke after de-convolution process (Normal load: 140 N, reciprocating speed: 12.5 Hz).

6.8 Comparison of Experiment with Numerical Simulations

In this section, the measured minimum film thickness results will be compared with the values obtained from a numerical model. The model has been developed by Andrew Spencer at Luleå University of Technology. The overview of the reciprocating test condition is given in Appendix B2.

In the model, the Reynolds equation incorporating cavitation, a modified version of the Giacopini et al. [111] mass-converging cavitation algorithm was used. More precisely, a two dimensional time dependent solution of the averaged Reynolds equation was formulated as a Linear Complimentary Problem (LCP) where the usual Poiseuille and shear flows in Reynolds equation are replaced with flow factors which take into account surface topography. The problem is solved using the finite difference method in 2D with zero pressure boundary conditions at the edges of the domain. The flow factors were calculated using the technique described by Almqvist et al. [112] over a real measured area of cylinder liner surface topography. To model contact between the piston ring and cylinder liner a boussinesq-type elasto-plastic contact mechanics model was used to calculate average asperity contact pressure as a function of separation.

The minimum oil film thickness calculated with the numerical model was compared to the values measured at the five sensor locations. Figure 6.32 illustrates this data at a constant speed of 10 Hz with a low, medium and high load. Both the simulated and experimental plots showed the same trend in film thickness, where the MOFT increased towards the mid-stroke and reduced again as the ring came to a halt at the end of the stroke. The film thickness was skewed so that the maximum MOFT occurred just past mid-stroke. This was due to the time dependent nature of the oil film build-up. In general, ultrasonically measured MOFT varied between 0.25 and 1.8 μm. The numerical simulation slightly overestimated the minimum oil film thickness when compared to the ones acquired with the ultrasound technique.

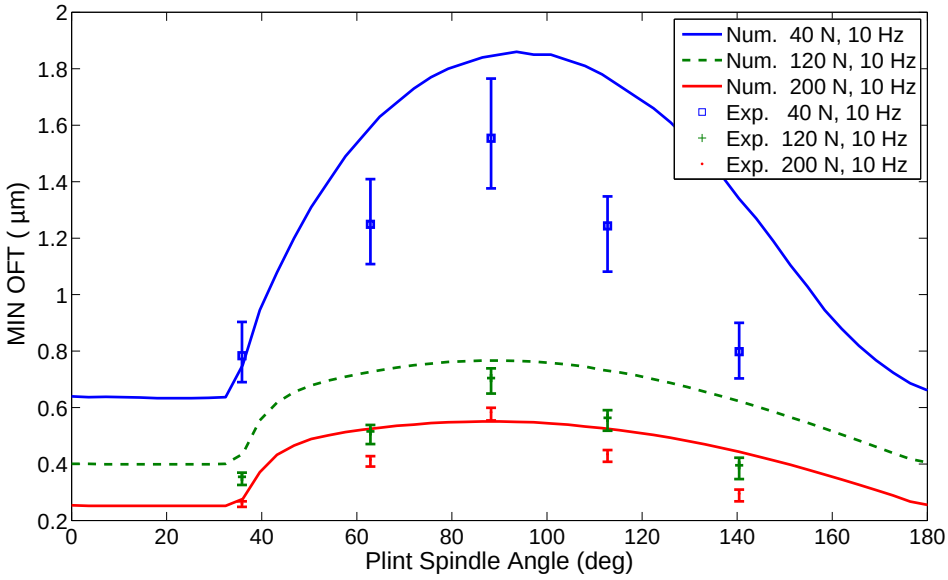

Figure 6.32: Comparison of calculated and measured film thickness at a constant speed of 10 Hz and loads of 40 N, 120 N and 200 N.

The model predicted almost constant minimum film thickness until approximately 35° spindle angle, this was due the sliding speed being too low to produce any significant hydrodynamic lift. At mixed lubrication regime occurred in medium and high load cases, there was a much closer match between simulation and experiment. However, for the low load case there was a greater difference at around mid-stroke where the sliding speed became sufficiently high and this allowed the surfaces to be separated by hydrodynamic effects. Any difference here (the maximum $\sim$0.55 μm) was most likely attributed to an inaccurate value of lubricant viscosity being used in the simulation, which was an estimate at 22°C based on the provided lubricant data. Any shear thinning or shear heating effects in the contact would lower the lubricant viscosity and lead to a lower film thickness in reality than that predicted by the iso-viscous model.

6.9 Conclusion

This chapter has demonstrated the application of the ultrasonic technique to the reciprocating bench test. The ring and liner sections were cut from the components of the heavy duty truck engine. Liner holder and also reciprocating head for the ring holder were both manufactured for this application. The ring-liner conformability was successively obtained and the conformal line contact across the liner width and through the stroke was shown with Fujifilm pressure paper.

The back of the liner section was instrumented with five piezo electric sensors. FFT analysis of the measurement signals showing the film thickness variation over the frequency was performed and the frequency independent region was presented for one ring passage. The successive reflections from the ring-liner contact were recorded while the ring reciprocated over the liner. Lubricant film thicknesses were calculated using the thin layer spring model.

The window size of the sensor was smaller than the ring width, so the film formed underneath the ring was measured. However, if the ultrasound wave is thought of as a series of discrete pulses over the sensor area, then their reflection depends on the ring profile in the sensor window and the cumulative results of reflections will be observed by the sensor. Thus, the obtained film thickness values are averaged by the sensor 'window'. To eliminate this effect on the minimum film thickness a de-convolution algorithm was put forward. The algorithm uses each discrete local thickness (*i.e.* between the liner and ring profile) and calculates the equivalent reflection coefficient. The true minimum reflection could be deduced from the reflection observed by the sensor.

Initial tests showed some fluctuations in the ultrasonically measured ring profile due to less oil availability and cavitation occurred in the contact. However, they only affected the tests in one sliding direction (*i.e.* up stroke) because of the ring profile which influenced the lubrication in the contact. The minimum film thickness variations over

the sensing areas were presented. The measured MOFT results were compared with values obtained from the numerical model. Overall the results were encouraging and the experimental data correlated reasonably well with simulation.

7

Parametric Study of Oil Film Thickness and Friction

In the previous chapter, the modified reciprocating test rig was introduced. The test rig provides simultaneous friction and oil film thickness data. This chapter presents the results of experiments which have been performed to understand the effect of normal load, reciprocating speed and viscosity on the lubricant film thickness. The transition of the lubrication regime at the ring-liner contact has been investigated at mid-stroke. In the final section, different liner samples ultrasonically instrumented with bespoke strips have been tested to investigate the effect of surface topography on the lubricant film.

7.1 Friction Measurement

A typical friction force measured by the friction transducer is shown in Figure 7.1a. This friction data was recorded at 120 N of normal load and 2.5 Hz of reciprocating speed. As seen, there were more than six cycles in the figure and the repeatability of the friction force trace was very good from cycle to cycle. Under the described instrumentation set up, it was not possible to obtain an absolute measure of the angle of rig spindle driving the scotch yoke mechanism. Thus the data in the figure was given in terms of data

points. However, there were sufficient and definite differences in the friction data and so an algorithm using a cross-correlation technique was written and performed on the friction data to identify the individual cycles. One complete cycle was selected by the user and it was cross correlated with the entire friction data set.

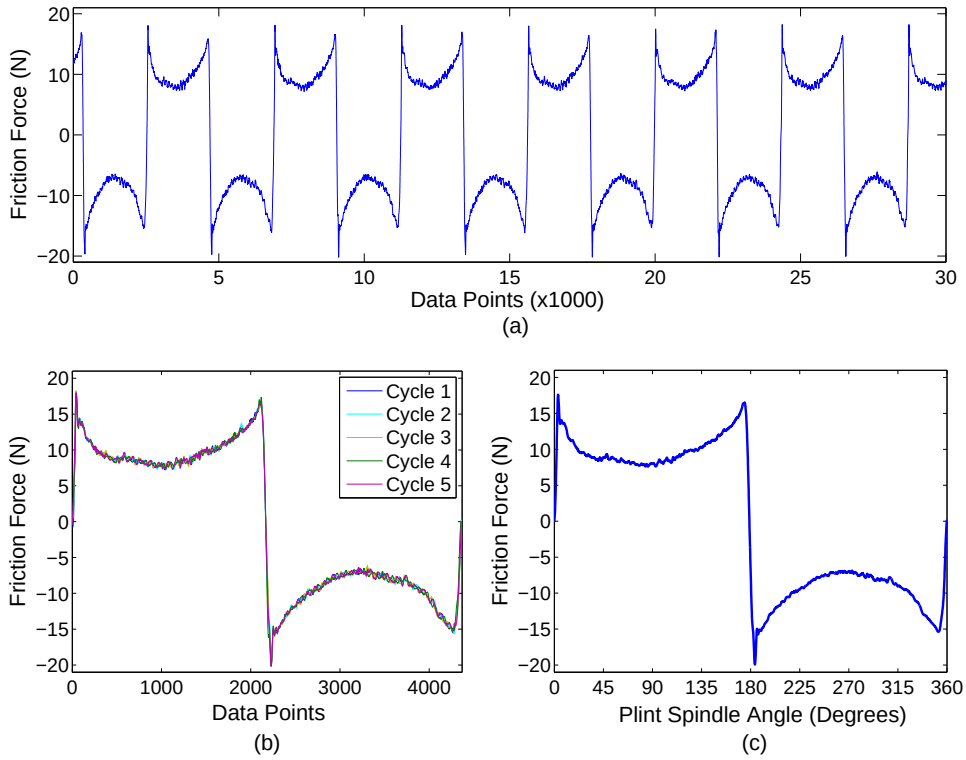

Figure 7.1: Graphs showing: (a) typical friction trace, (b) individual cycles and (c) mean friction force.

Figure 7.1b illustrates the five individual cycles from the friction data provided in Figure 7.1a and it is seen that all cycles have been well matched. Since the data capturing rate and the rotational speed of the plint spindle are constant, the horizontal axis (*i.e.* data points) can be replaced with plint spindle angles. The mean friction cycle calculated from all of the individual cycles is illustrated in Figure 7.1c where the negative sign simply indicates the direction of the piston ring stroke. This data represents one complete reciprocation of the piston ring. The friction coefficient can be calculated by dividing the friction force by the normal load between the specimens (see Figure 7.2). As seen, the friction is high at the reversal points where the contact operates in bound-

ary lubrication regime because of cessation of entraining motion. When the piston ring begins its movement with increasing speed, the lubricant film is formed in the contact. Thus, the friction reduces rapidly and reaches rather small in the mid-stroke (90°). While the ring is reaching near the end of the stroke (180°), the friction force rises again and then the same pattern occurs for the ring's return stroke (180° - 360°).

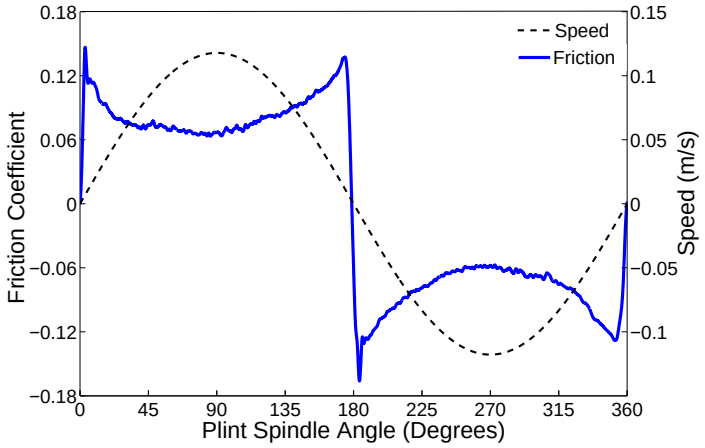

Figure 7.2: Friction coefficient for the ring operating under a load of 120 N.

7.2 Results

The standard production liner sample and the piston ring which were detailed in Chapter 6, were tested for nine different normal loads, from 40 N to 200 N with an increment of 20 N, and at seven different reciprocating speeds from 2.5 Hz to 17.5 Hz with an increment of 2.5 Hz. The piston ring sliding speeds at each sensor location and overview of the test conditions are given in Appendix B1-2. This test batch was repeated three times at room temperature and so the test matrix consisted of a 9x7x3 matrix, a total of 189 tests. The ring-liner contact was lubricated with base oil and the duration of each test was between three to ten second according to the sliding speed. A minimum of 25 cycles were captured for the lowest speed. Film thicknesses at five fixed sensor locations and friction data were simultaneously recorded for each test.

Figure 7.3 shows the minimum film thicknesses measured by sensors in a 3D plot. In the figure, data is presented in seven groups, each corresponded to one constant reciprocating speed test. The horizontal axes of these groups show the sensor numbers (*i.e.* from S1 to S5). As stated before, the each test has been repeated three times and so MOFT data points in the graphs show the average of these tests. The overview of friction results of the test matrix have been given in Figure 7.4. The data presented here is the average friction coefficient and for each test it was obtained by dividing the friction force (*i.e.* the RMS signal giving the friction force in oscillating sliding) by normal load.

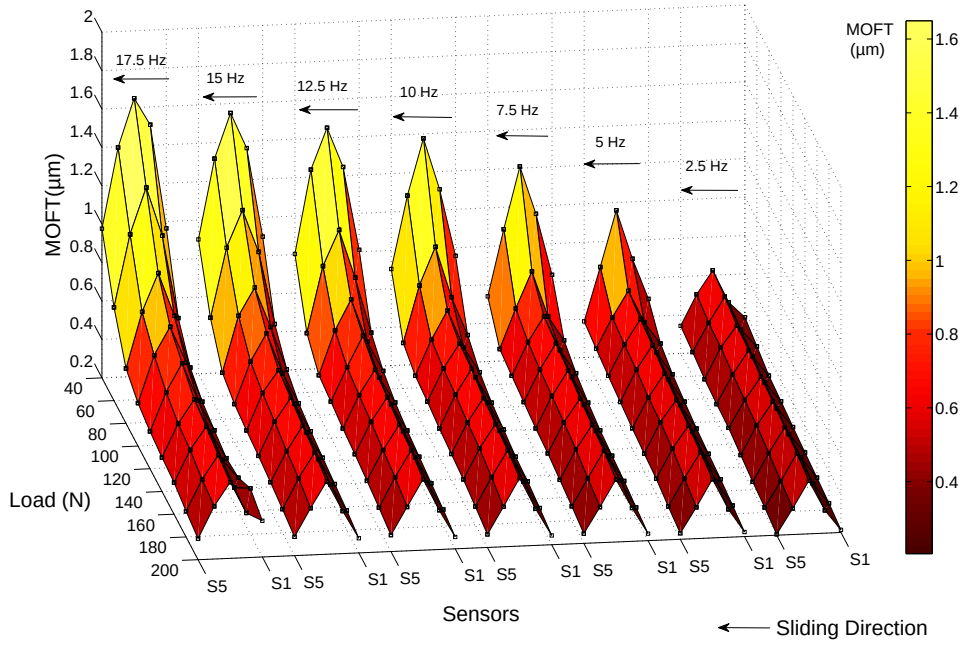

Figure 7.3: Average MOFT values measured by sensors for the test matrix.

The minimum film thickness and friction data are consistent such that if seven groups are considered, the minimum film thicknesses measured by sensors were formed as the reciprocating speed was the lowest. This is consistent with the friction data in which the highest friction occurred in the tests carried out at 2.5 Hz. Additionally, under low loading and high reciprocating speed, the minimum film thicknesses in the contact

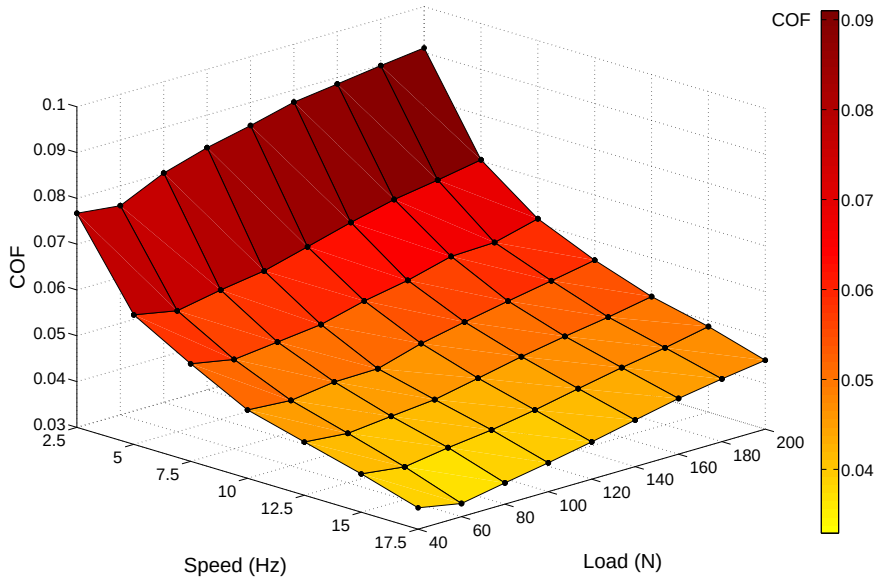

Figure 7.4: Mean coefficient of friction for the test matrix.

increase and it is expected to result in less friction as seen in Figure 7.4.

The relation between minimum film thickness, h_{min}, and the combined surface roughness of the samples is defined by the dimensionless film parameter, λ^*, or known as the lambda ratio. This ratio gives an indication of the possibility and severity of asperity interaction and wear [113].

$$\lambda^* = \frac{h_{min}}{\sigma^*} \tag{7.1}$$

where σ^* is the combined roughness of the two surfaces defined by,

$$\sigma^* = \sqrt{{\sigma_R}^2 + {\sigma_L}^2} \tag{7.2}$$

where σ_R and σ_L are the r.m.s. roughness of the ring and liner. If a value of 'λ^*' is more than 3, it suggests full film lubrication with no asperity contact. If its value is between 1 and 3, this suggests mixed lubrication whereas the value less than 1 indicates boundary lubrication regime [114].

Using the surface parameters of the specimens (given in Chapter 6), the combined surface roughness was calculated as 0.35 μm. Since the minimum film thickness was measured, the lambda ratio could be obtained from Equation (7.1). As seen from Figure 7.3, the MOFT values varied approximately from 0.3 to 1.5 μm, this is equivalent to the lambda ratio from 0.85 to 4.2. This suggests all three lubrication regimes occurred in the test matrix. However, mostly the contact was in the mixed lubrication regime. Measured friction coefficients in the range 0.03 to 0.09 also support this.

7.2.1 The Effect of Speed

To illustrate the effect of speed on film thickness formation, some tests results at 60 N are selected from the overview graph and given in Figure 7.5. The results indicate that increasing the ring sliding speed enhances the wedging action of the converging ring profile, providing better load carrying capacity and a thicker lubricant film. This trend is also seen for individual test data. At the beginning of the stroke a thin lubricant film was formed in the contact, for instance, the minimum film thickness was measured as 0.55 μm at Sensor-1 when the Plint was running at 12.5 Hz. However, as the sliding speed of piston ring increased and allowed the lubricant film to develop between the surfaces, the film thickness was increased to $\sim$1 μm at the location of Sensor-2. Then

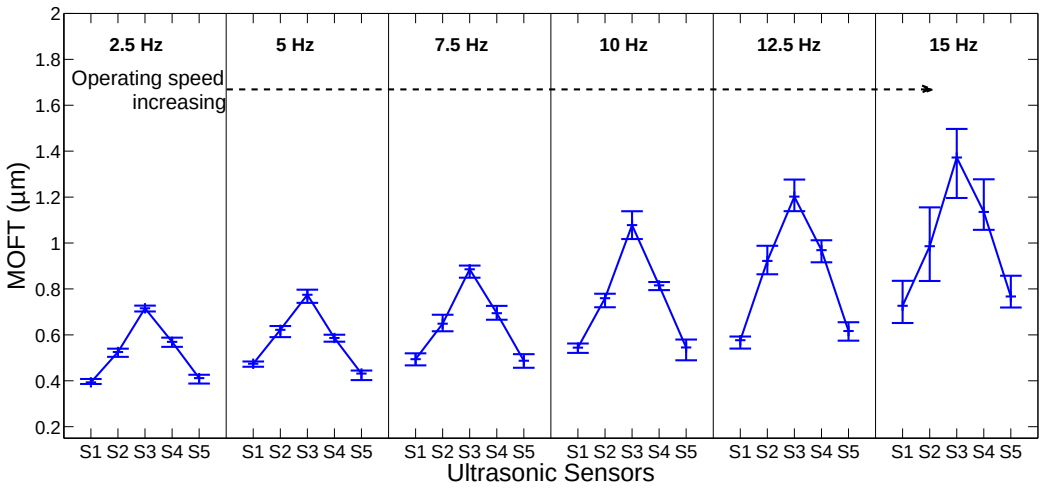

Figure 7.5: Measurement results of minimum film thickness for different operating speeds.

the thickest film in the stroke, 1.25 μm, was measured at Sensor-3 where the sliding speed was greatest in the stroke. As the piston ring decelerated towards BDC, thick oil film conditions between ring and liner could no longer maintained leading to a reduction in film thickness. 1.05 and 0.6 μm were measured respectively by Sensor-4 and Sensor-5.

Figure 7.6 shows a comparison of the experimental friction of the piston ring-liner contact for different operating speeds. As a general trend, the friction force decreases with increasing ring sliding speed. Analysing the results, it seen that this trend is limited at around mid-stroke such that there is no longer as reduction in friction force beyond 7.5 Hz and further increases in sliding speed does not seem to affect the friction force. However, it is noticeable that the trend begins to become distinguishable again towards the end of strokes. This is expected since the frictional force due to asperity interaction is generally much larger than viscous losses [103]. Therefore even a small increment in film thickness at near dead centres creates a difference in friction force due the less asperity pressure in the contact.

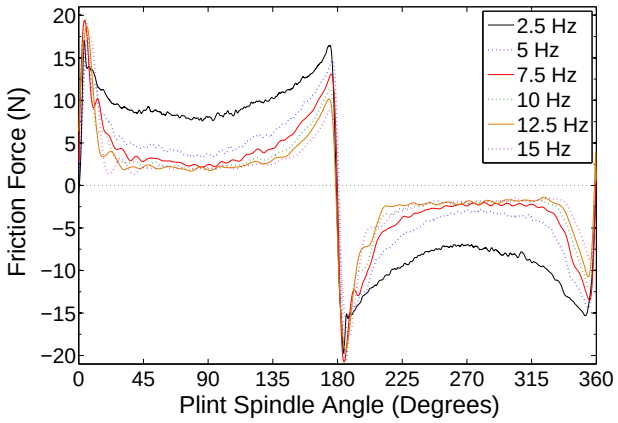

Figure 7.6: Measured friction force between piston ring and liner contact for different operating speeds.

The hydrodynamic effect is evident in Figure 7.7 illustrating friction force between piston ring and liner under two contact conditions, dry and lubricated. In dry conditions, the asperities of the matching surfaces are purely in contact and the friction force is almost independent of the sliding velocity. General frictional behaviour may be influenced by

the surface roughness, temperature, presence of moisture, oxygen and other surface contaminants [115]. However, if there is lubricant between the liner and ring, there is large friction falls due the low shear lubricant film developed by hydrodynamic action as the piston ring speed increase. It should be note that the maximum value of the friction spike at dead centres does not exceed the dry friction force.

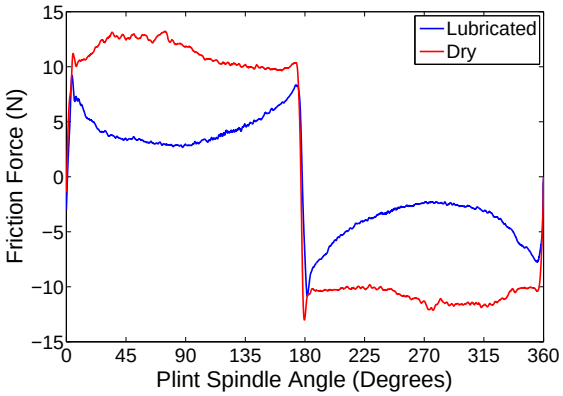

Figure 7.7: Comparison of dry and lubricated friction.

7.2.2 The Effect of Load

The loading effect on film thickness measurement is illustrated in Figure 7.8 which shows the minimum film thicknesses for three loading conditions, 60, 120 and 180 N, while the ring reciprocates at 7.5 and 15 Hz. The minimum film thickness measured at each sensor location decreased when the applied normal load increased. This trend can be seen from the general view of the test matrix (Figure 7.3) as well. It should be noted that the rate of reduction of film thickness became smaller as normal load increased. By increasing applied load, more asperities were in contact and this resulted in no further decreasing in the film thickness.

The effect of load on friction can be seen Figure 7.9, illustrating the different loading conditions of the ring-liner contact at a reciprocating speed of 7.5 Hz. The lowest friction during the stroke was observed for a low load of 40 N. As expected, the friction force was increased with increasing the normal load.

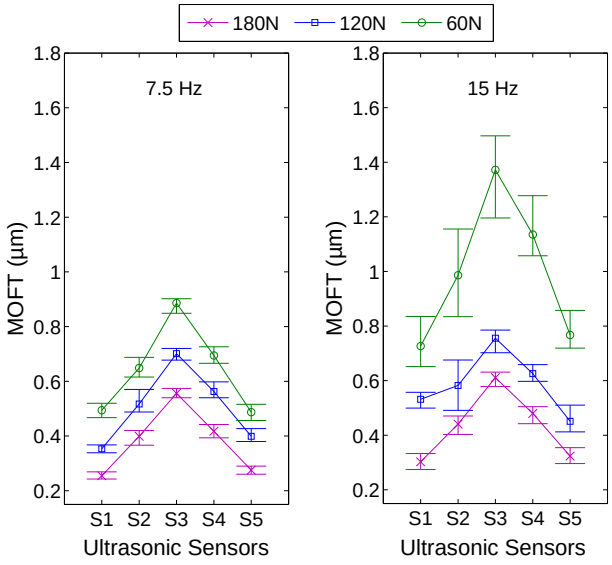

Figure 7.8: Measurement results of minimum film thickness for different normal loads.

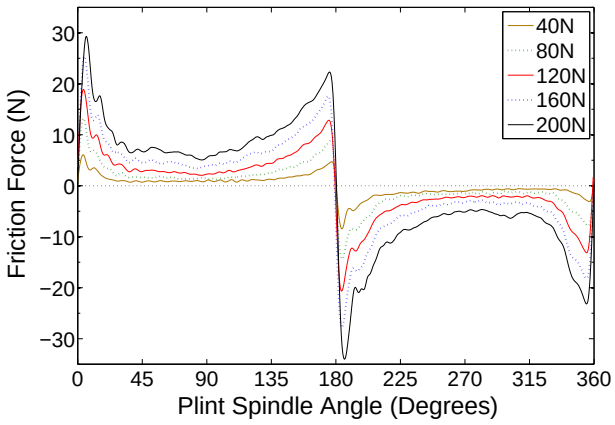

Figure 7.9: Friction force measurements at consant operating speed for different loading conditions.

7.2.3 The Effect of Viscosity

Lubricant viscosity significantly influences the performance and fuel economy of an engine. Using standard liner sample, additional three lubricant samples, S20, S200 and S600 (from Cannon Ltd.) viscosity standards, which are mineral oil (%100) were also tested under several loads and reciprocating speeds in order to investigate the effect

of viscosity on oil film formation in the simulated piston ring-liner contact. Table 7.1 shows the properties of these lubricants.

Table 7.1: Properties of the lubricants used in the tests.

	Base Oil	S20	S200	S600
Kinematic Viscosity (cSt.) at $40°C$	37	17.9	179.6	507.5
Kinematic Viscosity (cSt.) at $100°C$	6.5	3.7	16.5	32.7
Density (g/ml)	0.843	0.863	0.879	0.891
Speed of Sound (m/s) at $20°C$	1440	1445	1482	1521

Figure 7.10 shows the measurements of the mean friction and MOFT at the sensor locations for these three lubricant samples under a normal load of 120 N at 7.5 Hz operating speed and a normal load of 200 N at 12.5 Hz, respectively. The mean film thickness results show similar trends for both Figure 7.10a and 7.10c. As expected, the lubricant with lowest viscosity, S20, produced the smallest film formation at all sensor positions since it had less load carrying capacity. The mean MOFT was generally less than 0.5 μm with an exception at mid-stoke where there was a little increment in the MOFT. The mean friction data was also support this. The reduction in shear loss at mid-stroke and increase in friction near the end of the stroke can be seen in both cases (see Figure 7.10b and 7.10d). The highest friction force over the stroke was recorded for S20 as compared to the other samples.

It is seen from the figures that the mean MOFT increased when the contact lubricated with S200 which is more viscous sample than S20. The range of mean MOFT was approximately between 0.5 and 1 μm. The thickest film was occurred at mid-stroke where the sliding speed is highest in the stroke. Due to its relatively high viscosity, the change in mean MOFT during the piston ring strokes is more prominent than that of S20. Less friction force was observed for S200 and it was smooth throughout the stroke (apart from the dead centers) since the mean MOFT were raised.

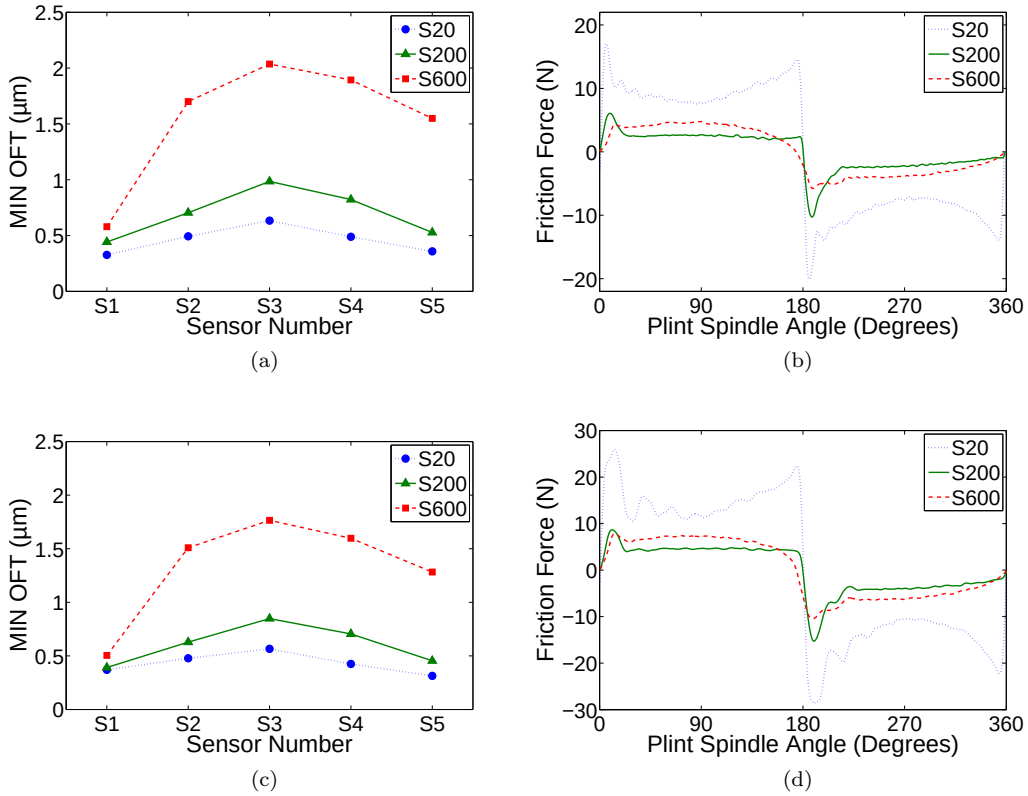

Figure 7.10: Friction and MOFT measurement results for different lubricant samples: (a) minimum oil film thickness results at 120 N and 7.5 Hz, (b) friction force at 120 N and 7.5 Hz, (c) minimum oil film thickness results at 200 N and 12.5 Hz, (d) friction force at 200 N and 12.5 Hz.

The thickest oil film over the stroke was observed for S600 which was a more viscous lubricant. The mean MOFT was initially measured at around 0.5 μm then it increased rapidly to above 1.5 μm at Sensor-2. The maximum film thickness occurred at mid-stroke and was approximately four times greater than the other samples. This thick oil film was maintained towards the end of the stroke and interestingly, there was no considerable drop in the mean film thickness at near BDC (*i.e.* Sensor-5) when compared to the other two lubricant samples. This was presumably due to the high viscosity leading to less oil transport under the ring. This was also consistent with the friction data of S600. Friction force increased at the mid-stroke due to the viscous force of the thick

lubricant film and the peak friction force at BDC was not observed due to the thick film present. This type of friction profile was also introduced by Cho et al.[116] and it is suggested that a thick film would not be completely squeeze out even at dead centers, hence hydrodynamic lubrication is possible over the entire stroke.

Figure 7.11 shows the minimum film thickness under the ring at mid-stroke as function of viscosity. As seen, an increase in the oil viscosity results in a thicker film. Although the data is given for several reciprocating speeds at a load of 120 N, this general trend has been observed in all tests carried out in this study.

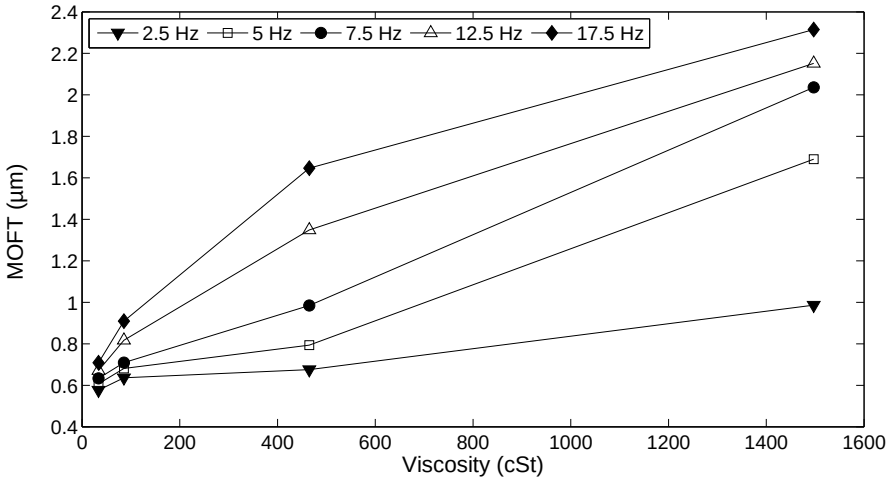

Figure 7.11: Minimum film thickness under the piston ring as a function of oil viscosity.

7.3 Transitions of the Lubrication Regime at the Ring-Liner Contact

During reciprocation of the piston ring, the lubrication regime between the ring and liner is varying through boundary to hydrodynamic regime. In this section, the lubricant regime transition under the ring was analyzed using the Stribeck diagram. Since the measurement system allowed the lubricant film thickness and friction data to be recorded simultaneously, correlations between the lubricant film and friction could also be drawn.

Figure 7.12 shows sample measurements of mean MOFT and friction coefficient results for down stroke (half cycle) together with a plot of the ring sliding speed across the stroke. As it seen the ring sliding speed variation is very small at mid-stroke (*i.e.* Sensor-3) when compared to the other sensor locations. Therefore only mid-stroke data from the previous experiments were used.

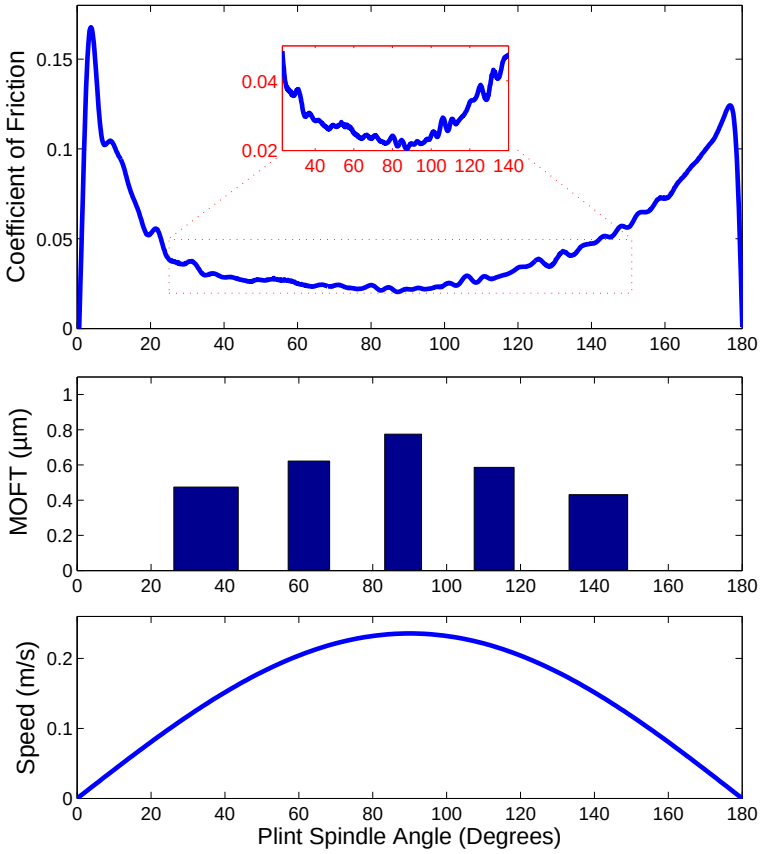

Figure 7.12: Measured minimum oil film thicknesses and friction together with the piston ring speed across the down stroke for a Plint reciprocating speed of 5 Hz and a load of 60N.

7.3.1 Stribeck Diagram

A typical Stribeck diagram, which relates the friction coefficient to the dimensionless parameters known as the Sommerfeld number, has already been presented briefly in Chapter 1. In this section, the Stribeck diagram will be detailed for the piston ring

application and the experiments carried out previously were placed into the Stribeck diagram to show the combined effects of oil viscosity, sliding velocity and normal load pressure on friction.

Stribeck diagrams are frequently used as a convenient tool to analyze the lubrication and wear performance for journal bearings [117]. However, this diagram is not really applicable for the ring-liner interface because it was originally developed using the journal bearing test results. During the piston stroke, the piston speed is varying due to the crank connecting rod mechanism and the ring contact pressure is changing according to the engine load. The dimensionless bearing parameters cannot, therefore, represent the entire stroke of the piston assembly. Ting [102] introduced the looping-type Stribeck diagram using the modified bearing parameters by substituting the rate of rotation for the instantaneous speed of piston. This relation is given,

$$S = \frac{\mu U}{PL} \tag{7.3}$$

where, μ, is the dynamic viscosity of the lubricant, U, is the sliding velocity, P, is the normal pressure load and , L, is the reference length. Dearlove [29] suggests that the appropriate reference length would be the ring face width.

From the relations given above, the non-dimensional group, S, was calculated for each tests performed previously and the results plotted in a Stribeck diagram. Figure 7.13 illustrates the friction coefficients at mid-stroke versus the non-dimensional group. Figure 7.13 appears similar to the Stribeck diagram given in Chapter 1 and it can also be seen that all three lubrication regimes were observed at mid-stroke. As oil viscosity and the ring sliding speed are low, meaning that the Sommerfeld number is small, the coefficient of friction can reach up to 0.11. Thus in this region, the frictional behaviour of the piston ring falls within the boundary lubrication regime. Less applied normal load or increment in sliding speed and viscosity lead to increase in the dimensionless parameter. As the Sommerfeld number increases, the lubrication regime shifts towards

mixed-lubrication regime and the coefficient of friction decreases down to a minimum of 0.014. The friction coefficient begins to increase again with further increase in the dimensionless parameter. This indicates that the regime falls into hydrodynamic lubrication and the increment in the friction could be attributed to the viscous shear losses in the thick lubricant film.

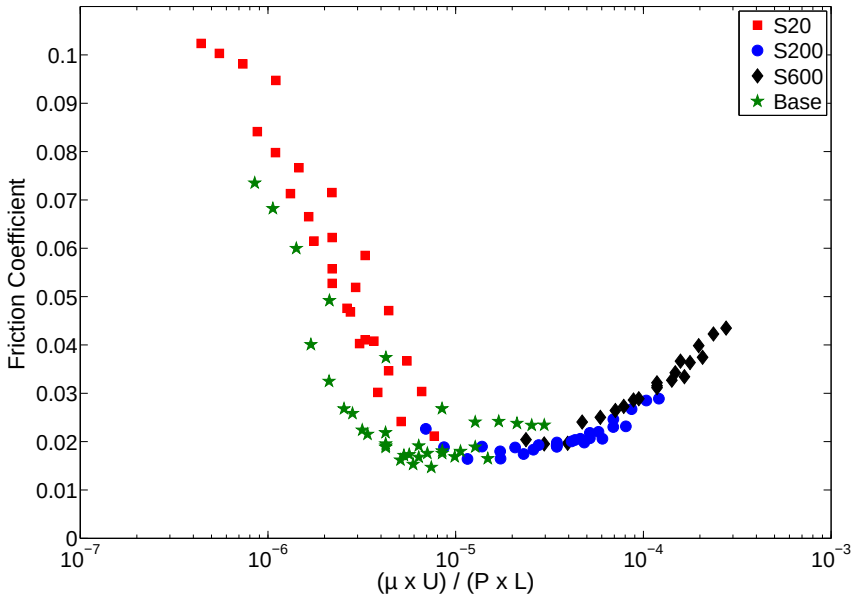

Figure 7.13: Stribeck diagram at mid-stroke for all the test results from the experiments; note that the modified Sommerfeld number was based on the ring face width.

7.3.2 Correlation between Minimum Lubricant Film Thickness and Friction

The friction and film thickness values measured at mid-stroke during the previous tests were plotted in Figure 7.14. The form of the curve is very similar to the typical shape of a Stribeck curve. The figure shows a clear trend that when the film thickness was higher than roughly 1.2 μm, the friction force tended to increase. At this point, the existence of relatively thick lubricant films prevents the asperity interaction and only oil viscous drag contributes the friction coefficient. Thus thicker film increase the viscous drag and hence the friction coefficient. Additionally, at the same film thickness, more viscous

lubricant showed a higher friction coefficient value than the other lubricants because of the high viscous forces.

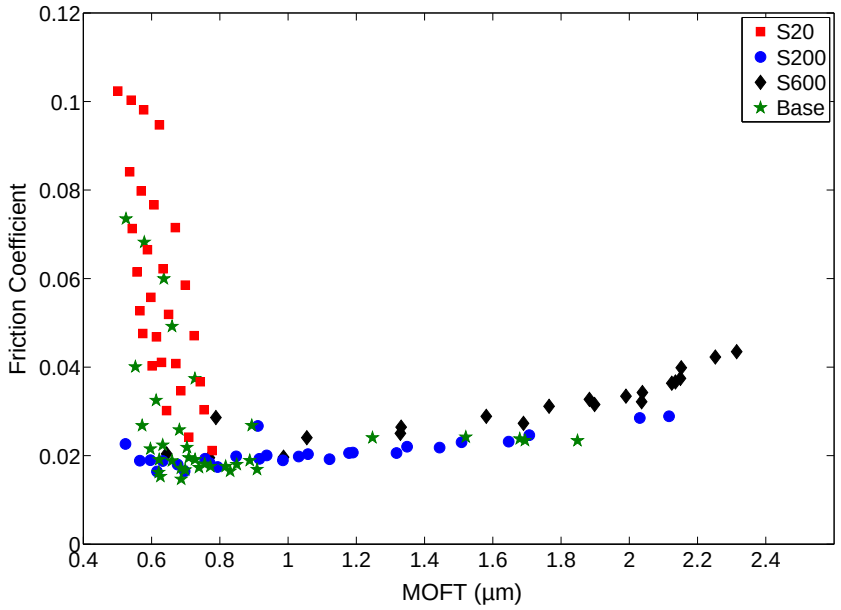

Figure 7.14: A variation of friction coefficient with minimum film thicknesses measured throughout this study.

It seen that there is a rapid increase in friction when the oil film thickness falls below 0.8 μm. This would represent the termination of hydrodynamic lubrication. In the film thickness region between 0.6 and 0.8 μm, the normal load is supported partly by the asperities solid contacts and partly lubricant film pressure in the contact. Therefore, friction coefficient is not exclusively caused by fully hydrodynamic characteristic and shows mixed behaviour. This also influences the ultrasonic film measurements since the technique yields only a combined liquid oil and asperity stiffness. However, it was found that most of the contact stiffness at close to dead centres (72-83 %) was attributed the liquid parts and it could be even more at mid-stroke due to the less asperity contacts occurring. Therefore, this may lead to underestimate of film thickness (*i.e.* roughly less than 20 %). The combined contact stiffness and the investigation detail are presented in Appendix B2.

7.4 Different Liner Specimens

Surface characteristics of the piston ring and cylinder liner are also a very important factor for the functionality of the IC engines; particularly cylinder liners require critical surface properties to achieve an effective engine life [101]. If the cylinder liner is very smooth and polished, it is not be able to retain oil and will have poor tolerance for wear debris leading to high wear and scuffing. On the other hand, rough liners in spite of having good oil retention capacity, would have high friction coefficient and wear rate. Thus optimum properties are required.

To investigate the effect of the liner surface finish on film thickness and friction, like the standard liner sample used in previous tests, another two liner samples were cut from the same place of each liner, *i.e.* around mid-stroke. They were from the same heavy duty diesel engine (a bore diameter of 130 mm) and also been run-in a fired engine by Scania. These liner samples were instrumented with five ultrasonic sensors by following the procedure given in sensor preparation section in Chapter 6. The sensor positions of each liner samples over the stroke are given in Table 7.2.

Table 7.2: Sensor positions over the stroke, (mm)

	Liner 1 (Std)	Liner 2	Liner 3
TDC	0	0	0
Sensor-1	1.42	1.42	1.44
Sensor-2	4.08	4.30	4.21
Sensor-3	7.27	7.39	7.13
Sensor-4	10.4	10.20	9.72
Sensor-5	13.28	13.20	13.17
BDC	15	15	15

All the liner samples were made from grey cast-iron. While the standard liner sample 1 and liner sample 3 had cross-hatch angle of 55°, liner sample 2 had cross-hatch angle of 35°. The liner sample 3 was ANS Triboconditioning® liner. The ANS triboconditioning

method is a dedicated metal finishing process. It combines elements of extreme-pressure mechanical burnishing of the component surface with a tribochemical deposition of a low-friction antiwear film of tungsten disulfide (WS_2) [118, 119]. This process is incorporated into the honing process with the use of a special honing tool and process fluid. The method modifies the liner surface due to the smoothing the asperities and coated with a layer of tungsten disulfide. The surface parameters of the samples were measured using a stylus surface profilometer. Severeal measurements were taken from the samples and the average of these measurements are given in Table 7.3. The microscopic images of the cylinder liner surfaces have been illustrated in Figure 7.15.

Table 7.3: The surface roughness values of samples

	Liner 1 (Std)	Liner 2	Liner 3
R_a (μm)	0.32	0.38	0.28
R_{pk} (μm)	0.13	0.17	0.10
R_{vk} (μm)	1.32	1.62	1.36
Honing Angle (Degree)	55°	35°	55°

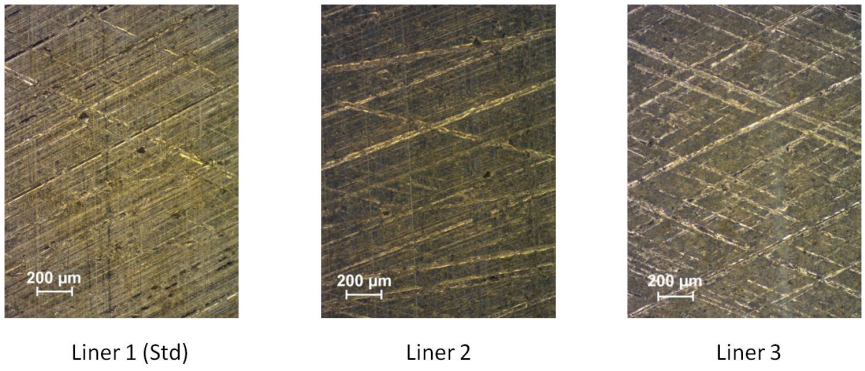

Figure 7.15: Surface images of the liner samples used in the tests.

In experiments, base oil was used as a lubricant and test conditions was the same as applied to the previous tests with the standard liner sample. According to the measurement results, the thickest lubricant film over the stroke, generally, was formed for the standard liner sample (denoted as 'STD') when compared to the other samples. However, particularly for the high speed and low load case (see Figure 7.16) where hy-

drodynamic film pressure was enough to separate the contact, and the surface interaction between the ring and liner was less; the film thickness difference between the samples was small and in general, minimum lubricant film thicknesses for the liner samples were very similar. Sample 1 and sample 3 (denoted as 'WS2') with smoother surfaces had a slightly thicker film (*i.e.* by roughly 0.1 μm) than Sample 2 (denoted as '145'). The smoother, especially less-peaked surfaces provide more hydrodynamic support and allow the lubricant film build up easily [120]. Michail and Barber [108] reported that in hydrodynamic regime, oil film thickness increased as the roughness decreased, but the differences in oil thickness were small about 0.05 to 0.125 μm. This was consistent with the results in Figure 7.16.

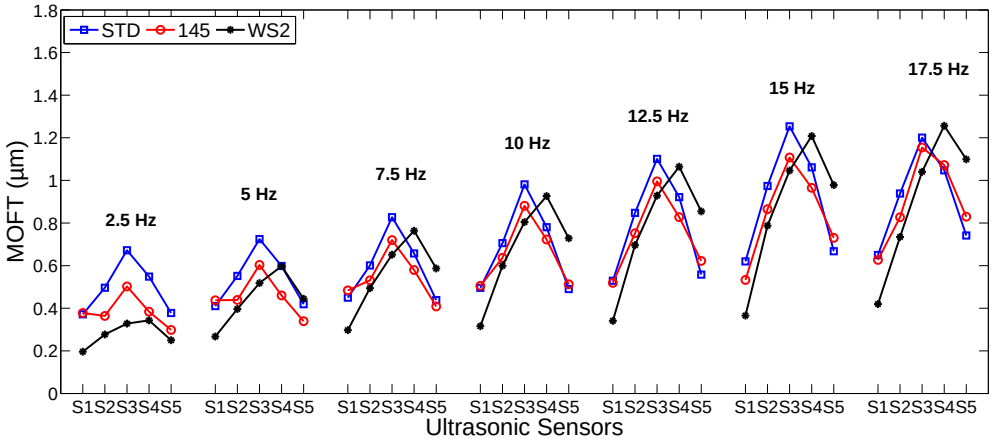

Figure 7.16: Mean minimum lubricant film thickness measured by sensors for the liner samples with different surface texture for a range of speeds (Load:60 N).

In the literature, there are very few works that have investigated the effect of honing angle on lubrication performance. Analytical published works [108, 121, 122, 123] suggested that decreasing honing cross-hatch angle increases the predicted lubricant film thickness. Recently, Spencer et al. [123] investigated the effect of honing angle (HA) on the hydrodynamic lubrication between the piston ring and liner numerically and highlighted that the variation in minimum film thickness with honing angle was minimal (about 20 nm variation was observed). Conversely, the results in Figure 7.16 indicates that MOFT of the 55° HA standard liner had always thicker than that of 35° HA liner

sample 2. However, it should be highlighted that the other surface properties of the samples were not the same such that they had different surface roughness, groove density etc. Therefore, the outcome would be the combination of these parameters.

Figure 7.17 shows the measurement results for a normal load 120 N. As it seen, the minimum film thickness variation between the samples is more prominent for low reciprocating speeds. The smallest film thicknesses were measured for liner sample 3 (WS2) which had smoother surface. This is probably because when the reciprocating speed decrease and the applied normal load increase, the lubricant more likely goes in mixed or boundary lubrication regime. The asperities are in contact; therefore, less peaked surface creates small separation. Interestingly, the lubricant film formed over the standard liner sample 1 was thickest across the tests. This is likely because of its groove density (due to the honing angle) and depth of the grooves. If liner sample has deeper machining grooves and high groove density, this would allow more volume of oil to escape from the contact. The depth of the grooves and the number of grooves were smaller for the standard liner. The lubricant oil could be trapped and compressed in the ring-liner contact, so hydrodynamic pressure is generated and this gives thicker lubricant films. This tendency for the grooves to channel the lubricant away from contact

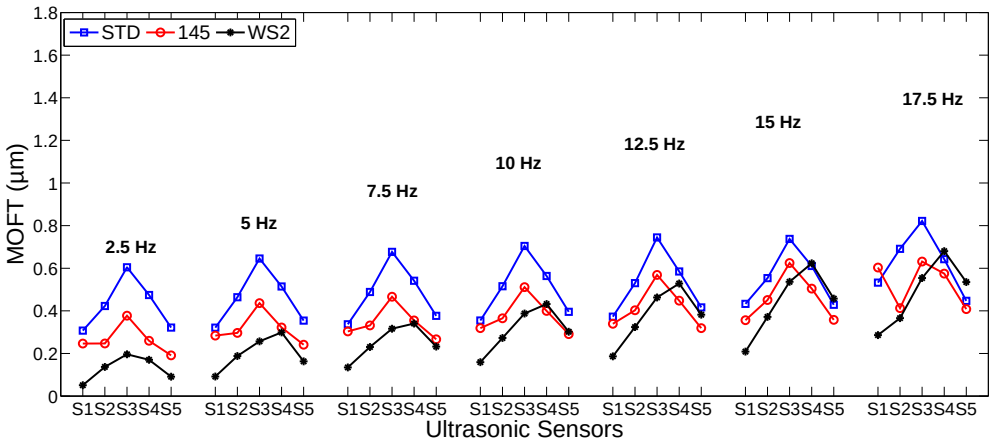

Figure 7.17: Mean minimum lubricant film thickness measured by sensors for the liner samples with different surface texture for a range of speeds (Load:120 N).

has also been reported in some published works [124, 125].

Following figures give comparisons of the friction cycles of the liner samples for two different constant loads of 60N and 140 N, but with a low speed of 5 Hz, a medium speed of 10 Hz and a high speed of 15 Hz. In general, there was no obvious difference between the liner samples especially for hydrodynamic conditions. Liner sample 1 and liner sample 2 (*i.e.* 145) followed the similar trend for almost all the tests; however, in boundary and mixed lubrication regimes, the friction force between liner sample 3 (*i.e.* WS2) and the piston ring was lower than the other samples.

For low load and high speed conditions, the effect of surface topography had little effect on the friction force, particularly at mid-stroke. It is seen from Figure 7.18 that these test samples have more or less the same friction data. As shown in Figure 7.16, there was a full film lubricant between the ring and liner at mid-stroke, therefore viscous force dominated the contact. Similar findings have been reported in previous experimental

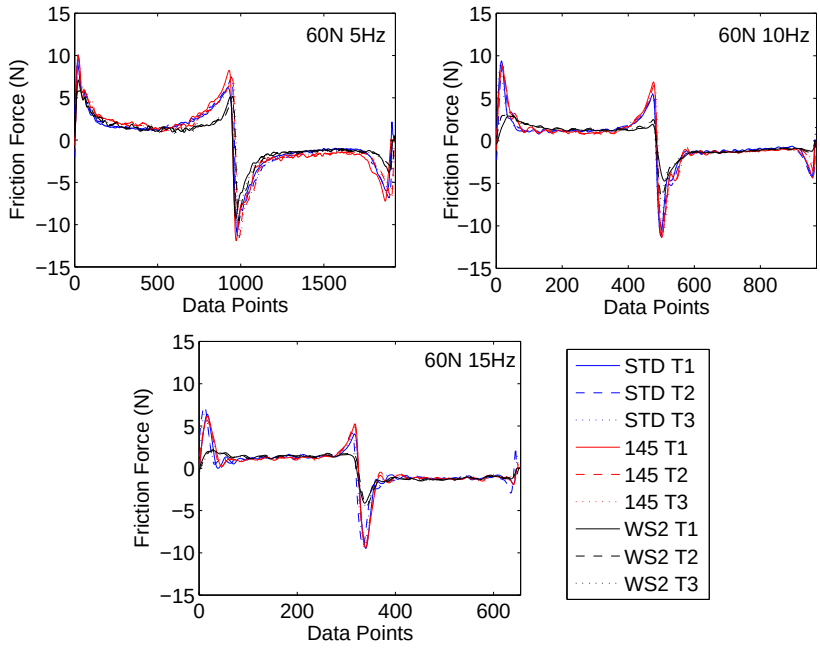

Figure 7.18: Measured mean friction cycles of test liner samples for a constant load of 60N and speeds of 5 Hz, 10 Hz and 15 Hz.

work carried out by Costa and Hutchings [124]. They tested patterned plane steel surfaces (*i.e.* circular depressions, grooves and chevrons) against cylindrical counter bodies under conditions of hydrodynamic lubrication and the film thicknesses measured by capacitance method. It was reported that the samples produced similar friction even though there was presence of significant changes in film thickness. Petterson [125] suggested that friction was rather insensitive to texturing when an ample amount of lubricant was supplied. It was also reported that whenever there was a full film between the surfaces, surface texturing did not significantly have an influence on friction.

It is important to note that the liner sample 3 (WS2) always had smaller friction peaks through dead centres when compared to the other samples. This behaviour was typical for all the tests carried out during study. This is because the sample 3 has a coating on its surface giving low shearing force. This is further evident for mixed and boundary conditions (see Figure 7.19). Although the liner sample 3 has small film thickness values, it produces smaller and smoother friction trace.

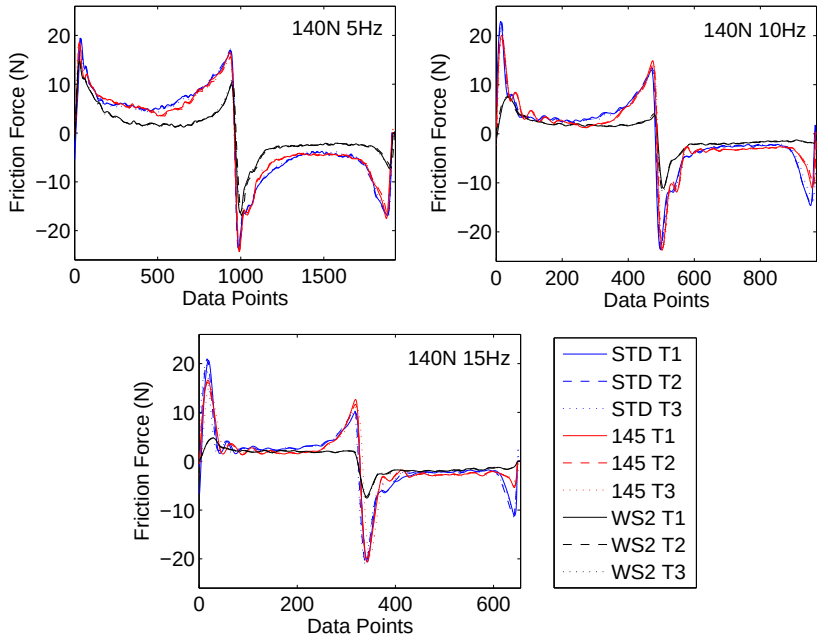

Figure 7.19: Measured mean friction cycles of test liner samples for a constant load of 140N and speeds of 5 Hz, 10 Hz and 15 Hz.

The effect of groove texture patterns on friction was numerically studied by Mezghani et al.[126] and showed that the minimum friction was obtained for a honing cross-hatch angle range 40° - 55°. However, in the other work [121] it was also reported that decreasing the honing cross-hatch angle decreased predicted ring-pack friction. The interesting point appeared in this work, even though thicker film thickness values were observed for the standard liner 1 with HA 55°, there was no significant difference in friction when compared to the liner 2 with HA 35°.

7.5 Conclusion

Using the modified reciprocating test rig, the piston ring and liner samples were tested under several operating conditions. The experimental results of ultrasonically measured film thickness and friction between the piston ring and cylinder liner were presented in this chapter. 3D measured film thickness and friction maps were plotted out for the standard tests components.

The results support the hydrodynamic lubrication theory and trends in the measured film thicknesses correlate to measurements of friction. Thicker film thicknesses were formed between the ring and liner for the low load and high sliding speed conditions, since thick film lubricant prevents the asperity interaction, low friction was observed. When the applied load was increased, the measured minimum film thickness decreased and therefore friction force in the contact increased. All three lubrication regimes were observed in the test matix and MOFT measurements for the standard liner were in the range of 0.3 to 1.5 μm.

Three lubricant samples with different viscosity properties were tested using the standard liner sample. It was found that the more viscous oil produced a thicker film in the contact. The transitions of the lubrication regime at the ring-liner contact were observed from the Stribeck diagram modified using the ring face width. The correlation between the friction coefficient and minimum oil film thickness at mid-stroke were

plotted out for all test results from the experiments. A rapid increase in friction when the lubricant film falls below 0.8 μm was found. It is believed that the asperity contacts begin to dominate the contact at this point. Additionally, when the film thickness is above 1.5 μm, higher friction coefficient were experienced.

Different liner samples were also instrumented with ultrasonic sensors and tested. The results suggest that for hydrodynamic lubrication case, the liner surface finish does not have a great influence on film thickness formation and also on friction due to the full film separation. The minimum film thickness variation between the samples was more prominent for mixed and boundary lubrication regime. For low reciprocating speeds and high loading case, the smallest film thickness measured for ANS triboconditioned liner® sample which had smoother surface. Even the triboconditioned liner sample had small film thicknesses; it had smaller friction trace due to low shear coating on its surface.

8

Ultrasonic Film Thickness Measurement in a Fired Engine

This chapter describes the application of the ultrasonic method to a four-stroke single cylinder gasoline engine. This was a collaboration work with Loughborough University and Robin Mills at University of Sheffield. The water-cooled cylinder barrel was ultrasonically instrumented at three locations; thrust, anti-thrust and one of the neutral sides. The oil film thickness measurements were taken in fired conditions. The reflection coefficients of the ring packs were produced successfully, however, in some cases, particularly for exhaust and intake strokes, the ultrasonic data was very noisy and impossible to detect the signal. Three loading conditions, 25, 37 and 42 Nm, were tested at an engine speed of 3200 rpm. The results showed that the minimum film thicknesses were formed over the liner during power stroke. At the beginning of the stroke the film thickness was less than 1 μm, but as the piston speed increased thicker lubricant films occurred up to 4 μm.

8.1 Test Apparatus

8.1.1 Test Engine

The Honda CRF450R engine designed for motocross bikes, was used in this work (based at a test cell in Loughborough University). It is single cylinder and 4-stroke engine. It has an over-square design, which means that the diameter of the cylinder is larger than the piston stroke. An engine crankshaft chain drives a single overhead camshaft which controls totally 4 valves (*i.e.* 2 for inlet and 2 for exhaust) via rocker arm system. The stroke of the engine is 62.10 mm and the volumetric displacement is 449 cm^3. This would generate a power of 41 kW (55 hp) at 9000 rpm. The engine is water-cooled and lubricant oil is delivered to the engine parts by an oil pump and oil splashing method. The brief key details of the engine are given in Table 8.1. In early work, this test engine has been used for the measurement of oil film between the piston skirt and cylinder [127]. At a single point, skirt oil film thickness was measured in the range of 2 to 21 μm. However, the skirt is a much larger target than the rings.

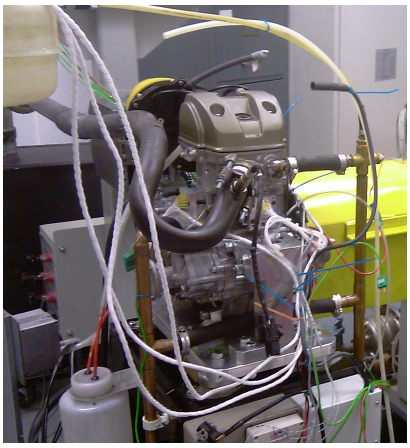

Figure 8.1: Single cylinder test engine.

The aluminium alloy cylinder 'barrel' is a separate piece from the block and it is bolted onto the crankcase. The inner cylinder surface (bore) is electroplated with a thin layer of NiSiC (produced by Capricorn), a matrix of silicon carbide in nickel to improve its wear

Table 8.1: Test engine specifications.

Number of Cycles	4
Number of Cylinder	1
Bore (mm) x Stroke (mm)	96 x 62.1
Connecting road length (mm)	105.6
Crank radius (mm)	31.05
Capacity (cm^3)	449
Compression Ratio	12:1
Cooling System	Liquid
Torque (Nm)	49.5 (at 7000 rpm)
Fuel System	Gasoline, Carburettor

resistance. The forged aluminium piston employs two piston rings both manufactured from steel. The compression ring has a barrel-shaped profile (see Figure C.1) with a tapered corner at top inner edge. It has a thickness of 0.90 mm. The oil control ring consists of two thin steel rails and a corrugated expander ring between them. The thickness of the thin steel rail is 0.40 mm and an overall thickness of the oil ring is 1.86 mm. The piston has a short skirt length of 25.8 mm. The nominal clearance is 150 micron between the piston skirt and cylinder. The mean roughness (R_a) of the cylinder was measured at 0.28 μm while it was measured at 0.2 μm for the compression ring.

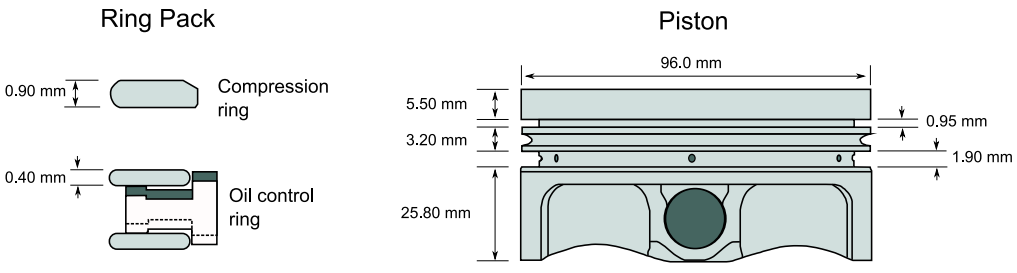

Figure 8.2: Schematic of the piston and ring pack.

The test cell included Oswald FQD series a.c. dynamometer, which was connected to the engine crankshaft by means of its gear box with a 4.02 reduction ratio. This type of dynamometer can be operated as either a generator or a motor. Therefore it absorbs

the engine output power and torque at different engine speed and throttle positions and also drives the engine for the motored tests. The S3000 Ricardo Taskmaster logs all the related data to compute the output power of the engine.

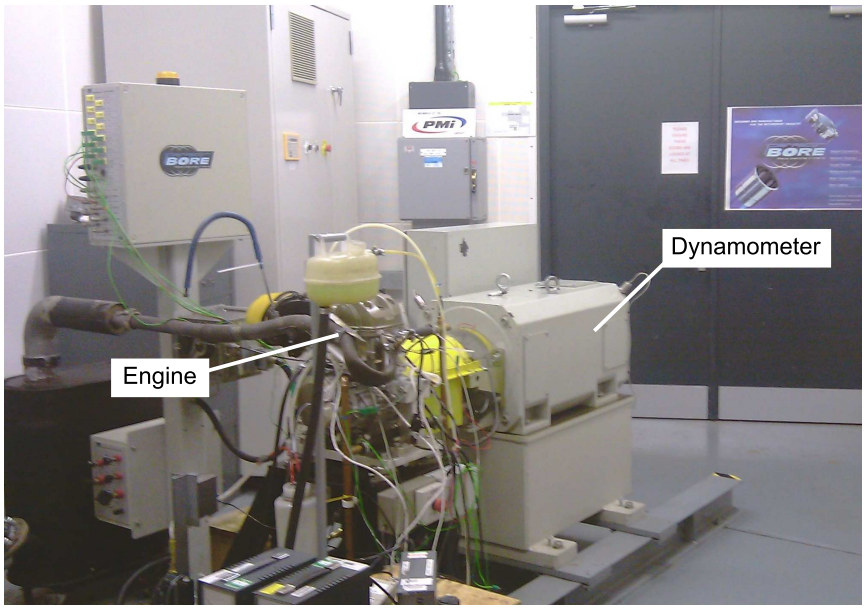

Figure 8.3: Test Engine and Dynamometer

8.1.2 Sensors on the Barrel

Thin piezo-electric elements, as have been mentioned in previous chapters, were used for monitoring the lubricant film formed between piston ring and cylinder. The machining of the barrel and the ultrasonic sensors placement were performed by *Robin Mills* who was a Research Associate at University of Sheffield.

The standard cylinder barrel of the CRF450R shown in Figure 8.4a was modified to have an access to the external surface of cylinder. As it is seen from the figure, three sides of the engine, which were the thrust, anti-thrust and one of the neutral sides, were accessible for the ultrasound instrumentation. The other neutral side was inaccessible due to the timing chain assembly. The external surface of the barrel was machined

through the water jacket providing three windows at the thrust, anti-thrust and neutral side (see Figure 8.4b). Using these windows, the exterior surface of cylinder (*i.e.* wet side of cylinder) was flattened by milling as the centre line of the flat surface was parallel to the tangent of the bore at these positions.

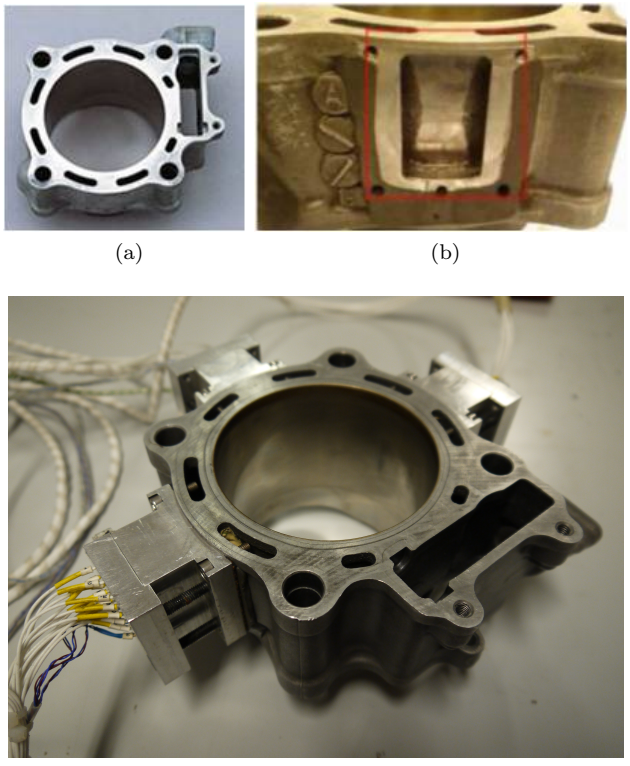

(a) (b)

(c)

Figure 8.4: Photographs showing: (a) standard barrel (b) machined window (c) ultrasonically instrumented barrel.

The same procedure, as explained in sensor preparation section in Chapter 6, was followed for bonding the ultrasonic sensors to the exterior surface of cylinder. The piezo crystals were cut into strips; their dimensions were 7.1 mm (length) by 1.0 mm (width) by 0.2 mm (thickness). Then 15 sensors for each side totally 45 piezo sensors were glued to these flat surfaces using Vishay's M-Bond 600 high temperature strain gauge adhesive. Figure 8.5 schematically shows the cut view of the engine and the arrange-

ment of sensor array. To seal and protect the connections of ultrasound sensors, high temperature resist epoxy (Scotch-Weld DP 760 produced by 3M) was applied on the sensors. Wires were transferred from the engine via specifically machined caps for each side (see Figure 8.4c and Figure 8.5). The original gasket material was placed between the cap and barrel to seal the engine.

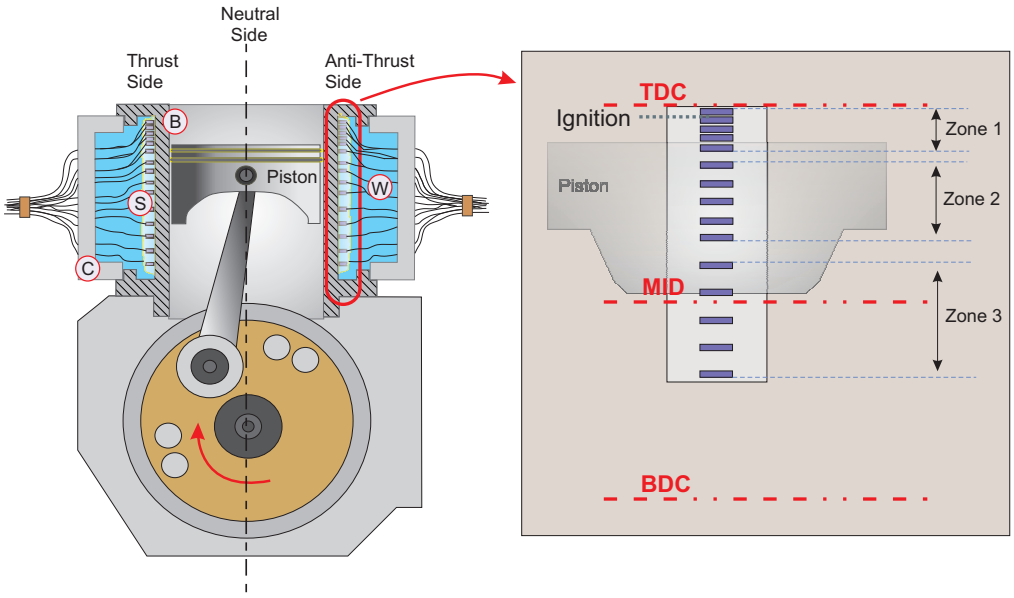

Figure 8.5: Schematic cutview of the instrumented engine (S: Sensor Array, B: Barrel, W: Water Jacket, C: Cap).

The axial length of the water jacket was shorter than the stroke of piston; it was approximately two thirds of the travel of the compression ring. This geometrical detail prevented sensors from being placed close to BDC. As illustrated schematically in Figure 8.5, the sensors were, therefore, non-uniformly positioned between TDC and 45 mm from the top of the bore. The distance between the sensors was 1 mm in Zone 1 (close to TDC) and this became 2.5 mm and 3.5 mm for Zone 2 and Zone 3 respectively. The reason for choosing the increased sensor density around TDC was to improve the overall effectiveness of the array because the piston was exposed to the highest load and had lowest velocities at this point.

For the experiments, all sensor outputs were checked and eight sensors located at the same position on each side were selected according to their signal strength and noise-signal ratio. The selected sensors and their positions in terms of crank angle and distance from the top of the barrel are both given in Table 8.2. The selected sensors allowed the film thickness measurement to be possible from a crank angle of 0° to angle of 87°, in other words from TDC to below the half of the stroke.

Table 8.2: The position of ultrasonic sensors used in the tests. (* from top of the barrel)

Sensor Number	Crank Angle (Degree)	Distance* (mm)
1	0	5.5
2	13	6.5
3	18	7.5
4	26	9.5
5	43	16.0
6	53	21.0
7	65	27.5
8	87	39.5

8.2 Data Capture and Signal Processing

The FMS-100 ultrasonic pulsing unit, detailed in Chapter 6, and a multiplexer were used in these tests. The sensors were connected to the multiplexer controlled by the ultrasonic unit. As the test was in progress, the multiplexer switched the sensors and connected the selected sensor to the pulsing unit in sequence. This allowed only one channel of the unit to be employed for the excitation of the sensor. Since high speed data acquisition was required, the system maximum pulse rate, 80k pulses/second, was set-up for this channel. The ultrasonic connections are illustrated in the schematic diagram given in Figure 8.6.

For each sensor, the ultrasonic reflection from the inner cylinder surface was isolated in a similar way given in previous chapters and then recorded continuously in a binary

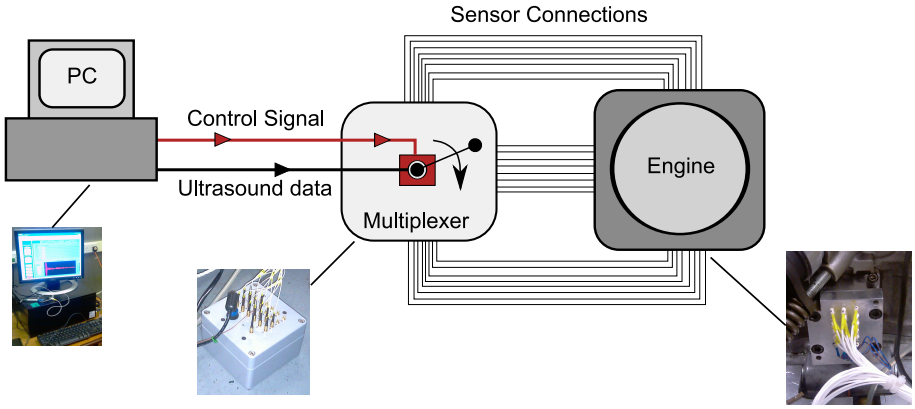

Figure 8.6: Schematic view of the ultrasonically instrumented engine.

format during the test. Later post processing was carried out to provide the reflection coefficient and determine the film thickness. As the main frame of the signal processing stages has already been drawn in Chapter 4, it will not be repeated here again. However, it should be noted that the materials of piston rings and skirt are different. As they are in contact with the aluminium liner, two different layer cases (*i.e.* al-oil-al and steel-oil-al) will be formed. Therefore, in the signal processing stage the spring model equation was applied to these cases separately. While the skirt film thickness was obtained by employing the skirt reflection data into Equation 3.18, the ring film thickness was obtained by employing the ring pack reflection data into Equation 3.19. Additionally, to limit the effect of ring profile on the minimum lubricant film thickness, the de-convolution algorithm described in Chapter 6 was put forward for a given ring profile and true minimum film thickness was obtained from the de-convoluted film thickness. The ring profile and the correction graph produced by the algorithm are given in Appendix C1.

The reference signal used in this chapter was created from the same pulse sequence or data string rather than its separate recording before the test. The reference pulse was performed by averaging the manually selected pulses in the pulse sequence, at which time no piston rings were present under the sensing area. As the increase in temperature can have an effect on the response of the ultrasonic transducer, this provides continual

updating of the reference measurement (*i.e.* test by test). Hence the reference and measurement signals have been taken at the same temperature, meaning that every pulse sequence has its own reference pulse. This provides automatic response calibration for the sensors.

8.3 Test Condition

The experiments were carried out when the engine was operated at 3200 rpm at low, medium and high load conditions (torques of 25 Nm, 37 Nm and 42 Nm respectively). The peak piston speed was about 10.85 m/s for this crank speed. Ultrasonic data from each sensor was recorded during a period of 2 seconds. The oil used in these tests was commercially available multi grade oil 10W40 from Castrol. Ultrasonic properties of the piston ring-liner materials and the oil were both given in Table 8.3. Torque measurements and the engine oil sump temperature at the beginning, T_b, and the end, T_e, of the each test were recorded from the display screen of S3000 Ricardo Taskmaster. Test conditions are given in Table 8.4.

Table 8.3: Acoustic properties of materials and lubricant used in the study.

Acoustic Impedance (z_2) of Steel Ring	45.7 MRayls
Acoustic Impedance (z_1) of Aluminium Liner	17.3 MRayls
Speed of Sound of Lubricant (m/s)	-3.169T+1524
Density of Lubricant (ρ)	873 kg/m^3
Kinematic Viscosity at 40°C	59.99 cSt
Kinematic Viscosity at 100°C	9.59 cSt

Table 8.4: Fired engine test condition

Engine Speed (rpm)	Torque (Nm)	Peak Pressure (bar)	Oil Temperature (T_b–T_e)
3200	25	48	45.4°C– 58.5°C
3200	37	57	68.5°C– 77.6°C
3200	42	74	86.5°C– 100°C

8.4 Results and Discussions

8.4.1 Reflection Coefficient Signal

The plots in Figure 8.7 show the reflection coefficient traces for selected sensors located at the anti thrust side as the engine was running at 3200 rpm. As the geometry of the piston and the positions of the sensor were known, each stroke of the piston can be identified. In the figures, these are roughly shown. The reflection coefficient data illustrated in Figure 8.7a was measured by Sensor-3. Since the sensor was located at 7.5 mm below the TDC, only the top compression ring could be monitored by this sensor. Figure 8.7b shows the reflection coefficient plot for Sensor-5 which is able to monitor both the top ring and oil control ring. If sensors positioned relatively far down from TDC point are selected, the skirt of the piston could also be observed. For instance, Sensor-8 located at 39.5 mm down from TDC, the skirt reflection coefficient trace becomes separated and it is visible for all strokes (see Figure 8.7c). As a comparison, the reflection trace from the neutral side of the cylinder is given in Figure 8.7d where the output of Sensor-8 located in the neutral side was used. As it is expected, there were no skirt traces for this side and only ring pack traces were observed.

Since this is a single-cylinder engine, the time for each stroke is not identical. In the power stroke, the piston accelerates more quickly to its maximum speed than the other strokes. The piston speed reduces until the next power stroke. This inherent asymmetry is highly visible in the reflection figures such that since the time between the pulses are constant, the power and exhaust stroke are shorter than the compression and induction stoke.

A detailed view of reflection coefficient trace is given in Figure 8.8 where the data was taken from thrust side and zoomed-in for the power and exhaust stroke. The skirt and ring pack passages are clearly seen. The skirt has lower speed than the ring at the sensor location and also has larger contact area so the skirt data is wider than ring

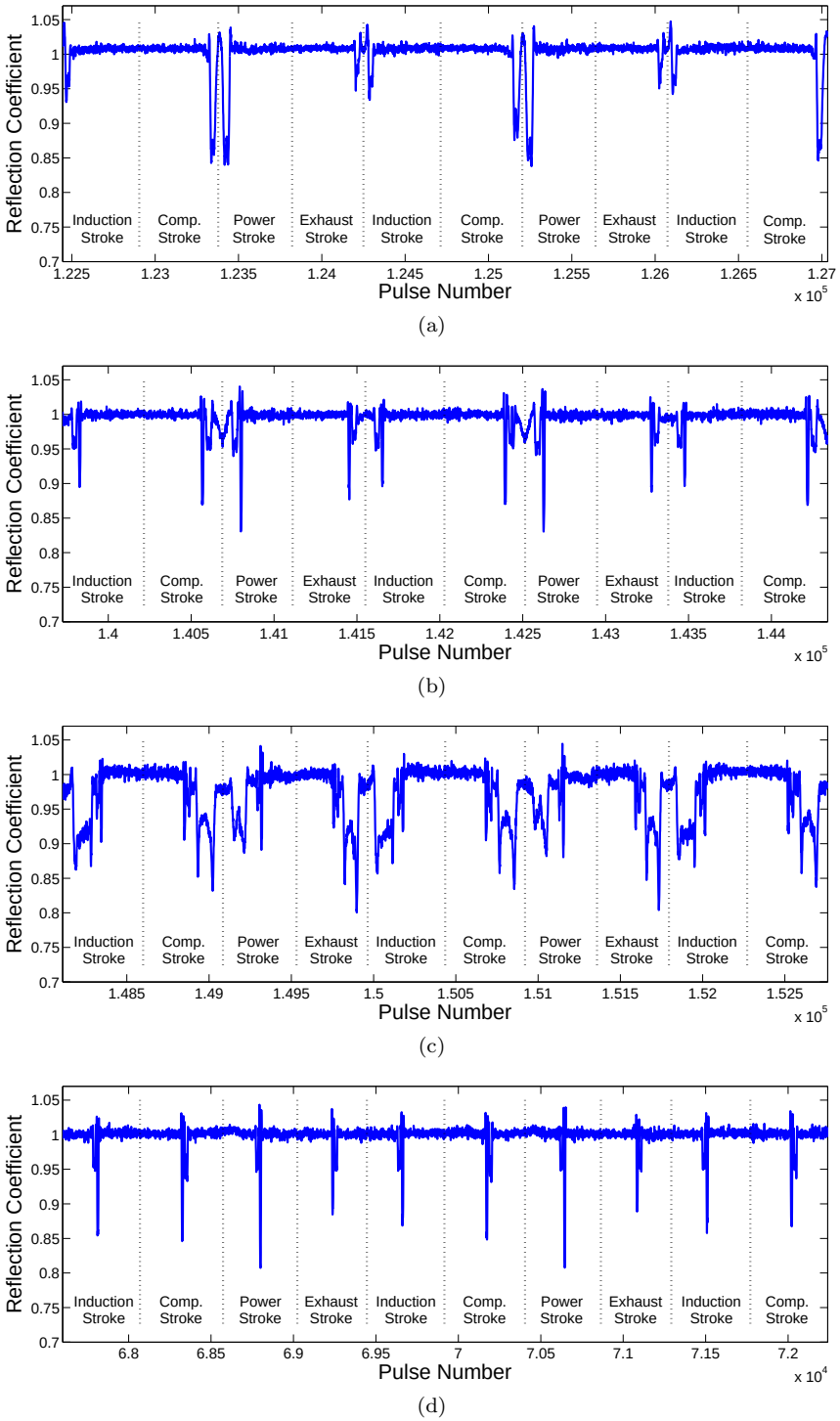

Figure 8.7: As the engine operating at 3200 rpm, the reflection coefficient traces measured by a) Sensor 3, b) Sensor 5, c) Sensor 8 at anti-thrust side and d) Sensor 8 at neutral side of the cylinder respectively.

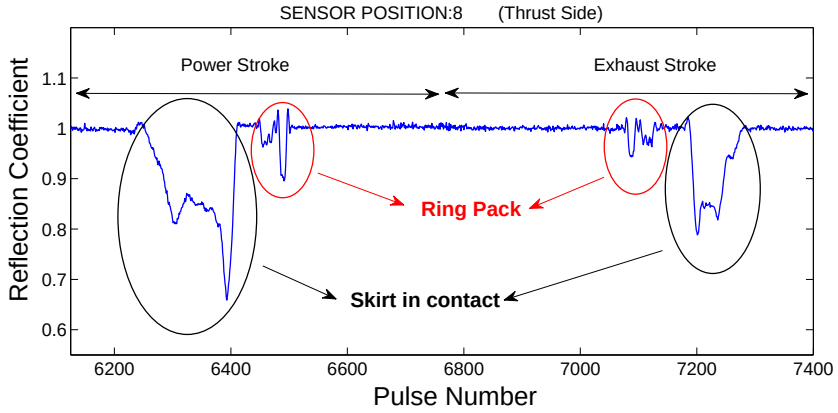

Figure 8.8: A Close view illustrating the reflection coefficient for the skirt and ring pack.

pack. As it is reported in previous Chapter 5, the variation in reflection data is high for the skirt due to the dynamics of the piston giving unknown contact size and location for the skirt.

8.4.2 Oil Film Thickness Measurements

Figure 8.9 illustrates typical lubricant film thickness data for the skirt and the ring pack. The presented data was obtained from the reflection coefficient signal illustrated in Figure 8.8. Oil film thickness variation over the skirt could be observed and the skirt has the minimum film thickness of 3 μm for power stroke and 4.5 μm for exhaust stroke. The following graphs in Figure 8.10 show a sample film thickness trace of the ring pack for each consecutive stroke. The values for the oil control ring are ranging from 6 μm to 8 μm and in general it has thicker oil film comparing to the top compression ring. However, it should be noted that the rails of the oil control ring is too thin and the width of sensors has fairly wide. This may cause the resolution issue mentioned in previous chapters and it makes the measurements suspicious. Also the minimum thickness value of the top compression ring must be de-convoluted to obtain 'true' film. Hence, only the top compression piston ring data will be analyzed in this chapter.

After the signal processing and deconvolution process, the minimum film thickness for top compression ring was obtained. Figure 8.11 shows sample results of top ring's

film thickness measured by the sensors positioned at 16 and 39.5 mm from the top of the cylinder. Each data point given in these figures is a mean value of minimum film thicknesses for each engine stroke and also shows the standard deviation bar indicating the maxima and minima. As seen, for each cylinder directions (*i.e.* thrust, anti-thrust and neutral side), the minimum film thicknesses were measured for the engine's power stroke. This is expected because the high combustion pressure is acting behind the ring

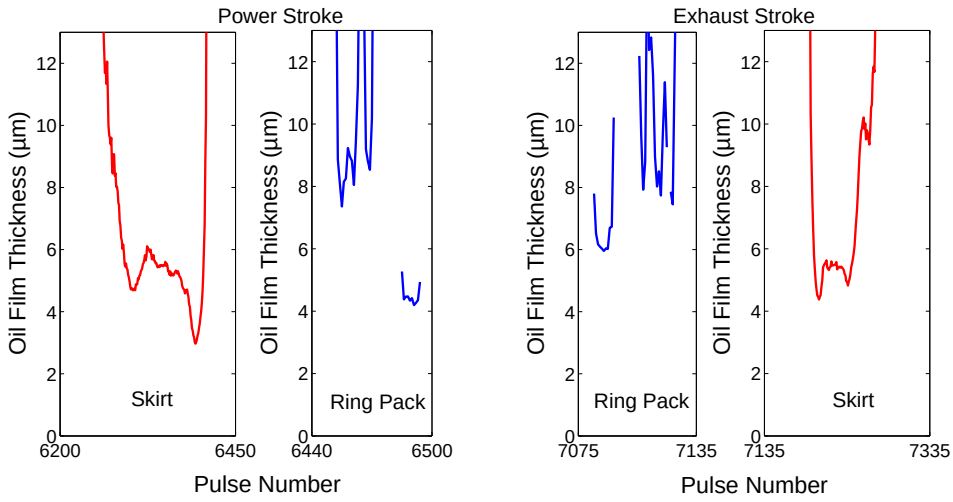

Figure 8.9: Oil film thickness measurement for skirt and ring pack; left hand side for power stroke and right hand side for exhaust stroke.

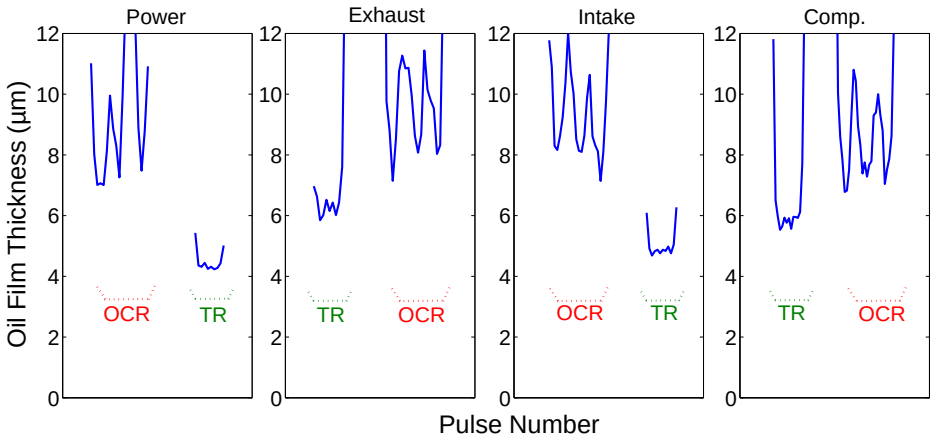

Figure 8.10: Ring pack film thicknesses for consecutive strokes starting from power stroke. (OCR: Oil Control Ring, TR: Top Ring).

and pushing it towards liner, hence minimum film thickness is decreasing. After the power stroke, generally compression stroke has thin film thickness and there is not very clear difference between the other strokes.

As graphs in Figure 8.11 show that there is a considerable variation in film thickness data for exhaust and intake stroke. The deviation of MOFT was less than $\pm$ 0.5 μm for the power stroke, while for the intake and exhaust stroke measured lubricant film thickness was varying $\pm$1.5 μm. Even in some cases, the ultrasonic data for these strokes was not very robust and the data was very close to noise limit. The detection of the reflections from the top compression ring was impossible in such situations as shown in the following graphs; the reflection from the top ring is very weak (Figure 8.12a) and sometimes disappears (Figure 8.12b).

As the engine was fired at 3200 rpm and operated at a load of 25 Nm, the minimum lubricant film formed during power and compression strokes are given in Figure 8.13. Since 'crank angle', has been mostly used in engine literature to describe the piston position, in the figures, the measured mean minimum film thicknesses for each cylinder direction were plotted over the engine crank angle. It is seen from the figures that the hydrodynamic effect which allows a thick lubricant film to be formed as the piston speed increased was observed for both power and compression strokes. However, it should be noted that the lubricant film data at the crank angle 0° for power stroke and 720° for compression stroke were considerably high. This data was recorded by sensors located at 5.5 mm down from the top of cylinder (*i.e.* Sensor-1), thus at this position the ring could not fully pass over the sensing area. This results in a bigger reflection coefficient and hence film thickness, so the lubricant film data at this position, does not actually represents 'minimum' film thickness. This is shown in schematically in Figure 8.14. Even as it occurs at neutral side, the ring stops before the sensing area then the output of the sensor exposure to noise. The film thickness data at the position of Sensor-1 is therefore missing for neutral side in the tests results.

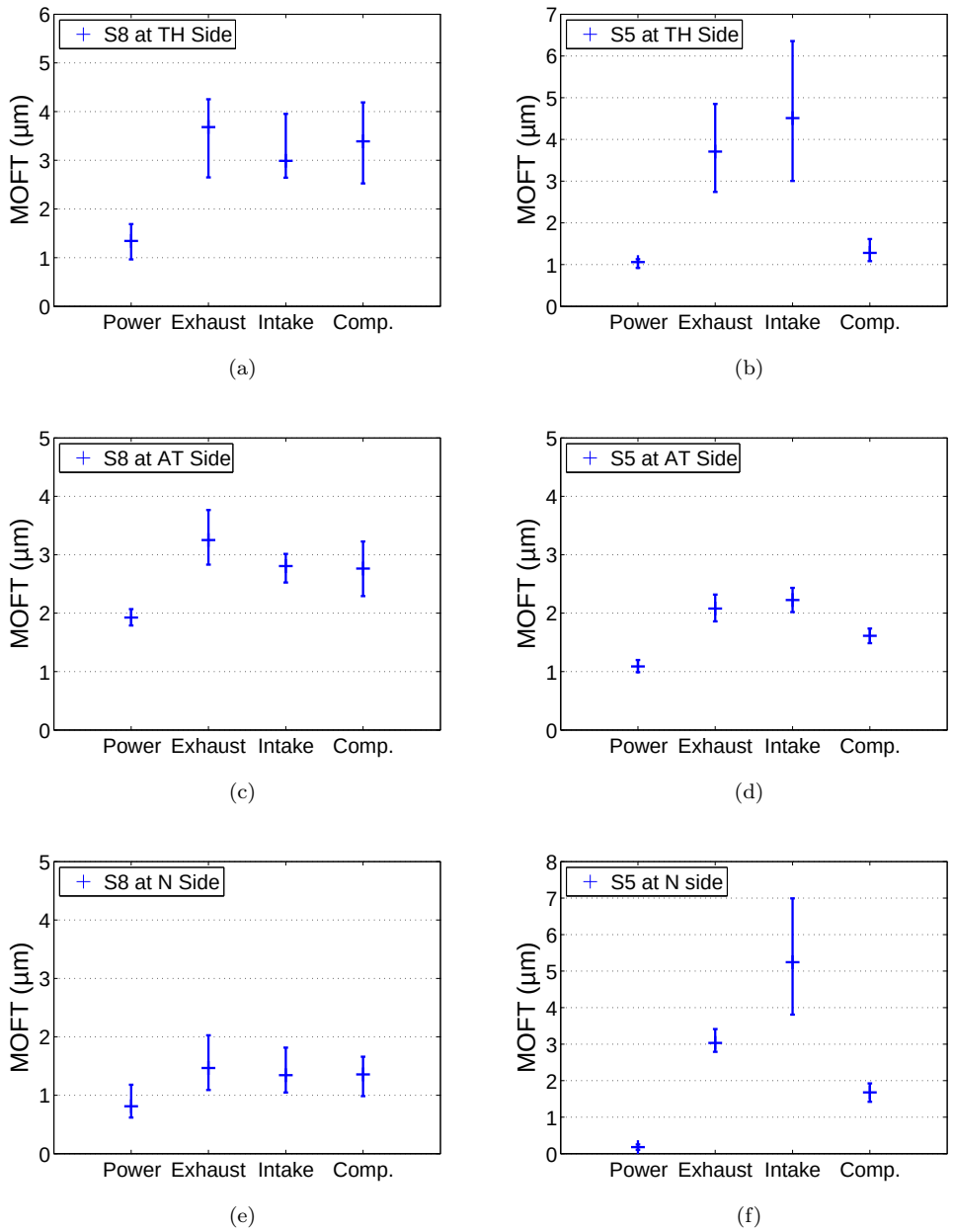

Figure 8.11: Results of minimum film thickness measured by sensors located at 16 and 39.5 mm down from TDC.

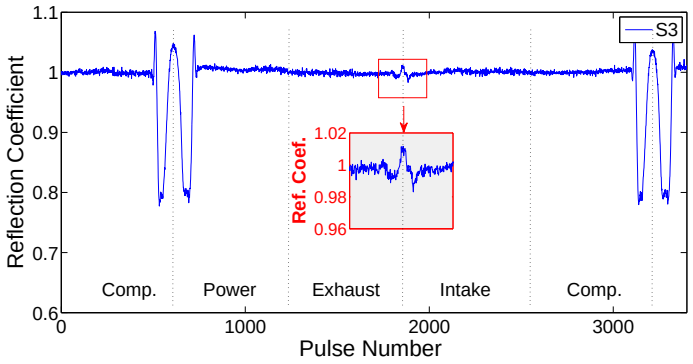

(a)

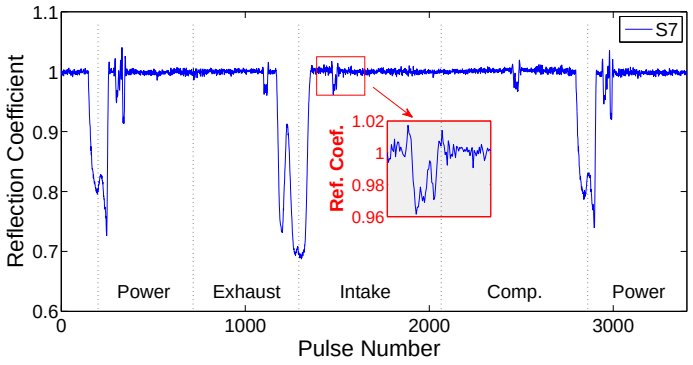

(b)

Figure 8.12: Top ring reflection issues for exhaust and intake strokes: (a) measured by Sensor-3 and (b) measured by Sensor-7.

The measurement results also indicate that at the position of Sensor-7 (shown at crank angle of 65° and 655° degrees for power and compression strokes respectively), there was relatively thick lubricant film formed for each cylinder directions comparing to the other crank angles that the measurement was taken. Clearly, this rapid increment in the measurement is not related to the solely sensor issue or its fault, since the same lubricant tendency was measured by three different sensors, placed in each three different cylinder directions at this position. The reason behind it could be a distortion of the ultrasonic barrel which may lead to observation of thick film formation at this crank angle.

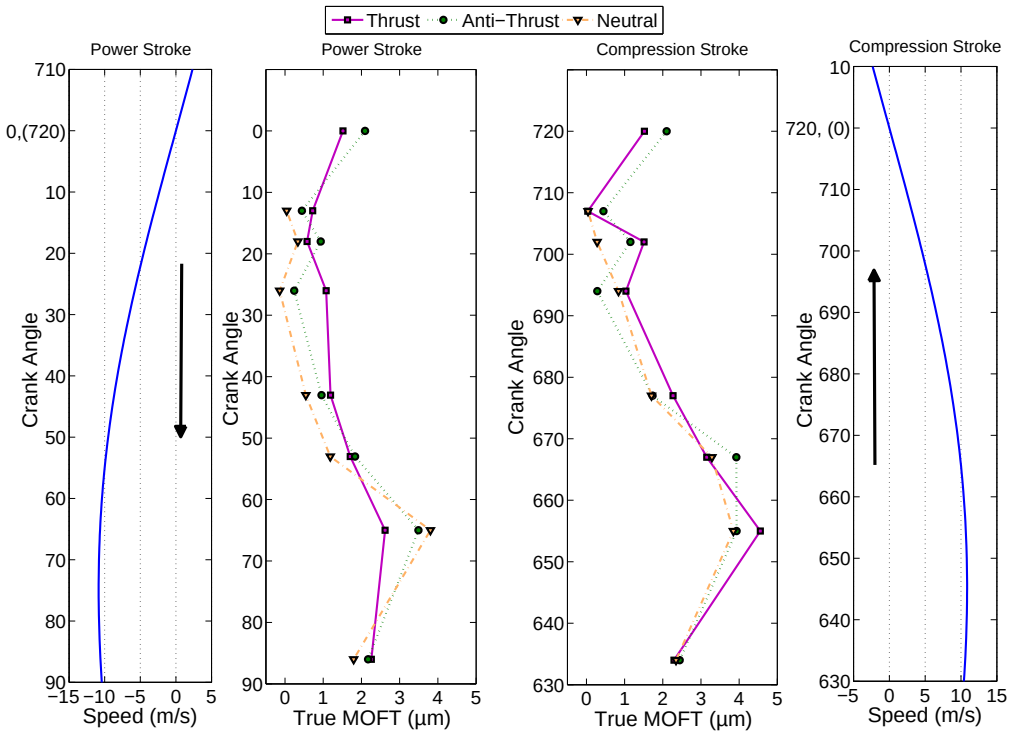

Figure 8.13: Piston speed variation and MOFT results measured by sensors positioned at thrust, anti thrust and neutral side of the cylinder during power and compression strokes.

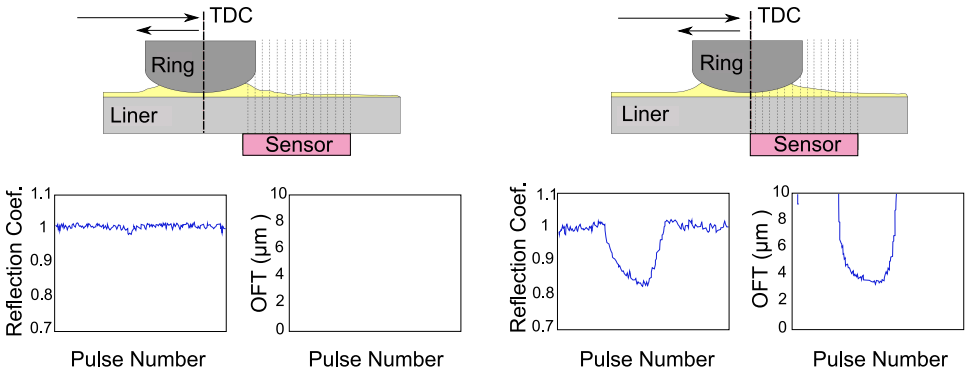

Figure 8.14: Schematic showing two cases possibly occurred at TDC.

As mentioned before, the fired engine tests were carried out at 3200 rpm for three loading conditions. The results of measurements recorded during power stroke for each cylinder direction are illustrated in Figure 8.15. It is seen that the circumferential top

ring film thickness measurements were broadly similar. At the beginning of the crank angle, the effect of load on power stroke is not very apparent. However, especially for anti-thrust and neutral side, after 40°, MOFT results for high loading case of 42 Nm become thinner than the low loading case of 25 Nm. The film thickness results were lying in a range less than 1μm, particularly close to TDC. As the piston ring speeds up and the combustion pressure decreasing, the thicker lubricant film up to 4 μm was formed.

The results showed that the de-convolution process was effective. During the experiments the minimum lubricant film thickness obtained after the de-convolution process remained above the zero with only one exception, *i.e.* -0.14 μm occured at neutral side. Of course, this is not physically possible. The one reason to this is the use of oil sump temperature which is significantly lower than the temperature of the ring. This could mislead the selection of the correlation line and hence true film thickness because an

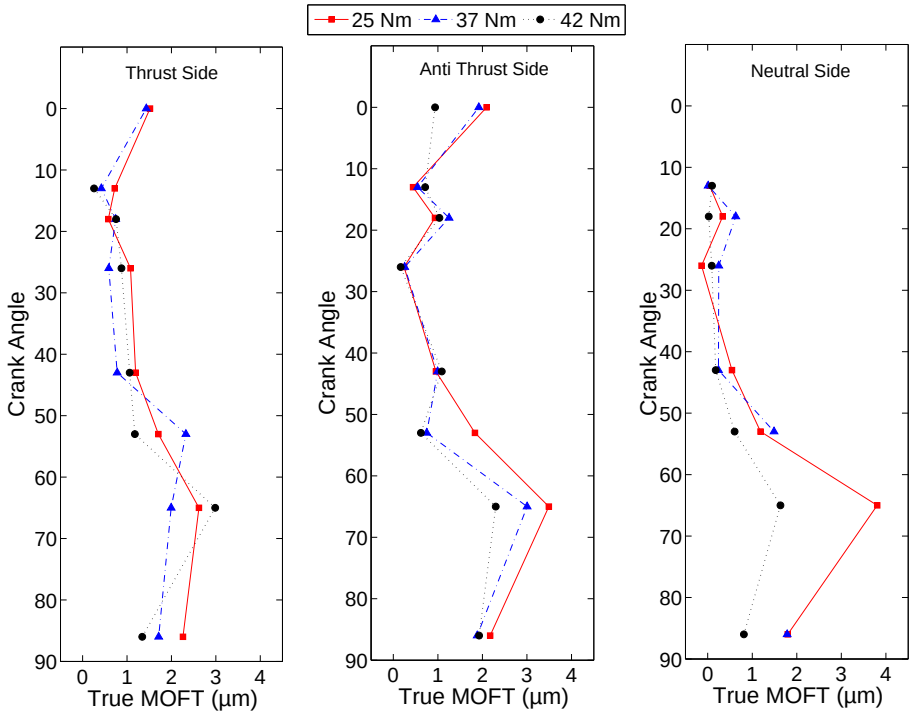

Figure 8.15: MOFT results measured by sensors positioned at thrust, anti thrust and neutral side of the cylinder for three loading conditions.

increase in oil temperature brings the true film value closer to the measured value. This can be seen from Figure C.3 in Appendix where the correlation line will move to the left for higher oil temperature. As an example, a measured film thickness of 3 μm is equivalent to a true film of 0.52 μm for 60°C on the other hand it corresponds to 0.82 μm for 100°C. The other reason which could cause the film thickness fall below zero is that the direct asperity contact occurs in the ring-liner conjunction. This would result in more ultrasound passing into the piston ring and hence a smaller reflection coefficient and film thickness.

8.5 Conclusion

The ultrasonic method developed in the previous chapters has been successfully employed in a fired single cylinder engine. Non-invasive measurement of lubricant film thicknesses in piston ring-liner contact have been performed at three cylinder directions as the engine operating at 3200 rpm with different loading conditions. In fired engine cycles, the minimum lubricant film thickness was measured for the power cycles. This is because the high combustion pressure force pushed the ring towards liner and causes the film thickness to be decreased.

Occasionally, the reflections from the top compression ring could not be monitored for exhaust and intake cycles due to the weak signals. The measured mean minimum film thicknesses for each cylinder direction were plotted over the engine crank angle. At the beginning of the crank angle, the effect of load on power stroke was not very evident but after 40°, MOFT results for high loading case of 42 Nm became thinner than the low loading case of 25 Nm, particularly for anti-thrust and neutral side. Sensors positioned at 27.5 mm down from top of the barrel measured relatively thick lubricant film comparing to the other sensor positions. This was attributed to the distortion of the ultrasonic barrel.

Typically the minimum film thicknesses were measured to less than 1 μm around TDC. However, as the piston speeds increased, the thicker films up to 4 μm were measured by the sensors. The de-convolution algorithm was effective and the film thickness data was fell below the zero minimum film thickness at one point. The possible reasons to this could be either the use of oil sump temperature in the analysis or more asperity contact occurred in the conjunction.

9

Conclusions and Recommendations

This chapter highlights the conclusions that can be drawn from this work on the development of a novel ultrasonic technique for measuring lubricant film thickness in piston ring-liner contacts. Improvements to the technique and possible future work are also suggested here.

9.1 Concluding Remarks

Piston ring-liner conjunction in an IC engine, responsible for 40-50% of typical engines frictional losses [9], is one of the important areas for automotive industry. The oil film formed between the piston ring and liner is an essential parameter. If the film is too thin then surfaces are in contact and this leads to high friction and wear. However, if an ample amount of oil is present in the contact, it would leak into the combustion chamber and be burnt away. Monitoring of the lubricant film can therefore become essential for optimum lubrication of the piston rings.

This work presents a novel ultrasonic technique to measure film thickness between the piston ring and cylinder liner. The technique was initially developed and trialled on the motored engine. A commercial contact transducer was coupled to the outer cylinder

wall so that ultrasonic pulses passed through the cylinder and reflected from the inside wall. High speed pulsing and triggering system was built thus pulses reflected from the rings as they pass the transducer were received and analyzed. The ultrasonic system allowed for measurements to be recorded from the ring pack in a limited operating conditions (*e.g.* no load), however there were some issues such as sensor's spatial resolution and the system internal memory capacity that require further development to obtain more accurate data in high resolution.

In light of the conclusions drawn by the trial motored engine tests, the ultrasonic system was upgraded and combined with Plint TE-77 reciprocating test rig. The reciprocator was used to provide a controlled, easily accessible and repeatable experiment. The most significant development in ultrasonic sensors was the use of bespoke strips of piezo elements. Due to their smaller size compared to the contact transducers, the spatial resolution of the measurements was enhanced. The reflections were recorded by five custom made sensors permanently mounted at the back of the liner section and then the lubricant film thickness traces were determined by employing the spring model. Ultrasonic film measurements were conducted with simultaneous measurements of friction. Key findings from the experiments were that:

- Very repeatable film thickness data was observed during the reciprocating bench tests MOFT varied between 0.25 and 2.1 μm.
- There were some fluctuations in the ultrasonically measured ring profiles due to less oil availability and cavitation occurred in the contact. However, this only affected the tests in one sliding direction (*i.e.* up stroke).
- Film thicknesses increased with increasing sliding speed due to the hydrodynamic effect.
- When the applied normal load increased, the lubricant film could not support the load and decreased until it reached its balancing point with the load partly supported by asperities.

- Three lubricant samples with different viscosity properties were tested using the standard liner sample. The more viscous oil produced thicker films in the contact.
- Oil film thickness data was consistent with the friction data. For the case of low load and high reciprocating speed, the hydrodynamic lubricant film was generated and this produced low friction values. On the other hand, high loading with low speed cases experienced the smaller film thicknesses and as expected high friction in the contact due to more asperities interactions.
- A rapid increase in friction was observed for the lubricant film below 0.8 μm. This suggests that the asperity contacts begin to dominate the contact at this point.
- Higher friction was experienced for the film thickness above 1.5 μm. This is highly likely due to the viscous forces in the layer.
- The effect of liner surface finish on friction and film thickness was small for hydrodynamic lubrication. Measured MOFT values were relatively similar and there was a full film separation in the contact.
- A clear difference between the samples was observed for mixed and boundary lubrication. The smallest film thickness was measured for ANS triboconditioned liner® sample and thicker film thickness for the standard liner sample.
- The effect of coating on the triboconditioned liner sample was obvious. It had small film thicknesses values but produced less friction due to low shear coating on its surface.

After successful measurements on the bench tests, the ultrasonic approach was applied to the single cylinder test engine. The strip piezoelectric elements were positioned on the outer liner surface of the engine at three cylinder directions; thrust, anti-thrust and one of the neutral sides. Using multiplexer, 8 sensors for each cylinder direction were pulsed at 80k pulses/s in a sequence. Depending on the sensor locations, the skirt-liner and ring-liner conjunctions were successfully detected by the sensors. The reflections from top compression ring were post-processed. The main results of this investigation as follows:

- Minimum lubricant films were measured for the engine's power cycles.
- There was a considerable variation in MOFT data for exhaust and intake stroke.
- The circumferential top ring film thicknesses were pretty similar and the minimum film thickness was typically measured less than 1 μm at around TDC but as the piston speeds increased, the thicker lubricant films up to 4 μm were recorded.
- During the power stroke, the effect of load was not very obvious at the beginning of the crank angle. After 40°, particularly for anti-thrust and neutral side, the MOFT values appeared to decrease for high loading case of 42 Nm.
- There were some unexpected sensors readings (*i.e.* positioned at 27.5 mm down from top of the barrel). This was thought to be due to the distortion of the cylinder bore that could deteriorate the conformability of the ring.

9.2 Achievement of Aims and Contribution to Knowledge

During the last decade, the ultrasonic technique has already been used for measuring oil film thickness in static or low speed applications. In this thesis, the technique has been further developed for high speed and more concentrated piston ring-liner contact. As surveyed in the background chapter, there are various methods to measure the film thickness in piston rings and with varying degrees of success. All of these measurement methods are invasive techniques, meaning that they require to penetrate the inner cylinder wall in order to access the ring-liner contact. The ultrasound technique is based on sending the high frequency pulses through the cylinder wall and sensing the reflections from the ring-wall contact. The ultrasonic sensors do not have to be flush with the inner cylinder wall; therefore, post grinding of the outer cylinder surface could be enough to retrofit the sensor on the liner. This localised non-invasive measurement of piston ring film thickness would help to monitor lubricant condition in the contact and make a significant contribution to the literature.

Before the complicated fired engine tests, the technique was initially developed and applied to a motored engine and then a reciprocating test rig. The ultrasonic instrumentation of the reciprocating test rig provides simultaneous and comparative measurement of friction and lubricant film thickness. To build confidence, the measured piston ring film thicknesses were compared to the numerical simulation and also judged by considering the measured friction data. Furthermore, the bespoke piezo crystals developed during the reciprocating test stage were used for the single cylinder engine. The lubricant film thickness formed in the ring-liner contact was successfully measured by these sensors in fired condition. Thus the work successfully achieved its primary aim.

The ultrasonic implementations from bench test rig to fired engine test rig have demonstrated that the non-invasive measurement of piston ring-liner film thickness is viable and more practical compare to the current measurement techniques. Knowledge gained during testing would provide an aid to the design and development of future film thickness measurements. The other benefit of this work is that the results would be used by other researchers for comparing their empirical data or validating of current numerical models of piston ring-liner contact.

9.3 Critical Assessment of Approach

This thesis suggests that the ultrasonic technique has the potential to provide non-invasive route to assess the lubricant in the piston ring-liner conjunction. The instrumentation of the ultrasound technique is compact and insensitive to test environment so it could be used outside an engine test cell. By contrast with the other techniques, the ultrasonic technique does not require an in-situ calibration of the setup as the quantification of lubricant thickness is derived by direct physical correlation (i.e. spring model).

The fired engine tests prove that the ultrasonic sensors placed on the exterior surface of cylinder are robust and could withstand the elevated temperatures experienced on the engine. Normally, thermal variations lead to drift in sensor response. The piston ring is

present in the sensing area for a short time, therefore the large portion of the recorded signal is from air-liner interface (*i.e.* reference interface). The developed post-processing software program uses this interface and provides continual updating of the reference. Since the measurement and reference are recorded at the same temperature, this gives automatic response calibration.

The measurement values experienced during the reciprocator and engine tests were comparable to results of other published data given in the literature. The measured film thickness data shows good consistency between cycle sets. In reciprocator tests, the deviation bars of the minimum film thickness were less than 0.05 μm for high load but tended to increase up to 0.25 μm for low load high speed cases. Since the fired engine was more chaotic, the deviations were different from cycle to cycle. For the power stroke, the deviation of MOFT was less than $\pm$ 0.5 μm while for the intake stroke measured lubricant film thickness was varying $\pm$1.5 μm. It should be noted that any inhomogeneous regions in the contact due to cavitation or lack of oil would result in the impression of greater film thickness measurements being recorded than is actually the case. Other measurement techniques (*i.e.* capacitance, inductance, resistance) are also sensitive to air-oil mixture.

The one of the current limitations of the ultrasonic technique is the spatial resolution of the sensor. The size of the sensor in relation to the piston ring-liner contact will limit the ability to resolve the true minimum film formed under the ring. This sensor issue is present in other techniques as well. The other limitation is the local conditions in the contact, *i.e.* temperature and pressure, which both affect the bulk modulus of oil hence the film thickness results. The temperature calibration of lubricant speed of sound has been carried out using a simple time of flight principle. To more accurate measurement, the speed of sound value corresponding to the measured lubricant temperature in the contact should be employed into the spring model. The bulk modulus is also dependent on pressure, but it is challenging the measure pressure within the contact. For the content of this thesis, the properties of the lubricant were assumed to be equivalent to

those at ambient pressure. Various computational simulations estimated the maximum hydrodynamic pressure in the contact, ranging from 8 MPa to 50 MPa. If such higher pressures are assumed to exist, the contact becomes stiffer and more ultrasound will pass through the ring. For given such pressures, an error of the order of 10-15% in film measurement is estimated [128].

Hardware also limits the ultrasonic film thickness measurement particularly for high speed applications where maximum pulsing and sampling rate are both important parameters. Any improvements will increase the resolution. However, it should be noted that cylinder liner material has a finite speed of sound which characterizes the transit time of the pulse. The pulse echo should sufficiently decay before a subsequent pulse is initiated. This physical fact therefore limits the maximum pulse rate that can be achieved. However, this would only be an issue for engines where the piston speed is very high (above 30 m/s).

9.4 Future Research

The key recommendations for future work are summarised below.

- ***Sensor Development*:** Piezoelectric element transducers with a width of 1 mm were used in this study. This size might be small enough for the piston rings of the engine used in heavy truck-bus engine or marine industry. However, smaller size of sensor provides a greater resolution over a smaller area. To achieve this, the focusing type of transducer can be used for the piston ring-liner contact. At this point the water jacket of the engine could be used as a required water bath to focus the ultrasonic beam into a point. However, their size is much bigger than piezoelectric elements and so this could be a trouble due to limited space in the engine. Alternatively, high frequency piezoelectric films could be used as well. This involves the deposition of a thin layer of aluminium nitride film onto the surface. The film coating has a highly columnar structure and this gives them

a strong piezoelectric property. Using this approach, ultrasound with a centre frequency of 200 MHz was achieved to measure the oil film in a rolling element bearing [129]. This sputtered coating would be applied to anywhere on the exterior surface of the liner and possibly be patterned around the liner. This probably gives the circumferential lubricant film thickness map. Additionally, at this frequency, the resonance technique may also used to measure film thickness in piston ring but the attenuation problem would need to be overcome.

- ***More reciprocating tests*:** Using the reciprocating test rig developed in this study further experimentation would be recommended to investigate the effect of soot particles, different dimples on the liner surfaces, coatings etc. Moreover, it would be useful to conduct tests over an extended period of time to investigate and quantify running in effects. The lack of oil or cavitation in the contact adversely affects the measurements. To gain further understanding, visualization tests could be carried out using a transparent liner section in the bench reciprocating rig. If the ring sensor is placed into the ring holder, the image and ultrasonic measurement from the contact would be compared and the reliable correlation between the cavitation and reflection coefficient could be achieved.

- ***More engine tests*:** By measuring lubricant film thickness over a long period of time, the sensor robustness or possibly thermal fatigue failure could be explored. Different ring profile and lubricants may be tested. As highlighted before, the ultrasound technique requires the lubricant density and speed of sound value to determine the lubricant thickness. It would be useful to investigate the temperature distribution along the liner surface and this would increase the accuracy of the technique.

- ***Ring Sensor*:** In this current work, the ultrasonic sensors were placed to the exterior surface of the liner. Another further investigation which would be recommended is the application of piezoelectric elements or thin films outlined above to the back of piston ring. This would provide continuous film thickness through the whole stroke but there are some challenges such as referencing, wiring issue and

harsh combustion environment. Since the ring is always in contact with liner, the reference interface needs to be created to normalize the measurement reflection according to the reference. This could be achieved by machining a reference groove on the liner or using an external apparatus (may be containing the same separate liner section). An expensive linkage system (see Figure 2.14) is also required to transmit the measurement cables to the engine exterior. Although the fired engine tests showed that the piezoelectric elements could survive at the high temperature that liner exterior surface experienced, the piston and ring exposure to much higher temperature and pressure. This could have an effect on the bounding layer and the sensor response.

- ***Test vehicle*:** The main differences of the ultrasonic method from the other measurement techniques are portable and non-invasive. It would be used in the field tests as well as in the lab environment. Thus, eventually the ultrasonic measurement technique might be carried to a test vehicle and measurements could be performed in road driving tests.

List of Publications

***Journal and Technical Papers*:**

- R. Mills, E. Y. Avan, and R. Dwyer-Joyce. Measuring Lubricant Films at the Piston-Cylinder Contact: An Overview of Current Technologies with Focus on Ultrasound. *SAE International Technical Paper*, No:2013-01-0294, 2013.

- E. Y. Avan, A. Spencer, R. Dwyer-Joyce, A. Almqvist, and R. Larsson. Experimental and Numerical Investigations of Oil Film Formation and Friction in a Piston Ring-Liner Contact. *Proc. IMechE Part J: Journal of Engineering Tribology*, 227(2):126 – 140, 2013.

- E. Y. Avan, R. Mills, and R. Dwyer-Joyce. Frictional Characteristic of Ultrasonically Measured Lubricant Films in a Simulated Piston Ring Liner Contact. *SAE International Technical Paper*, No:2011-01-1400, 2011.

- E. Y. Avan, R. Mills, and R. Dwyer-Joyce. Ultrasonic Imaging of the Piston Ring Oil Film During Operation in a Motored Engine-Towards Oil Film Thickness Measurement. *SAE International Journal of Fuels and Lubricants*, 3(2):786 – 793, 2010.

***Conference Papers, Extended Abstracts*:**

- E. Y. Avan, R. Mills, and R. Dwyer-Joyce. Simultaneous Film Thickness and Friction Measurement for a Piston Ring-Cylinder Contact. In *Proceedings of the STLE/ASME 2010 International Joint Tribology Conference*, IJTC2010-41081, San Francisco, USA,October, 2010.

- E. Y. Avan, R. Mills, R. Dwyer-Joyce and N. Akturk. Oil Film Thickness Measurement between an Automotive Piston Ring and Cylinder using an Ultrasonic Technique. In *Proceedings of the 4th World Tribology Congress*, Kyoto, Japan, September, 2009.

Appendices

A

Piston Ring Terminology

***Ring face (or front face)*:** This is the face contacting the cylinder wall. This face profile varies depending on the intended application. Barrel face for top compression rings and tapered face for second compression rings are the most commonly used in automobile engines.

***Side faces*:** These are the top and bottom surfaces of the piston ring.

***Back face*:** This is the inner face of the piston ring.

***Ring width*:** This is thickness of the ring and measured from one side face to the other in the axial direction.

***Radial wall thickness*:** This is the ring measured from the front face to the back

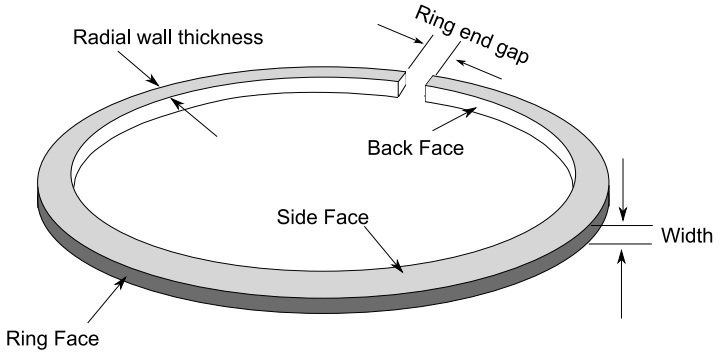

Figure A.1: Compression ring.

face of the ring. A specification, called 'D-wall', was established by the Society of Automotive Engineers (S.A.E.) that dictates the radial wall thickness of a standard automotive piston ring. It is calculated by dividing a bore diameter by 22 (*e.g.* 130 mm bore diameter divided by 22 is 5.9 mm).

***End gap*:** The space between the ends of the compression ring.

***Rail (or Segment)*:** It is a part of a there-piece oil ring (see Figure A.2). Two flat steel rails (top rail and bottom rail) do the scraping and sealing of lubricant oil.

***Expander*:** This piece is placed between the rails and holds them in axial position. It provides oil ring tension which pushes the rails to the cylinder bore and also allows for oil drain-back.

***Radial clearance*:** The distance between the back face of the ring and the back side of the ring groove when the ring is installed on the piston (see Figure A.3).

***Side clearance*:** The clearance between the top side faces of the ring and groove when the ring bottom side face is flush with the groove bottom side.

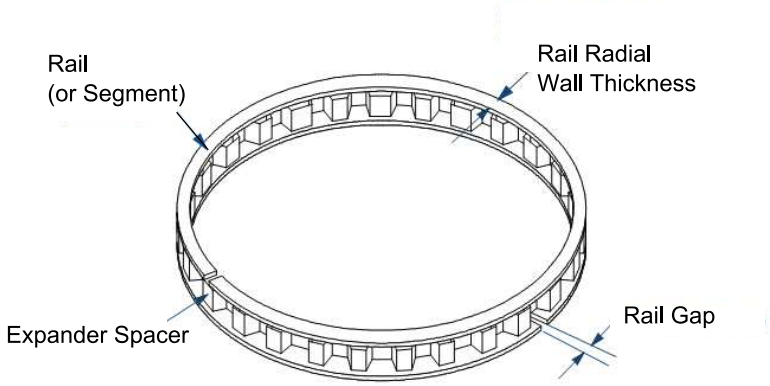

Figure A.2: Oil control ring.

***Positive Twist*:** An asymmetric change in the ring cross section causes the ring to twist in the groove. If the ring has a tapered corner or a step at the top back face, this creates a positive twist in an upward direction. This improves the sealing of the top and bottom side of the ring groove, so positive twist is used only for top compression rings.

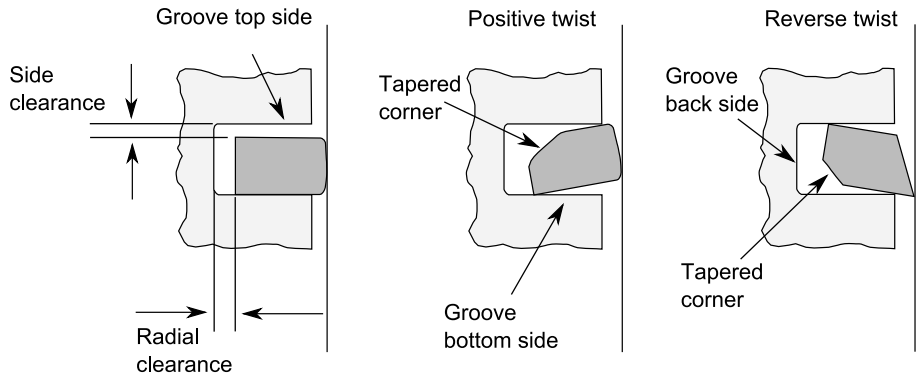

Figure A.3: Side clearances, positive twist and reverse twist.

***Reverse Twist*:** A bottom internal bevel (or step) creates a negative twist (toward the piston skirt). Hence, the ring touches to the cylinder bore at its bottom outer edge that helps scraping of the oil and touches to the piston groove at its top inner edge that prevents the blow-by. In general, reverse twist are preferred for second compression rings.

B

Reciprocating Work Appendix

B.1 Piston Ring Sliding Speed at Measurement Locations

Since the lubricant film thickness was measured at five locations over the liner sample and each measurement location had different sliding speed, in this study Plint oscillation

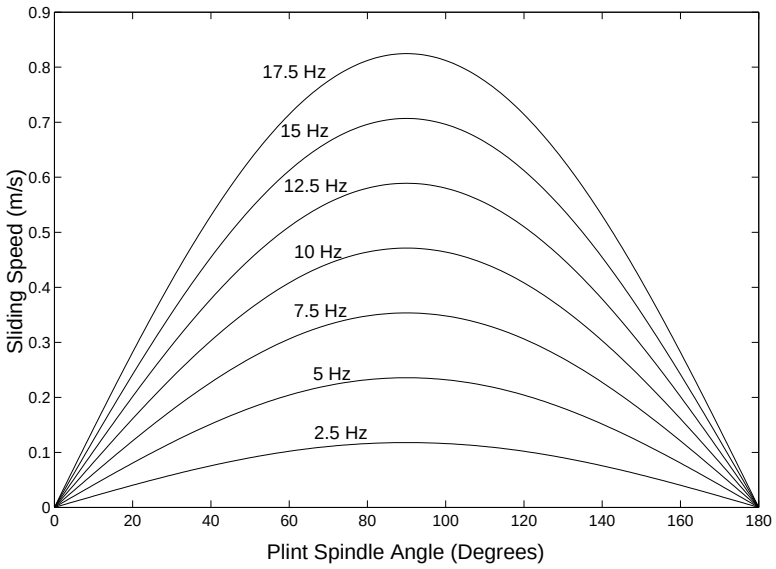

Figure B.1: Piston ring sliding speed versus spindle angle of Plint.

speed in terms of Hz was used to specify the test condition. The piston ring sliding speed as a function of spindle angle is illustrated in Figure B.1 for several operating speeds used during this study. Table B.1 gives the ring sliding speed at these measurement locations.

Table B.1: Piston ring sliding speeds at lubricant film thickness measurement locations.

	Operating	Speed	in (Hz)	(Velocity	in m/s)	
	2.5 Hz	5 Hz	7.5 Hz	10 Hz	12.5 Hz	15 Hz	17.5 Hz
Sensor-1	0.069	0.138	0.207	0.276	0.345	0.414	0.483
Sensor-2	0.105	0.209	0.315	0.419	0.524	0.629	0.734
Sensor-3	0.118	0.235	0.353	0.471	0.589	0.706	0.824
Sensor-4	0.109	0.217	0.326	0.434	0.543	0.652	0.760
Sensor-5	0.075	0.150	0.225	0.300	0.375	0.450	0.525

B.2 Overview of Plint Test Conditions

Table B.2 shows an overview of the reciprocating test condition. The table has been drawn by considering the use of standard piston ring and liner specimen lubricated with base oil. Other oil samples and liner specimens tested in this work have already been presented in Table 7.1 and Table 7.3 respectively. Normal load can also be given in terms of per unit length (load/contact length), for instance a normal load of 60 N equals to 3 N/mm.

Table B.2: Test parameters.

Reciprocating stroke	15 mm
Piston ring type	Full keystone ring (top ring)
Piston ring profile	Asymmetric barrel shaped
Ring coating	Running face coated with a chrome ceramic (CKS®)
Ring face width	3 mm
Ring surface roughness (R_a)	0.14 μm
Liner specimen	Cast iron, plateau honing, HA of 55°
Liner surface roughness (R_a)	0.32 μm
Bore diameter	130 mm
Contact length	20 mm
Reciprocating speed (Hz)	2.5, 5, 7.5, 10, 12.5, 15 and 17.5
Normal load (N)	40, 60, 80, 100, 120, 140, 160, 180 and 200
Temperature	$22°C$
Lubricant	Castrol base oil without additive package
Method of lubrication	Immersed
Lubricant viscosity	37 cSt (at $40°C$), 6.5 cSt (at $100°C$)
Lubricant density	843.4 kg/m^3

B.3 Ring-Liner Contact Stiffness

When the contact operates in mixed-lubrication regime, the total load on the contact is shared between contacting asperities and compressed lubricant. Then the total stiffness of the interface, K_{total}, becomes a combination of the stiffness of the asperity contact, K_{asp}, and the stiffness of the liquid film, K_{liq}. This can be modelled as shown in Figure B.2 where the mixed lubrication regime interface is represented by two springs in parallel. If the surface separation is high, the asperity contact is negligible so K_{asp} term falls to zero. Therefore, the load is entirely carried by the liquid spring, K_{liq}. This is the reason why the spring representing the asperity interaction is free at one end.

$$K_{total} = K_{liq} + K_{asp} \tag{B.1}$$

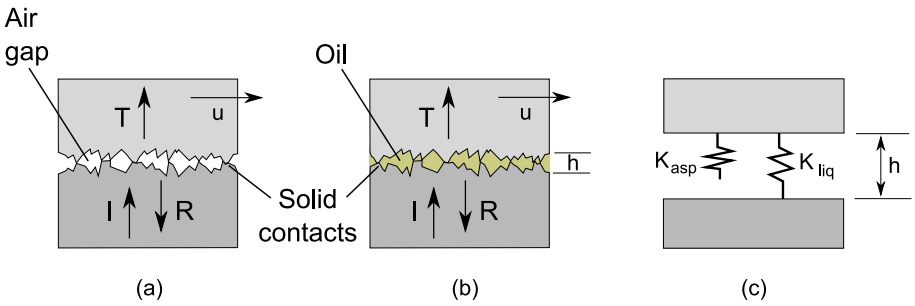

Figure B.2: Schematic diagrams of tribological interfaces (a) a dry contact, (b) a wet contact, (c) spring model representation.

To investigate the effect of asperities on the film thickness measurement, limited numbers of dry and lubricated tests were conducted for a range of loads (60 N, 80 N and 120 N) at a low speed of 2.5 Hz. Unfortunately high loading dry test above 120 N was not possible due to wear of the liner specimen. The reflections from the ring-liner interface were recorded by the sensors as the piston ring reciprocated over the liner. Figure B.3 shows a sample reflection coefficient signal captured by sensor-5 for dry ring-liner contact. As seen most of the ultrasonic signal was reflected back and the reflection coefficient was about 0.97 at the ring passages. The results for the other sensor locations are illustrated in Figure B.6. The spring model (Equation (3.12)) was

used to covert reflection coefficient to the interfacial stiffness for each sensor location. The stiffness results of dry and lubricated tests carried out at 80 N and 2.5 Hz are given in Figure B.4. For the dry tests, the contact was made up of asperity contact and air gaps. Since there was no lubricant present in the contact (K_{liq}=0) and air stiffness was zero, the stiffness of the contact K_{dry} was equal to K_{asp}. As seen, the asperity stiffness at each sensor location was almost similar and equal to 0.34 GPa/μm. When the lubricant was added to the reciprocating ring-liner contact, the contact stiffness increased at each sensor location. At near dead centres (*i.e.* Sensor 1 and 5), the contact was likely to be in mixed lubrication regime due to the ring low speed. The contribution of the liquid part, K_{liq}, at the location of Sensor 5 was about 1.25 GPa/μm. Since the sliding speed increased towards mid-stroke, the contact stiffness was decreased due to the surface separation by compressed lubricant. So at this point, the comparison between K_{asp} and K_{liq} would be more tricky because the asperity interaction in lubricated case was not similar to that in dry case.

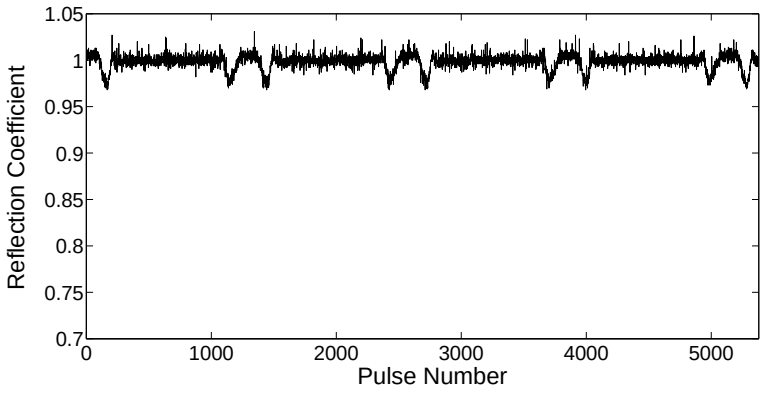

Figure B.3: Reflection coefficient signal measured by Sensor-5 located at near BDC while the dry contact was operating at a speed of 2.5 Hz under a load of 80 N.

The relative contributions of the asperity and liquid film to the contact stiffness at the location of sensor 1 and 5 are given in Figure B.5. From around 17 to 28 % of the total contact stiffness was attributed to the asperity contacts so the remaining (i.e. 72-83 %) was attributed the liquid parts. Once these liquid parts were placed into Equation (3.17), slightly thicker film values were obtained when compared to the film

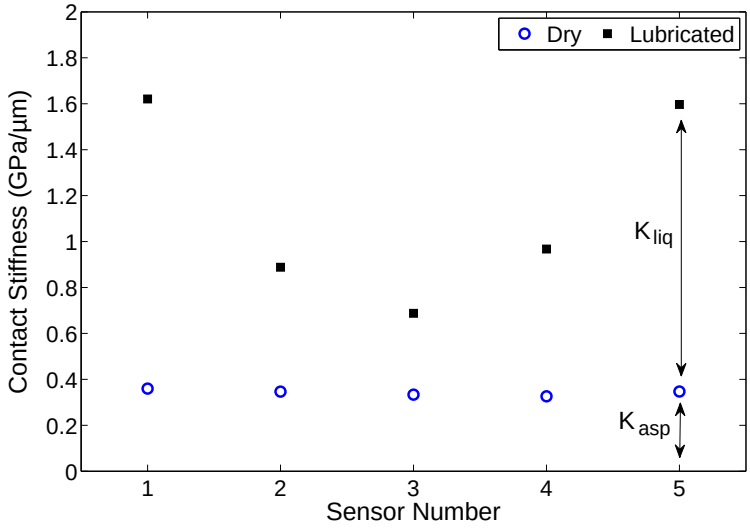

Figure B.4: The stiffness values of the contact at measurement locations for dry and lubricated cases.

thickness obtained from the total contact stiffness. The difference (Δh) was 0.2 μm for 60 N and $\sim$0.4 μm for 120 N. It must be noted that these given values represent the variation only at near dead centres. High liquid contribution and so less film thickness differences (Δh) are expected for the other sensor locations (*i.e.* Sensor 2, 3 and 4) due to the less asperity contacts occurring at these locations.

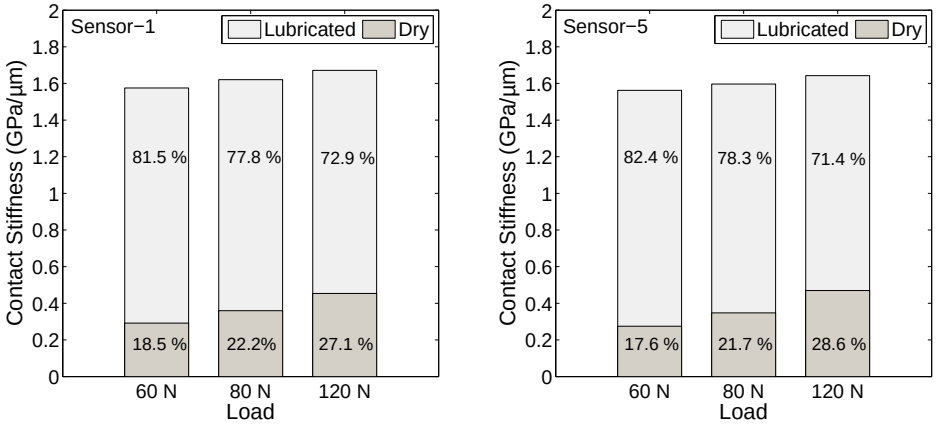

Figure B.5: The stiffness of the contact at near dead centres for several loads as the ring reciprocates at 2.5 Hz.

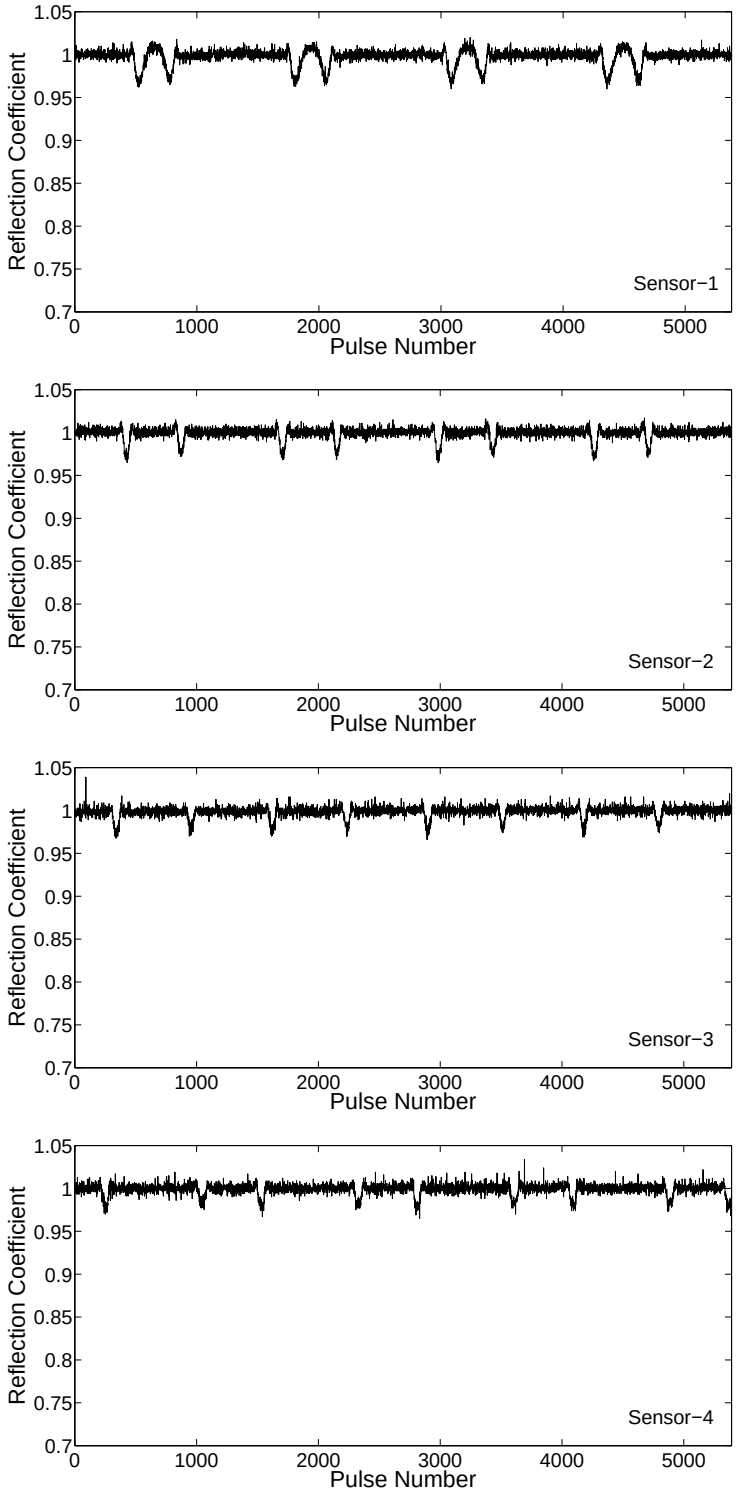

Figure B.6: Reflection coefficient signals measured by sensors while the dry contact was operating at a speed of 2.5 Hz under a load of 80 N.

C

Fired Engine Work Appendix

C.1 De-convolution Process for Compression Ring

The ring profile of the compression ring is given in Figure C.1. This profile was used to de-convolute the film thickness over a sensor window. The comparison graph obtained from the de-convolution algorithm is illustrated in Figure C.2 for a range of oil temperatures. As seen, at higher oil temperature the observed film thickness is getting closer to the true film thickness (see Figure C.3).

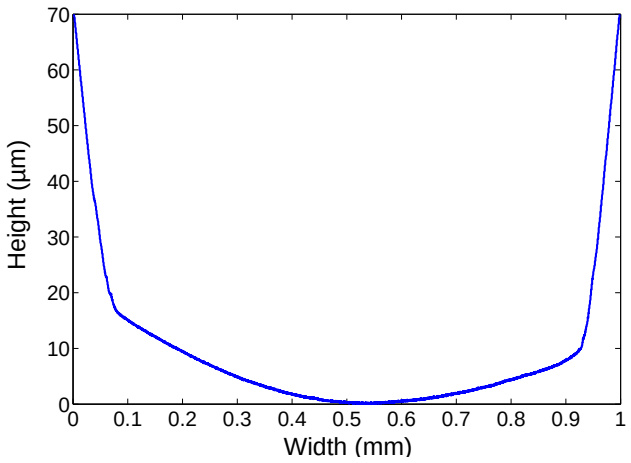

Figure C.1: Top compression ring profile of the single cylinder Honda engine.

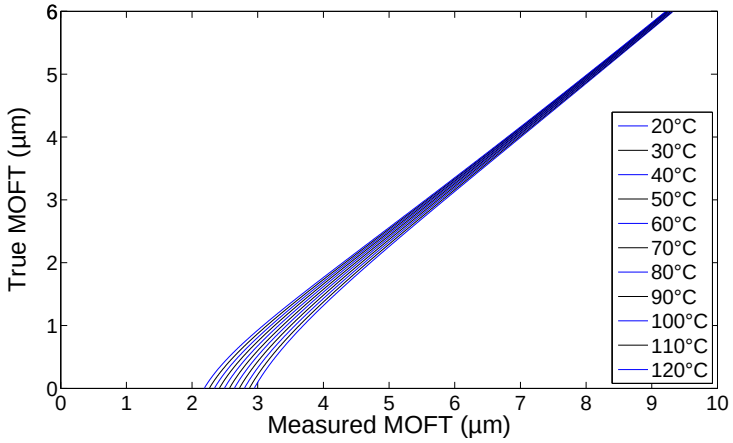

Figure C.2: True minimum film thickness plots for a range of lubricant temperatures.

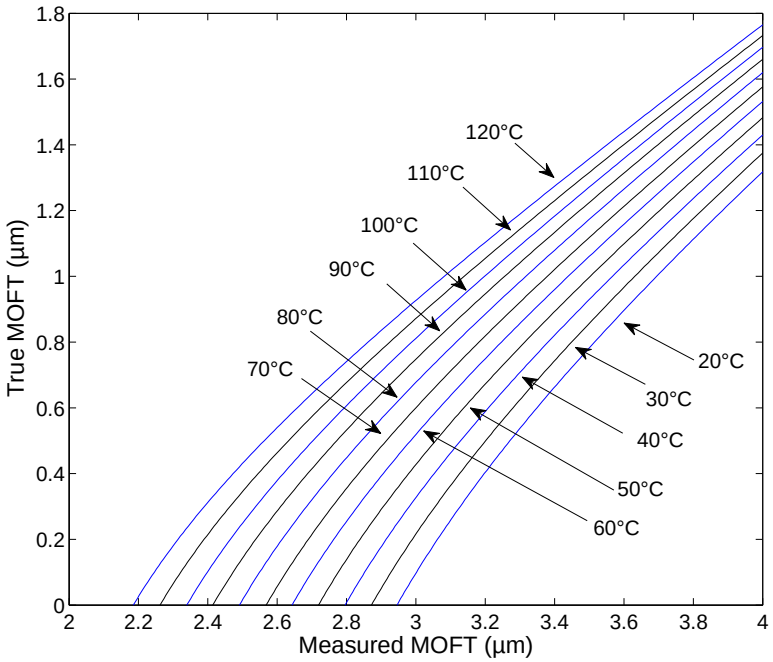

Figure C.3: A close view of Figure C.2.

Bibliography

[1] J. C. Bell. Engine lubricants. *Engine Tribology (Taylor, C.M. (ed.)), Tribology Series, Elsevier*, 26:287–301, 1993.

[2] R. K. Rajput. *Internal Combustion Engines*. Laxmi Publications, 2005.

[3] Engine cutway. *URL: http://www.cadillacfaq.com/faq/imglib/engtranny.html*, Accessed on 31 March 2013.

[4] Federal-Mogul Burscheid GmbH. Piston ring handbook. *URL: http://www.federalmogul.com/korihandbook/en/index.htm*, Accessed on 14 August 2008.

[5] Mahle GmbH. *Cylinder Components*. Mahle, Stuttgart, 2010.

[6] B.J Taylor and T.S. Eyre. A review of piston ring and cylinder liner materials. *Tribology International*, April:79–89, 1979.

[7] The European Parliament and the Council of the EU. Regulation (eu) no 510/2011. *Official Journal of the European Union*, L 145/1., 2011.

[8] C. M. Taylor. Lubrication regimes and the internal combustion engine. *Engine Tribology (Taylor, C.M. (ed.)), Tribology Series, Elsevier*, 26:75–89, 1993.

[9] B.S. Andersson. Company perspectives in vehicle tribology - Volvo. *17th Leeds-Lyon Symposium on Tribology - Vehicle Tribology, Tribology Ser., Elsevier.*, 18: 503–506, 1991.

[10] J. A. Spearot. Friction, wear, health, and environmental impacts - tribology in the new millennium. In *A keynote lecture at the STLE Annual Meeting, Nashville, Tennessee, May 2000*, 2000.

[11] D. Dowson. Piston assemblies: Background and lubrication analysis. *Engine Tribology (Taylor, C.M. (ed.)), Tribology Series, Elsevier*, 26:213–240, 1993.

[12] S.C. Tung and M.L. McMillan. Automotive tribology overview of current advances and challenges for the future. *Tribology International*, 37:517–536, 2004.

[13] M.C. Shaw and T. Nussdorfer. Visual studies of cylinder lubrication - part i: The lubrication of the piston skirt. *NACA Wartime R E*, 66, 1945.

[14] M. C. Shaw and T. J. Nussdorfer. Camera techniques expose oil-film behaviour. *SAE J.*, 66:54–68, 1946.

[15] A. B. Greene. Initial visual studies of piston cylinder dynamic oil behaviour. *Wear*, 13:345–360, 1969.

[16] U. Todsen and Niethus K. U. Optical ways to improve the tribological system piston-ring-liner. *SAE Technical Paper Series*, 2006-01-0527, 2006.

[17] I. Sherrington and E.H. Smith. Experimental methods for measuring the oil-film thickness between the piston-rings and cylinder-wall of internal combustion engines. *Tribology International*, 18(6):315–320, 1985.

[18] A. E. Smart and R. A. J. Ford. Measurement of thin liquid films by a fluorescence technique. *Wear*, 29:41–47, 1974.

[19] R.A.J. Ford and C.A. Foord. Laser based fluorescence techniques for measuring thin liquid films. *Wear*, 51:289–297, 1978.

[20] L. L. Ting. Development of a laser fluorescence technique for measuring piston-ring oil-film thickness. *J. Lubr. Technology*, 102:165, 1980.

[21] D. P. Hoult, J. P. Lux, and V. W. Wong. Calibration of laser fluorescene measurements of lubricant film thickness in engines. *SAE Technical Paper Series*, 881587, 1988.

[22] J. P. Lux and D. Hoult. Lubricant film thickness measurements in a diesel engine piston ring zone. *Lubrication Engineering*, 47(5):353–364, 1991.

[23] M. A. Brown, H. McCann, and D. M. Thompson. Characterization of the oil film behaviour between the liner and piston of a heavy-duty diesel engine. *SAE Technical Paper Series*, 932784, 1993.

[24] D. E. Richardson and G. L. Borman. Using fibre optics and laser fluorescence for measuring thin oil films with applications to engines. *SAE Technical Paper Series*, 912388, 1991.

[25] B. T. Shaw, D. P. Hoult, and V. Wong. Development of engine lubricant film thickness diagnostics using fibre optics and laser fluorescence. *SAE Technical Paper Series*, 920651, 1992.

[26] M. Takiguchi, K. Nakayama, S. Furuhama, and H. Yoshida. Variation of piston ring oil film thickness in an internal combustion engine - comparison between thrust and anti-thrust sides. *SAE Technical Paper Series*, 980563, 1998.

[27] K. Frølund and J. Schramm. An investigation of the cylinder wall oil film development during warm-up of an si-engine using laser induced fluorescence. *SAE Technical Paper Series*, 971699, 1997.

[28] R.I. Taylor and P.G. Evans. In-situ piston measurements. *Proc. IMechE Part J: Journal of Engineering Tribology*, 218:185–200, 2004.

[29] J. Dearlove and W.K. Cheng. Simultaneous piston ring friction and oil film thickness measurements in a reciprocating test rig. *SAE Technical Paper Series*, 952470, 1995.

[30] C. Arcoumanis, M. Duszynski, H. Lindenkamp, and H. Preston. Measurements of the lubricant film thickness in the cylinder of a firing diesel engine using lif. *SAE Technical Paper Series*, 982435, 1998.

[31] T. Seki, K. Nakayama, T. Yamada, A. Yoshida, and T. Takiguchi. A study on variation in oil film thickness of a piston ring package: variation of oil film thickness in piston sliding direction. *JSAE Review*, 21:315–320, 2000.

[32] H. Yoshida, H. Kobayashi, T. Yamada, M. Takiguchi, and K. Kuwada. Effects of narrow-width, low-tangential-tension, 3-piece oil ring on oil consumption. *JSAE Review*, 21:21–27, 2000.

[33] Y. Baba, H. Suzuki, Y. Sakai, D. L. T. Wei, T. Ishima, and T. Obokata. Piv/lif measurements of oil film behaviour on the piston in i. c. engine. *SAE Technical Paper Series*, 2007-24-0001, 2007.

[34] A. Cameron and R. Gohar. Theoretical and experimental studies of the oil film in lubricated point contact. *Proceedings of the Royal Society of London. Series A, Mathematical and Physical Sciences*, 291:520–536, 1966.

[35] A. D. Roberts and D. Tabor. The extrusion of liquids between highly elastic solids. *Proceedings of the Royal Society of London. Series A, Mathematical and Physical Sciences*, 325:323–345, 1971.

[36] H. A. Spikes. Thin films in elastohydrodynamic lubrication: The contribution of experiment. *Proc. IMechE Part J: Journal of Engineering Tribology*, 213:335–352, 1999.

[37] L. Gustafsson, E. Hoglund, and O. Marklund. Measuring lubricant film thickness with image analysis. *Proc. IMechE Part J: Journal of Engineering Tribology*, 208: 199–205, 1994.

[38] Y. Wakuri, S. Ono, M. Soejima, and N. Woguchi. Oil-film behaviour of reciprocating slider with circular profile: Observation of oil-film by means of thin-film interferometry. *Bulletin of the JSME*, 22(167):755–762, 1979.

[39] C. Myant, T. Reddyhoff, and H. A. Spikes. Laser-induced fluorescence for film thickness mapping in pure sliding lubricated, compliant, contacts. *Tribology International*, 43:1960–1966, 2010.

[40] B. E. Courtney-Pratt and G. K. Tudor. An analysis of the lubrication between the piston-rings and cylinder-wall of a running engine. *Proceedings of IMechE*, pages 155–293, 1946.

[41] S. Furuhama and T. Sumi. A dynamic theory of piston-ring lubrication, 3rd report: Measurement of oil-film thickness. *Bulletin of the JSME*, 4(16):744–752, 1961.

[42] S. C. Tung and H. Gao. Study of break-in film development with different piston ring coatings and correlation with electrical contact resistance measurement. *Tribology Transactions*, 46:326–331, 2003.

[43] P. Saad, L. Kamo, M. Mekari, W. Bryzik, V. Wong, N. Dmitrichenko, and R. Mnatsakanov. Modeling and measurement of tribological parameters between piston rings and liner in turbocharged diesel engine. *SAE Technical Paper Series*, 2007-01-1400, 2007.

[44] M.G. Lewis. A miniature mutual inductive proximity transducer. *Journal of Physics E: Scientific Instruments*, 7:269–271, 1974.

[45] R. D. Wing and O. Saunders. Oil-film temperature and thickness measurements on the piston-rings of a diesel engine. *Proceedings of IMechE*, 186:1–9, 1972.

[46] T. A. Dow, C. A. Schiele, and R. D. Stockwell. Technique for experimental evaluation of piston-ring/cylinder film thickness. *Journal of Lubrication Technology*, 105:353–360, 1983.

[47] R. Golloch, G. P. Merker, U. Kessen, and S. Brinkmann. Functional properties of microstructured cylinder liner surfaces for internal combustion engines. *Tribotest.*, 11(4):307324, 2005.

[48] L. Shenghua, L. Jijun, Z. Longbao, and W. Rong. An experimental investigation of the oil film lubricating piston rings. *SAE Technical Paper Series*, 961912, 1996.

[49] J. Tamminen, C. E. Sandström, and P. Andersson. Influence of load on the tribological conditions in piston ring and cylinder liner contacts in a medium-speed diesel engine. *Tribology International*, 39:1643–1652, 2006.

[50] Patranabis. *Sensors and Transducers*. Prentice-Hall of India Pvt.Ltd, Amsterdam; London, 2004.

[51] A. Chiba. *Magnetic Bearings and Bearingless Drives*. Elsevier/Newnes, Oxford, 2005.

[52] G. M. Hamilton and S. L. Moore. Measurement of the oil-film thickness between the piston rings and liner of a small diesel engine. *Proceedings of IMechE*, 188: 253–261, 1974.

[53] G. M. Hamilton and S. L. Moore. Comparison between measured and calculated film thicknesses of the oil-film lubricating piston-rings. *Proceedings of IMechE*, 188:262–268, 1974.

[54] S. Furuhama, C. Asahi, and M. Hiruma. Measurement of piston ring oil film thickness in an operating engine. *ASLE Transactions*, 26(3):325–332, 1982.

[55] K. Shin, Y. Tateishi, and S. Furuhama. Measurement of oil-film-thickness between piston ring and cylinder. *SAE Technical Paper Series*, 830068, 1983.

[56] N. Grice and I. Sherrington. An experimental investigation into the lubrication of piston-rings in an internal combustion engine - oil film thickness trends, film stability and cavitation. *SAE Technical Paper Series*, 930688, 1993.

[57] C. Mattsson. Measurement of the oil film thickness between the cylinder liner and the piston rings in a heavy duty directly injected diesel engine. *SAE Technical Paper Series*, 952469, 1995.

[58] D. O. Ducu, R. J. Donahue, and J. B. Ghandhi. Design of capacitance probes for oil film thickness measurements between the piston ring and liner in internal combustion engines. *Journal of Engineering for Gas Turbines and Power*, 123 (3): 633–643, 2001.

[59] S.J. Söchting and I. Sherrington. The effect of load and viscosity on the minimum operating oil film thickness of piston-rings in internal combustion engines. *Proc. IMechE Part J: Journal of Engineering Tribology*, 223:383–391, 2009.

[60] M. Takiguchi, R. Sasaki, I. Takahashi, F. Ishibashi, S. Furuhama, R. Kai, and M. Sato. Oil film thickness measurement and analysis of three ring pack in an operating diesel engine. *SAE Technical Paper Series*, 2000-01-1787, 2000.

[61] L. E. Bird and M. R. Gartside. Measurement of bore distortion in a firing engine. *SAE Technical Paper Series*, 2002-01-0485, 2002.

[62] A. Dhar, A. K. Agarwal, and V. Saxena. Measurement of dynamic lubricating oil film thickness between piston ring and liner in a motored engine. *Sensors and Actuators, A: Physical*, 149 (1):7–15, 2009.

[63] A. Dhar, Agarwal A. K., and V. Saxena. Measurement of lubricating oil film thickness between piston ring-liner interface in an engine simulator. *SAE Technical Paper Series*, 2008-28-0071, 2008.

[64] C. Arcoumanis, M. Duszynski, H. Flora, and P. Ostovar. Development of a piston-ring lubrication test-rig and investigation of boundary conditions for modelling lubricant film properties. *SAE Technical Paper Series*, 952468, 1995.

[65] I. Sherrington. Oil film thickness measurement: a contribution to the understanding and control of lubrication in the piston-ring packs of ic engines. *Proc. IMechE Part J: Journal of Engineering Tribology*, 225:595–601., 2009.

[66] M. Marshall. *An Ultrasonic Investigation of Real Engineering Contacts*. PhD thesis, The University of Sheffield, 2005.

[67] J. Kräutkramer and H. Kräutkramer. *Ultrasonic testing of materials*. Springer-Verlag, New York, 1977.

[68] J. L. Rose. *Ultrasonic Waves in Solid Media*. Cambridge University Press, Cambridge, 1999.

[69] W. J. McGonnagle. *Nondestructive testing*. McGraw-Hill, New York, 1961.

[70] A. B. Wood. *A Textbook of Sound*. Bell and Sons, London, 1964.

[71] W. P. Mason and R. N. Thurston. *Physical acoustics*. Academic Press, New York, 1979.

[72] R. S. Dwyer-Joyce, T. Reddyhoff, and B. W. Drinkwater. Operating limits for acoustic measurement of rolling bearing oil film thickness. *Tribology Transactions*, 47(3):366–375, 2004.

[73] L. S. Gournay. Conversion of electromagnetic to acoustic energy by surface heating. *Journal of the Acoustical Society of America*, 40:1322–1330, 1966.

[74] R. M. White. Generation of elastic waves by transient surface heating. *Journal of Applied Physics*, 34:3559–3567, 1963.

[75] C. B. Scruby, R. J. Dewhurst, D. A. Hutchins, and S. B. Palmer. *Research techniques in NDT*, volume 5, chapter Laser Generation of Ultrasound in Metals, pages 281–325. Academic Press, London, 1982.

[76] H. L. Grubin. Direct electromagnetic generation of compressional waves in metals in static magnetic fields. *IEEE Transactions of Sonics and Ultrasonics*, 17(4): 227–228, 1970.

[77] D. Hutchins, J. Hu, and K. Lundgren. A comparison of laser and emat techniques for noncontact ultrasonics. *Materials Evaluation*, 44:1244–1253, 1986.

[78] J. Blitz. *Fundamentals of Ultrasonics*. Butterworths, London, 1967.

[79] M. G. Silk. *Ultrasonic Transducers for Non-destructive Testing*. Adam Hilger, Bristol, 1984.

[80] T. Reddyhoff. *Ultrasonic Measurement Techniques for Lubricant Films*. PhD thesis, The University of Sheffield, 2006.

[81] J. Souquet, P. H. Defranould, and J. Desbois. Design of low-loss wide-band ultrasonic transducers for non-invasive medical application. *IEEE Transactions of Sonics and Ultrasonics*, 26:75–80, 1979.

[82] G. Bradfield. Ultrasonic transducers-1. introduction to ultrasonic transducers, part a. *Ultrasonics*, 8(2):112–123, 1970.

[83] G. Kosoff. The effects of backing and matching on the performance of piezoelectric ceramic transducers. *IEEE Transactions of Sonics and Ultrasonics*, 13:20–30, 1966.

[84] R. S. Dwyer-Joyce, B. W. Drinkwater, and C. J. Donohoe. The measurement of lubricant film thickness using ultrasound. *Proceedings of the Royal Society A: Mathematical,Physical and Engineering Sciences*, 459:957–976, 2003.

[85] B. Hosten. Bulk heterogeneous plane waves propagation through viscoelastic plates and stratified media with large values of frequency domain. *Ultrasonics*, 29:445–450, 1991.

[86] V. K. Kinra, P. T. Jaminet, C. Zhu, and V. R. Iyer. Simultaneous measurement of the acoustical properties of a thin-layered medium: The inverse problem. *Journal of the Acoustic Society of America*, 95:3059–3074, 1994.

[87] T. Pialucha and P. Cawley. The detection of embedded layers using normal incidence ultrasound. *Ultrasonics*, 32(6):431–440, 1994.

[88] T. Pialucha, C. C. H. Guyott, and P. Cawley. Amplitude spectrum method for the measurement of phase velocity. *Ultrasonics*, 27:270–279, 1989.

[89] H. G. Tattersall. The ultrasonic pulse-echo technique as applied to adhesion testing. *Applied Physics*, 6:819–832, 1973.

[90] K. Kendall and D. Tabor. An ultrasonic study of the area of contact between stationary and sliding surfaces. *Proceedings of the Royal Society*, 323:321–340, 1971.

[91] B. W. Drinkwater, R. S. Dwyer-Joyce, and P. Cawley. A study of interaction between ultrasound and a partially contacting solid-solid interface. *Proceedings of the Royal Society*, 452:2613–2628, 1996.

[92] M. B. Marshall, R. Lewis, R. S. Dwyer-Joyce, U. Olofsson, and S. Bjorklund. Ultrasonic characterisation of a wheel/rail contact. *Proceedings of 30th Leeds-Lyon Symposium on Tribology*, 2003.

[93] M. Gonzalez-Valadez, R. S. Dwyer-Joyce, and R. Lewis. Ultrasonic reflection from mixed liquid-solid contacts and the determination of interface stiffness. *Tribology and Interface Engineering Series*, 48:313–320, 2005.

[94] M. J. W. Povey. *Ultrasonic Techniques for Fluids Characterisation*. Academic Press, San Diego, 1997.

[95] R. Dwyer-Joyce, P. Harper, and B. Drinkwater. Oil film measurement in polytetrafluoroethylene-faced thrust pad bearings for hydrogenerator applications. *Proc. IMechE Part A: Journal of Power and Energy*, 220:619–628, 2006.

[96] R. S. Dwyer-Joyce, P. Harper, and B. Drinkwater. A method for the measurement of hydrodynamic oil films using ultrasonic reflection. *Tribology Letters*, 17:337–348, 2004.

[97] J. Zhang, B.W. Drinkwater, and R.S. Dwyer-Joyce. Calibration of the ultrasonic lubricant-film thickness measurement technique. *Measurement Science and Technology*, 16:1784–1791, 2005.

[98] P. Harper. *Measurement of film thickness in lubricated components using ultrasonic reflection*. PhD thesis, The University of Sheffield, 2008.

[99] T. Reddyhoff, S. Kasolang, R. S. Dwyer-Joyce, and B. W. Drinkwater. The phase shift of an ultrasonic pulse at an oil layer and determination of film thickness. *Proc. IMechE Part J: Journal of Engineering Tribology*, 219:387–400, 2005.

[100] Y.C. Tan and Z.M. Ripin. Frictional behaviour of piston rings of small utility two-stroke engine under secondary motion of piston. *Tribology International*, 44(5): 592–602., 2011.

[101] D.K. Srivastava, A.K. Agarwal, and J. Kumar. Effect of liner surface properties on wear and friction in a non-firing engine simulator. *Materials and Design*, 28(5): 1632–1640, 2007.

[102] L.L. Ting. Development of a reciprocating test rig for tribological studies of piston engine moving components - part i: Rig design and piston ring friction coefficients measuring method. *SAE Technical Paper Series*, 930685, 1993.

[103] N.W. Bolander, B.D. Steenwyk, F. Sadeghi, and G.R. Gerber. Lubrication regime

transitions at the piston ring-cylinder liner interface. *Proc. IMechE Part J: Journal of Engineering Tribology*, 219:19–31, 2005.

[104] O. Akalin and G.M. Newaz. Piston ring-cylinder bore friction modeling in mixed lubrication regime: Part I, analytical results. *ASME: Journal of Tribology*, 123: 211–218, 2001.

[105] O. Akalin and G.M. Newaz. Piston ring-cylinder bore friction modeling in mixed lubrication regime: Part iicorrelation with bench test data. *ASME: Journal of Tribology*, 123:219–223, 2001.

[106] S.E. Hartfield-Wunsch, S.C. Tung, and C.J. Rivald. Development of a bench test for the evaluation of engine cylinder components and correlation with engine test results. *SAE Technical Paper Series*, 932693, 1993.

[107] J.J. Truhan, J. Qu, and P.J. Blau. A rig test to measure friction and wear of heavy duty diesel engine piston rings and cylinder liners using realistic lubricants. *Tribology International*, 38:211–218, 2005.

[108] S. K. Michail and G. C. Barber. The effects of roughness on piston ring lubrication-part ii: The relationship between cylinder wall surface topography and oil film thickness. *Tribology Transactions*, 38:173–177, 1995.

[109] M. K. Wan Ibrahim, D. Gasni, and R. Dwyer-Joyce. Profiling a ball bearing oil film with ultrasonic reflection. *Tribology Transactions*, 55:409–421, 2012.

[110] P. Dellis and C. Arcoumanis. Cavitation development in the lubricant film of a reciprocating piston-ring assembly. *Proc. IMechE Part J: Journal of Engineering Tribology*, 218:157–171, 2004.

[111] M. Giacopini, M. T. Fowell, D. Dini, and A. Strozzi. A mass-conserving complementarity formulation to study lubricant films in the presence of cavitation. *ASME: Journal of Tribology*, 132:1–12, 2010.

[112] A. Almqvist, J. Fabricius, A. Spencer, and P. Wall. Similarities and differences

between the flow factor method by Patir and Cheng and homogenization. *Journal of Tribology*, 133:1–5, 2011.

[113] I. M. Hutchings. *Tribology - friction and wear of engineering materials.* Butterworth-Heinemann, Oxford, 1992.

[114] M. T. Ma, I. Sherrington, and E. H. Smith. Analysis of lubrication and friction for a complete piston-ring pack with an improved oil availability model .1. circumferentially uniform film. *Proc. IMechE Part J: Journal of Engineering Tribology*, 211:1–15, 1997.

[115] P. Freeman. *Lubrication and Friction.* Pitman, London, 1962.

[116] S.W. Cho, S.M. Choi, and C.S. Bae. Frictional modes of barrel shaped piston rings under flooded lubrication. *Tribology International*, 33(8):545–551, 2000.

[117] J. A. Williams. *Engineering tribology.* Oxford University Press, Oxford, 1994.

[118] B. Zhmud, E. Akerlund, S. Jacobson, J. Hardell, L. Hammerstrom, and R. Ohlsson. Ans triboconditioning: In-manufacture running-in process for improving tribological properties of mechanical parts made of steel or cast iron. In *Proceedings of the 18th International Colloquium Tribology- Industrial and Automotive Lubrication*, TAE, Stuttgart/Ostfildern, Germany, 10-12 January 2012.

[119] B. Zhmud, G. Flores, C. Verpoort, and U. Morawitz. Ans triboconditioning: A novel surface finishing process for improving tribological properties of cylinder bores. In *Proceedings of the 6th VDI-Conference 'Zylinderlaufbahn, Kolben, Pleuel'*, Baden, Germany, 19-20 June 2012.

[120] E. Tomanik. Friction and wear bench tests of different engine liner surface ?nishes. *Tribology International*, 41:10321038, 2008.

[121] J. Jocsak, Y. Li, T. Tian, and V. W. Wong. Modeling and optimizing honing texture for reduced friction in internal combustion engines. *SAE Technical Paper Series*, 2006-01-0647, 2006.

[122] S. K. Michail and G. C. Barber. The effects of roughness on piston ring lubrication-part i: Model development. *Tribology Transactions*, 38:19–26, 1995.

[123] A. Spencer, A. Almqvist, and R. Larsson. A numerical model to investigate the effect of honing angle on the hydrodynamic lubrication between a combustion engine piston ring and cylinder liner. *Proc. IMechE Part J: Journal of Engineering Tribology*, 225:683–689, 2011.

[124] H. L. Costa and I. M. Hutchings. Hydrodynamic lubrication of textured steel surfaces under reciprocating sliding conditions. *Tribology International*, 40:1227–1238, 2007.

[125] U. Pettersson and S. Jacobson. Friction and wear properties of micro textured dlc coated surfaces in boundary lubricated sliding. *Tribology Letters*, 17(3):553–559, 2004.

[126] S. Mezghani, I. Demirci, H. Zahouani, and M. El Mansori. The effect of groove texture patterns on piston-ring pack friction. *Precision Engineering*, 36:210 217, 2012.

[127] R. S. Dwyer-Joyce, D. A. Green, P. Harper, R. Lewis, S. Balakrishnan, P. D. King, H. Rahnejat, and S. Howell-Smith. The measurement of liner-piston skirt oil film thickness by an ultrasonic means. *SAE Technical Paper Series*, 2006-01-0648, 2006.

[128] R.S. Mills, E.Y. Avan, and R.S. Dwyer-Joyce. Piezoelectric sensors to monitor lubricant film thickness at pistoncylinder contacts in a fired engine. *Proc. IMechE Part J: Journal of Engineering Tribology*, 227(2):100–111, 2013.

[129] B. W. Drinkwater, J. Zhang, K. J. Kirk, J. Elgoyhen, and R. S. Dwyer-Joyce. Ultrasonic measurement of rolling bearing lubrication using piezoelectric thin films. *ASME: Journal of Tribology*, 131:1–8, 2009.